

**Removal Of
Model Sulphur Compounds
From Hydrocarbon Fractions
By Selective Adsorption**

vom Fachbereich Chemie
der Technischen Universität Kaiserslautern
zur Erlangung des akademischen Grades
"Doktor der Naturwissenschaften"
genehmigte Dissertation

vorgelegt von
SRIDHAR ADAPA

Betreuer der Arbeit: Prof. Dr.-Ing. S. Ernst
Tag der wissenschaftlichen Aussprache: 16.09.2008

Kaiserslautern 2008

Promotionskommission:

Vorsitzender der Promotionskommission: Prof. Dr. Helmut Sitzmann
1. Berichterstatter: Prof. Dr.-Ing. Stefan Ernst
2. Berichterstatter: Prof. Dr. Werner R. Thiel

Die vorliegende Arbeit entstand zwischen Juni 2004 und August 2008 im Fachbereich Chemie, Fachrichtung Technische Chemie, der Technischen Universität Kaiserslautern.

Acknowledgements

I would like to express my sincere gratitude to Prof. Dr.-Ing. Stefan Ernst for giving me an opportunity to work in his group. I also thank him for his critical discussions, guidance and support that have been instrumental in improving my research skills.

I thank Prof. Dr. Martin Hartmann for his support at the initial days of my work.

I thank Prof. Dr. Helmut Sitzmann for immediately accepting to be the chairman of the committee and Prof. Dr. Werner R. Thiel for accepting to be a reviewer of this work.

I am grateful to my colleagues Thomas Hecht, Matthias Oberlinger, Helwig Thiel, Supak Tontisirin, Gunder Dörr, Alex Wagener, Markus Schindler, Thomas Philippi, Dirk Jung and Simon Kullmann for their hospitality.

I would also like to extend my thanks to the former and the present secretaries of the research group Ms. H. Schramm and Ms. I. Berwanger-Nicklas for their help and support.

To my Parents and Sisters

I. Contents

1. Introduction and scope.....	4
2. Theory	11
2.1 The structure and properties of zeolites.....	11
2.1.1 MFI.....	14
2.1.2 FAU.....	15
2.1.3 MWW.....	17
2.1.4 MOR.....	18
2.2 Techniques of characterization.....	19
2.2.1 Powder X-ray diffraction.....	19
2.2.2 Scanning electron microscopy (SEM).....	20
2.2.3 Nitrogen adsorption isotherms.....	22
2.2.4 Thermogravimetric and differential thermal analysis (TG-DTA).....	24
2.2.5 Elemental analysis.....	24
2.2.5.1 Atomic absorption spectroscopy.....	24
2.2.5.2 Energy dispersive X-ray analysis (EDAX).....	24
2.3 IR-spectroscopic studies of thiophene adsorbed on zeolites.....	24
2.4 UV-Vis spectroscopy.....	27
2.5 Post-synthesis modification of FAU zeolites by ion-exchange.....	27
3. Experimental section.....	29
3.1 Materials.....	29
3.2 Characterization of the adsorbents.....	31
3.2.1 Powder X-ray diffraction	31
3.2.2 Scanning electron microscopy.....	31
3.2.3 Nitrogen adsorption.....	31
3.2.4 Thermogravimetric and differential thermal analysis.....	32

3.2.5 Elemental analysis.....	32
3.2.5.1 Atomic absorption spectroscopy.....	32
3.2.5.2 EDAX.....	32
3.3 UV-Vis spectroscopy.....	33
3.4 Infrared spectroscopy.....	33
3.5 Applied zeolites.....	34
3.5.1 H-ZSM-5 ($n_{\text{Si}}/n_{\text{Al}} = 13$).....	34
3.5.2 H-ZSM-5 ($n_{\text{Si}}/n_{\text{Al}} = 20$).....	35
3.5.3 H-ZSM-5 ($n_{\text{Si}}/n_{\text{Al}} = 40$).....	37
3.5.4 Silicalite-1.....	38
3.5.5 H-MCM-22.....	40
3.5.6 H-MOR.....	41
3.5.7 Na ⁺ -Y.....	43
3.5.8 H ⁺ -Y.....	44
3.5.9 Ag ⁺ -exchanged Na ⁺ -Y.....	45
3.5.10 Ni ²⁺ -exchanged Na ⁺ -Y.....	46
3.5.11 Cu ²⁺ -exchanged Na ⁺ -Y.....	48
3.5.12 Ce ³⁺ - and Ce ⁴⁺ -exchanged Na ⁺ -Y.....	49
3.5.13 La ³⁺ -exchanged Na ⁺ -Y.....	50
3.5.14 Y ³⁺ -exchanged Na ⁺ -Y.....	52
3.6 Batch adsorption experiments.....	53
3.7 Continuous flow fixed-bed adsorption experiments.....	54
4. Results and discussion.....	59
4.1 Kinetics of thiophene adsorption: Batch experiments.....	59
4.1.1 Acid zeolites.....	59
4.1.2 Ion-exchanged Na ⁺ -Y zeolite.....	66

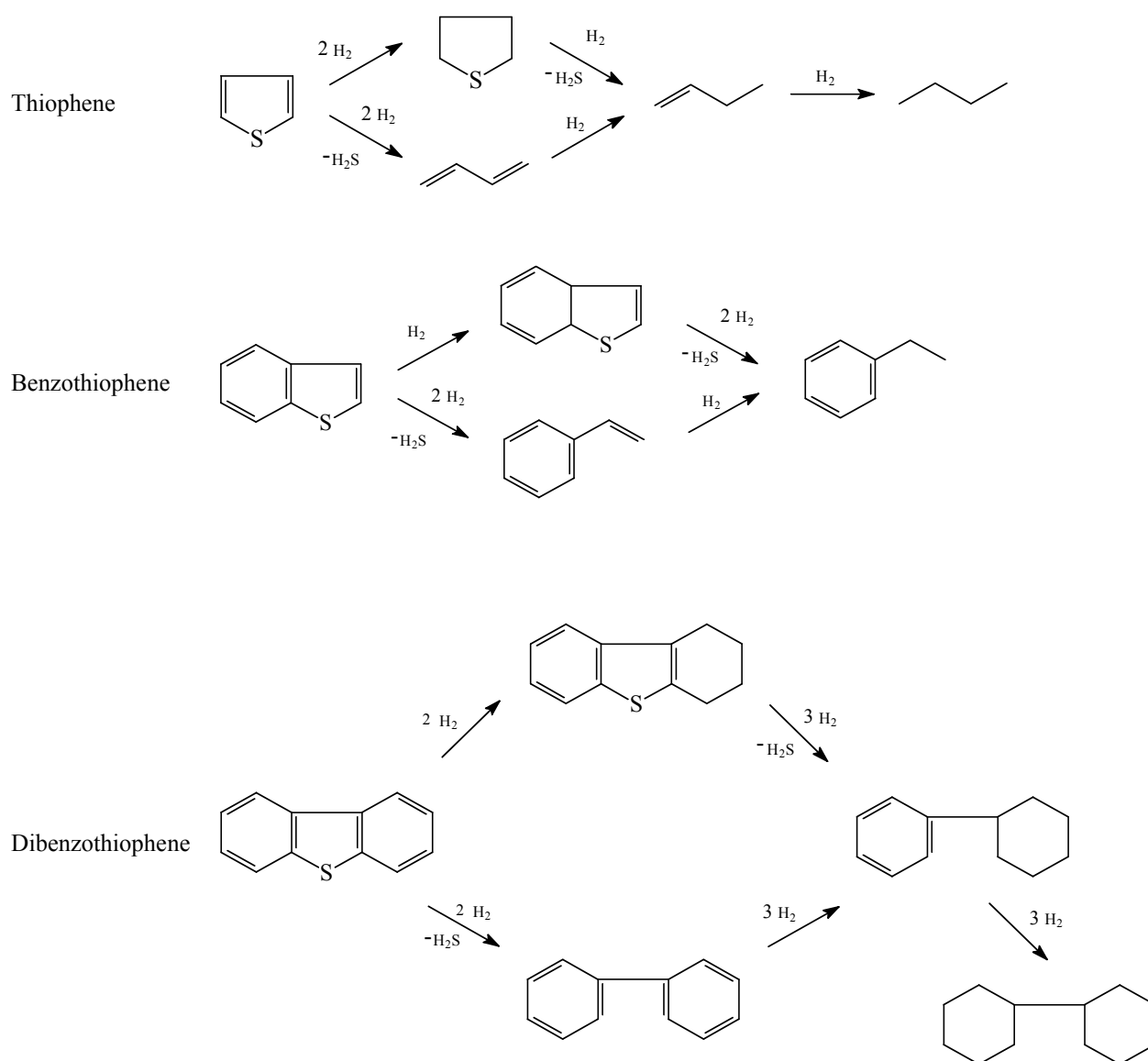
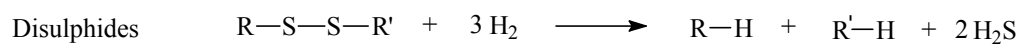
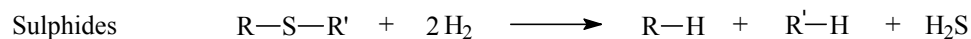
4.1.3	Cu ²⁺ -exchanged Na ⁺ -Y zeolite.....	68
4.1.4	Ce ³⁺ -, La ³⁺ - and Y ³⁺ -exchanged Na ⁺ -Y zeolites.....	70
4.1.5	Ce ⁴⁺ -Y zeolite.....	72
4.2	Continuous flow fixed-bed adsorption of sulphur-containing compounds.....	72
4.2.1	Breakthrough curves for sulphur-containing compounds on Cu ⁺ - and Ni ²⁺ -exchanged Na ⁺ -Y zeolites as adsorbents.....	72
4.2.2	Breakthrough curves for the adsorption of thiophene on Ce ³⁺ -, La ³⁺ - and Y ³⁺ -exchanged Na ⁺ -Y zeolites.....	78
4.3	IR spectroscopic studies on the adsorption of thiophene on metal ion-exchanged zeolites.....	81
4.4	Regeneration of used adsorbents.....	87
4.4.1	Regeneration of acidic zeolites.....	87
4.4.2	Regeneration of metal ion-exchanged zeolites.....	89
5.	Selective adsorption of 4,6-DMDBT from toluene solution.....	93
6.	Conclusions.....	95
7.	Abbreviations and indices.....	97
8.	References.....	99

1 Introduction and scope

Increasing concern over limited reserves of crude oil has created an interest in alternative fuels. One of the alternative routes to produce synthetic fuels is biomass to liquid conversion. The pyrolysis oil obtained by high temperature biomass pyrolysis can be upgraded to produce bio-fuels. The pyrolysis oil produced by this process contains, e.g., thiophene and thiophenic derivatives as impurities. Desulphurization of such oil is therefore required due to environmental concerns. Desulphurization is being used in petroleum refineries not only to meet the environmental regulations but also to protect catalysts that are being used in downstream processes. The sulphur compounds can also poison the catalysts used in the exhaust systems of the automobiles. Desulphurization is currently achieved by a hydrodesulphurization (HDS) process with Co-Mo/Al₂O₃ or Ni-Mo/Al₂O₃ catalysts. The reactions involved in hydrodesulphurization are shown in Figure 1.1 [1]. These processes require H₂, often at high temperature and pressure. Removal of thiophene and substituted thiophene-like compounds like benzothiophene or dibenzothiophene requires much higher pressures of H₂, which makes HDS less effective in removing sulphur from thiophene and thiophene derivatives (benzothiophenes, dibenzothiophenes) than from thiols, sulphides and disulphides.

Several non HDS-based desulphurization technologies such as adsorptive desulphurization, charge-transfer complex formation, extraction using ionic liquids, bio-catalytic treatment etc. have been proposed recently for the desulphurization of liquid fuels [2, 3]. In the context of this thesis, desulphurization by selective adsorption on zeolites has been explored.

The reason for expecting zeolites to be good adsorbents is that they offer the advantage of possessing adsorption sites as well as the possibility of easy separation and recovery. Properties like ion-exchange ability, alumina content and porosity of the zeolites can be well exploited in the purification of solutions through adsorption.

**Type of
organic sulphur
compounds**
Mechanism of hydrotreating reaction ^{a)}


^{a)} Reaction pathway for alkylated thiophene, benzothiophene and dibenzothiophene is similar to the reaction pathway of non-alkylated counterparts

Figure 1.1: Sulphur-containing compounds and their hydrotreating pathways [1].

Removal of sulphur-containing compounds by adsorption dates back to the use of Bauxite, a porous mineral, for the removal of mercaptanes from various petroleum fractions [4]. Red mud, a waste product from aluminium production, has also been used as an adsorbent for the removal of sulphur-containing compounds and other impurities from petroleum fractions. Singh et al. [5, 6] have used red mud for the removal of 1-butanethiol from kerosene and diesel oils in the temperature range from 25 °C to 45 °C. They concluded that higher temperatures favour the removal efficiency.

Thiophene adsorption on various oxides has been previously reported [7-9]. Among zeolites, De Angelis et al. [10] reported thiophene adsorption on zeolite Na⁺-X. Moreover, Ulendeeva et al. showed an interaction of thiophene through its S atom with Na⁺ and Ca²⁺ ions in zeolites and, in the case of aromatic compounds, through their π -system [11]. Salem [12,13] published the results of using activated carbon as well as zeolites Ca²⁺-A and Na⁺-X for removing sulphur-containing compounds from naphtha containing about 50 ppm sulphur at 20 °C. Their data indicate that activated carbon had greater adsorption capacity for sulphur-containing compounds, when the initial sulphur content is higher than 25 ppm. For lower concentrations, Na⁺-X proved to be more effective. Ca²⁺-A did not show an appreciable removal of sulphur-containing compounds from the petroleum fractions used in this study.

With respect to high-silica zeolites, Weitkamp et al. [14] reported ZSM-5, Silicalite-1 and ZSM-11 as promising adsorbents for the removal of thiophene from benzene. These adsorbents can be regenerated simply by flushing them with nitrogen at 350 °C. Later, Garcia and Lercher [15] predicted surface reactions of thiophene on H-ZSM-5 zeolites. Ring opening and oligomerization of thiophene on H-ZSM-5 were reported for longer exposures, indicating that these processes are relatively slow. Chica et al. [16] claimed that oligomerization occurs both on H-ZSM-5 and H-Y zeolites and these thiophene oligomers were shown to decompose at 261 °C to form molecular thiophene with oxygen, helium, hydrogen or propane as purge gas. However, thiophene-derived adsorbed species are completely removed only with oxygen containing streams at 600 °C. Richardeau et al. [17] studied the adsorption and the reaction of thiophene over H-FAU zeolite with dilute and concentrated solutions of thiophene. Their studies revealed the competition of unsaturated hydrocarbons with thiophene in adsorbing on acid sites of H-FAU. From these studies, it could be concluded that the removal of thiophene by adsorption on acidic zeolites is more effective when carried out from dilute solutions containing non-olefinic hydrocarbons as solvent. In another study Chica et al. investigated the

adsorption of thiophene on various acid zeolites like H-ZSM5, H-Y and H-Beta [18]. Thiophene oligomers with different sizes are formed during adsorption, depending on the spatial constraints within the zeolite channels.

Beside acid zeolites, efforts to develop metal ion-exchanged zeolites were undertaken in parallel. Among metal ion-exchanged Y zeolites, a Cu^{2+} -exchanged Y-type zeolite was the first to be shown as an useful adsorbent for the removal of thiophene from benzene [19]. However, thiophene can not be recovered as it is chemically converted by Cu^{2+} -Y and the only way left is to burn-off the adsorbate. While exploring Ni-Co-H-ZSM-5, Ni-Co-H-MOR and Ni-Na-Y zeolites as catalysts for their application to hydrodesulphurization reactions [20], apart from a catalytic conversion, adsorption of thiophene was also observed on these materials.

From the year 2000 onwards, the interest and the research activities in desulphurization by adsorption increased rapidly. This is due to the advent of strict administrative regulations and fuel specifications in many countries for environmental protection purposes. Consideration of sulphur-free liquid fuels as primary fuels for automotive and portable fuel cells also demands a good desulphurization adsorbent. Especially for a polymer electrolyte membrane (PEM) fuel cell, where the Pt electrode is readily poisoned by the sulphur-containing compounds.

New sorbents for the desulphurization of liquid fuels were developed on the basis of the π -complexation mechanism [21]. Through the π -complexation mechanism, cations can form a σ -bond with their vacant s-orbital and π -electrons of the adsorbate and the electron density of the d-orbital of the cation is back donated to the antibonding π -orbitals of the adsorbate. Already a number of new π -complexation adsorbents were developed for several applications. These include adsorbents for (a) olefin/paraffin separations, b) diene/olefin separation or purification and (c) aromatic/aliphatic separation and purification [22].

The bond strength between sorbate and sorbent depends on:

- 1) Vacancy in the outer shell s-orbital of the cation located on the surface of the adsorbent.
- 2) The amount of π -electrons in the target adsorbate molecule and the ease with which these π -electrons can be donated to the s-orbital of the cation.

- 3) The amount of d-orbital electrons of the cation and the ease with which they can be donated to the adsorbate molecule.

The best π -complexation adsorbents studied so far include Cu^+ -Y, Ag^+ -Y, Cu^{2+} -Y, Ni^{2+} -Y and Na^+ -Y. Among them, Cu^+ -Y was found to be the best for the removal of sulphur-containing compounds from hydrocarbon fractions. Cu^+ -Y was prepared by ion-exchanging Na^+ -Y with a Cu^{2+} -salt by conventional liquid phase ion-exchange (LPIE) and followed by reduction of Cu^{2+} to Cu^+ . The main drawback of these adsorbents is the high competition from aromatics, which can form a similar bond through π -complexation mechanism with the π -electrons of their double bonds like sulphur-containing compounds, e.g., thiophene and benzothiophene. Adsorbents based on metal ion-exchanged Y zeolites (with Cu^{2+} , Ni^{2+} , Zn^{2+} , Pd^{2+} and Ce^{3+} ions) were evaluated by Velu et al. for the adsorptive desulphurization of jet fuel [23]. In this evaluation, Ce^{3+} -exchanged zeolites were found to be highly selective adsorbents for sulphur-containing compounds as compared to the selectivity for aromatics. After performing some comparative studies, it was concluded that the reason for the higher selectivity is an adsorption via a direct metal-sulphur interaction (M-S) between the lone electron pair of sulphur in thiophene and the metal cation rather than binding via π -complexation (of C=C double bonds). To improve the adsorption capacity of Cu^+ -Y zeolite, an alternative route to introduce Cu^+ -ions directly was proposed and tested [24-25], viz. the so-called vapour phase ion-exchange (VPIE) or solid state ion exchange (SSIE) method. This technique was used to prepare a faujasite-type zeolite containing almost 57 copper ions per unit cell. The same method was also applied to Ni^{2+} -Y- and Ni^{2+} -X-type adsorbents [26]. In all cases, the sulphur adsorption capacity of the adsorbents prepared by SSIE was proven to be higher than with the adsorbents prepared by LPIE.

Selective adsorption of thiophene and benzothiophene on zeolites metal ion-exchanged in organic media was studied by Xue et al. [27]. Na^+ -Y zeolites exchanged with Ag^+ , Cu^{2+} , Ce^{3+} ions and NH_4^+ -Y exchanged with Ce^{3+} were used. The sulphur uptake increased in the order Cu^{2+} -Y < Ag^+ -Y < Ce^{3+} -Y. K-exchanged Ni^{2+} -Y zeolite was shown to be a promising adsorbent for desulphurizing model jet fuels [28]. The promoting effect of K on the ability to adsorb sulphur-containing compounds was attributed to an improved reducibility and surface dispersion of Ni when K was present as a co-cation. The effect of K as a co-cation on the performance of the adsorption of sulphur-containing compounds on Ni^{2+} -Y zeolite was also studied earlier in connection with coal desulphurization [29]. Yang et al. [30], in another

work, reported Zn^{2+} -Y zeolite as an additional π -complexation adsorbent, although its performance is not as good as Cu^+ -Y and Ni^{2+} -Y.

As shown in Figure 1.2, there are eight possible types of interaction of thiophene with metal species through one or more C=C bonds to form organometallic complexes [31-35]. In reviewing previous works, it should be noted that only two types of adsorption modes of thiophene on zeolite-based adsorbents have been proposed and very little spectroscopic information on the adsorption modes of sulphur compounds on zeolite-based adsorbents is provided. Having a thorough knowledge on the type of interaction is necessary to avoid the competitive adsorption of other organic compounds. In other words, the competitive adsorption between organic sulphur compounds and aromatics is one of the crucial factors that effect adsorption selectivity and hence, efficiency for sulphur-containing molecules.

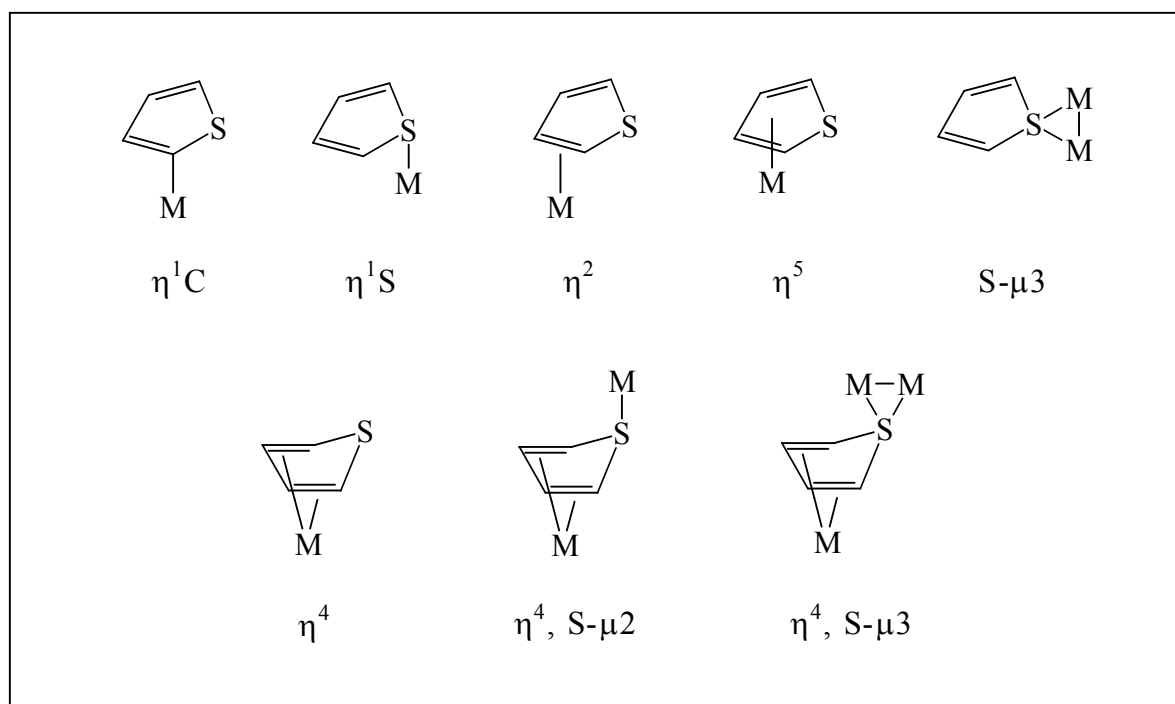


Figure 1.2: Known coordination geometries of thiophene with metal species in organometallic complexes [31].

In the present work, thiophene was selected as model sulphur-containing compound to explore the properties of zeolite-type adsorbents for the selective removal of sulphur-containing compounds from hydrocarbon fractions. To study the effect of an aromatic or aliphatic nature of the hydrocarbon fractions on the adsorption of thiophene over zeolites, two

different compounds, viz. toluene (aromatic) and *n*-heptane (aliphatic) were selected as solvents of the model solutions. The two selected model solutions were 0.5 wt.-% thiophene in toluene and 0.5 wt.-% thiophene in *n*-heptane. Acid zeolites like H-Y, H-ZSM-5, H-MCM-22, H-MOR and metal ion-exchanged zeolites like Na⁺-Y, Cu⁺-Y, Ag⁺-Y, Ni²⁺-Y, Ce³⁺-Y, La³⁺-Y and Y³⁺-Y were screened using the model solutions in batch-type and continuous systems. All the above mentioned zeolites were able to remove thiophene from toluene and *n*-heptane solutions. Adsorption of benzothiophene and dibenzothiophene from their solutions in toluene was also studied for the case of Cu⁺-Y as adsorbent. The reaction of thiophene on acidic zeolites and the interacting-mode of thiophene with metal ions of metal ion-exchanged zeolites was studied using UV-Vis spectroscopy and IR-spectroscopy, respectively. The regeneration procedure after adsorption was studied using thermogravimetry and differential thermal analysis. The removal of sulphur from dimethyl dibenzothiophenes is extremely difficult using the classical catalytic hydrodesulphurization technology. Therefore, the adsorption of 4,6 dimethyl dibenzothiophene on zeolites Cu⁺-Y and Ce³⁺-Y was also studied in complementary batch experiments.

2 Theory

2.1 The structure and properties of zeolites

In 1756 the Swedish mineralogist Cronstedt observed that the mineral stilbite seems to boil when heated, liberating steam. This led him to coin the term “zeolite”, which is derived from the Greek words “zeo”, to boil, and “lithos”, stone. Since then, approximately 40 mineral, or natural, zeolites have been discovered. Many of the naturally occurring zeolites can be produced synthetically, while some are only synthesized in the laboratory. Chemically, zeolites are crystalline aluminosilicates of group 1A and 2A elements. Structurally, these are complex, crystalline inorganic polymers based on an infinitely extending three-dimensional, four-connected framework of AlO_4^- and SiO_4 tetrahedra linked to each other by the sharing of oxygen ions. These AlO_4^- and SiO_4 tetrahedra are called primary building units of zeolites and are represented as TO_4 units. In this, T can be either Si or Al. These are the smallest units with which the entire framework can be built up. The next larger units that were found to occur in tetrahedral frameworks are secondary building units (SBU's). These SBU's, which contain up to 16 T-atoms, are derived assuming that the entire framework is made up of one type of SBU only. All SBUs known today are listed in Figure 2.1. A typical convention in drawing framework topologies is by using short straight line segments. Each line represents a bridging oxygen ion while the intersections locate the T-atoms (Si or Al).

Zeolites appear in over 170 different crystal structures that exhibit channels and cages of molecular dimensions from 0.4 to 1.32 nm in diameter. The pore openings are characterized by the size of the ring that defines the pore, designated as n-ring, where n is the number of T-atoms in the ring. The 8-ring-, 10-ring- and 12-ring-zeolites are called small, medium, and large pore zeolites, respectively. What makes zeolites unique is that their pores are uniform in size and there is no large pore size distribution. Therefore, zeolites may be good agents for separating different molecules from each other according to the size difference. Thus, zeolites are also called molecular sieves and this property is also very well exploited in using zeolites as catalysts for size selective and shape selective reactions.

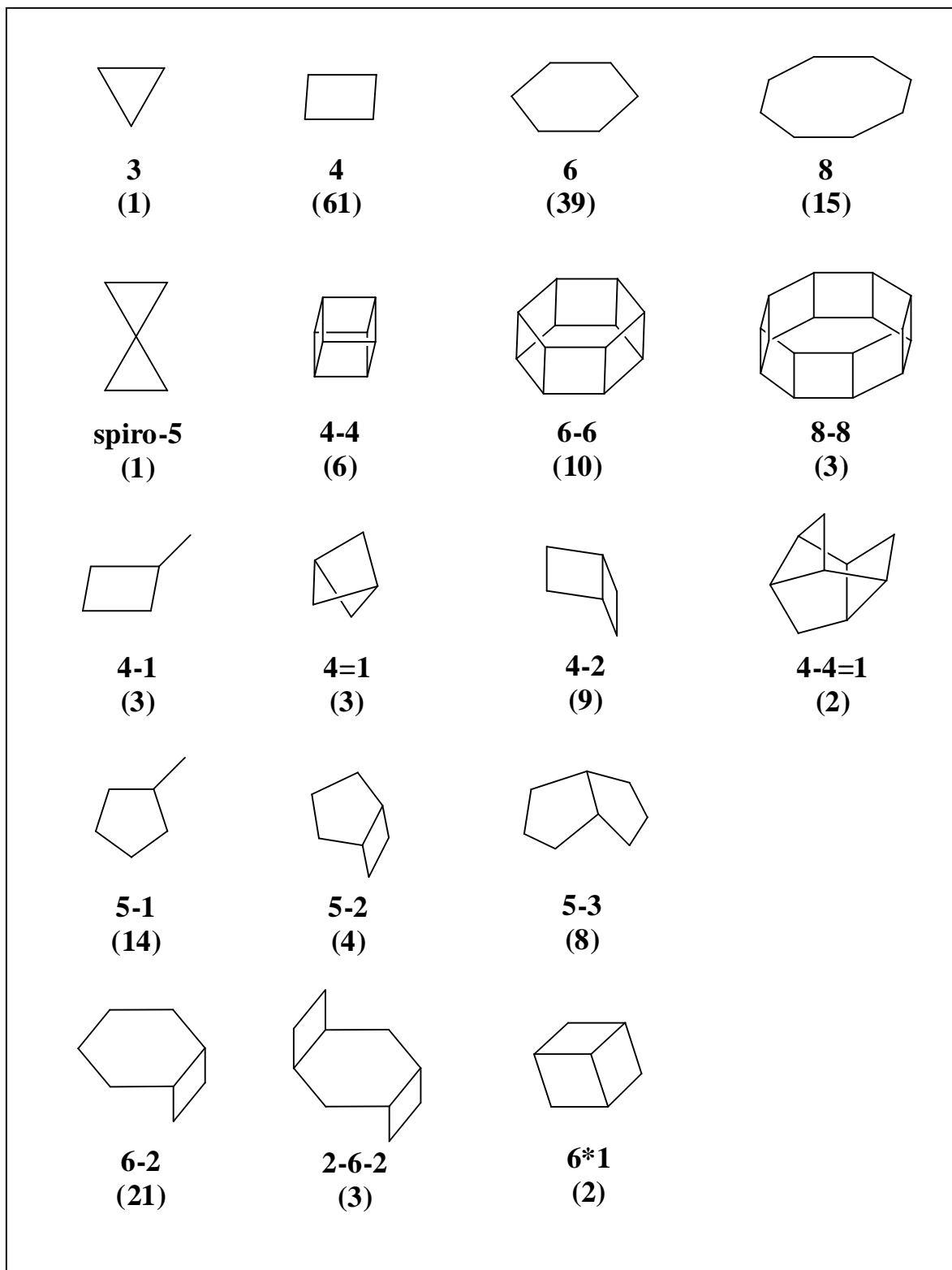


Figure 2.1: Secondary building units occurring in zeolite framework types [36].

The other important property of zeolites is their ion-exchange capability. Each aluminium atom in a zeolite introduces one negative charge into the framework which must be balanced by a metal cation or a proton attached to the oxygen atoms. These cations are mobile and exchangeable. When the charge is balanced by a proton, a bridge to a hydroxyl link is formed which acts as Brønsted-acid site. At high $n_{\text{Si}}/n_{\text{Al}}$ ratio, a zeolite contains fewer acidic or cationic sites, and hence lower adsorption affinity or capacity when it is used to remove polar compounds from a mixture. The exchangeable metal cations may be located at preferred sites within the framework and play an important role in determining the adsorptive properties. It is well established that the adsorptive properties of zeolites can be modified by ion-exchange.

Zeolites are very attractive materials for many applications. The use of zeolites in different segments is shown in Figure 2.2 [37].

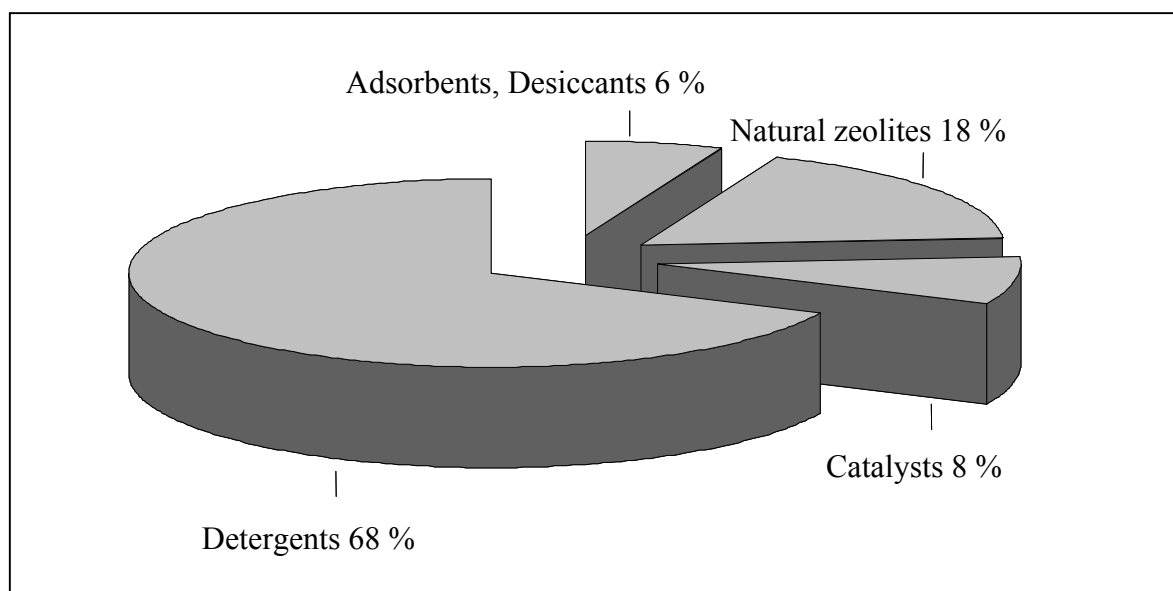


Figure 2.2: Zeolite market volumes.

As adsorbents, zeolites have very wide applications which include

- drying of petrochemicals like ethene, propene, ethylene oxide, natural gas etc.
- drying and purification of compressed technical gases like air, nitrogen or rare gases.

Zeolites with the topologies MFI, FAU, MWW and MOR are applied in this work for the selective removal of model sulphur compounds from hydrocarbon fractions. MFI, FAU, MWW and MOR are three letter codes assigned to the known zeolite framework topologies by the structure commission of the International Zeolite Association (IZA).

2.1.1 MFI

Zeolite ZSM-5, one of the most popular zeolites in modern hydrocarbon processing, has been assigned by the structure commission of the International Zeolite Association (IZA) a three letter code “MFI” (from Mobil Five). This zeolite, discovered by Mobil Oil Corp., is an aluminosilicate with high silica and therefore low alumina content. It consists of pentasil units as shown in Figure 2.1. These pentasil units are linked together to form pentasil chains and mirror images of these chains are connected via oxygen bridges to form corrugated sheets with 10-ring pore openings (e.g. the gray sheet perpendicular to the x-axis in Figure 2.3 c).

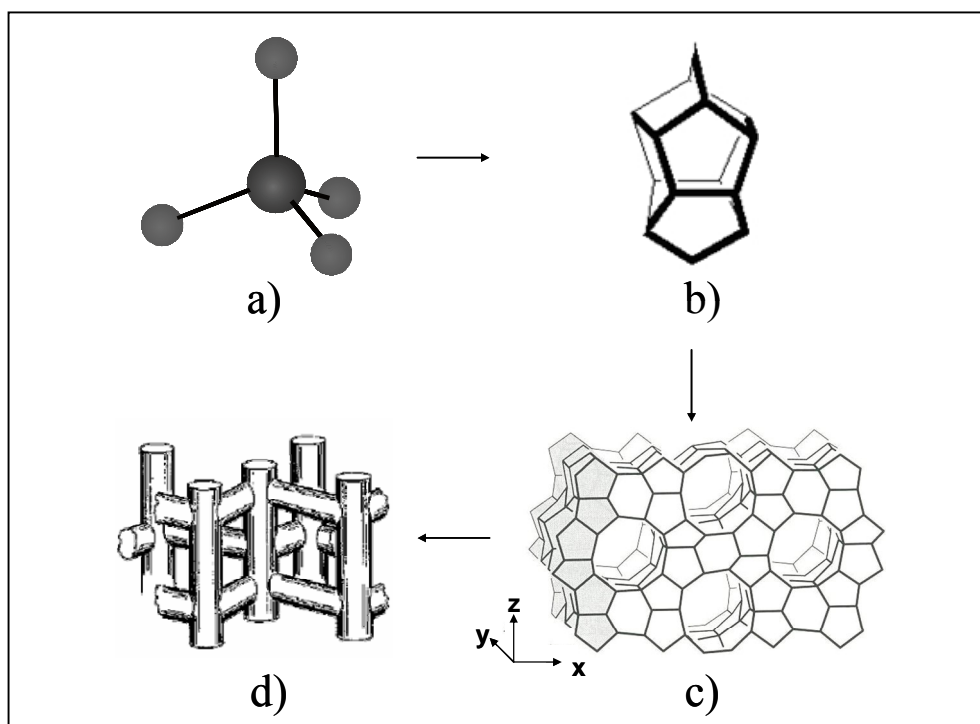


Figure 2.3: a) TO₄, the primary building unit, b) pentasil unit, c) MFI framework type, one corrugated sheet has been highlighted in gray, d) channel system in MFI.

Each sheet is linked by oxygen bridges to the next to form the 3-dimensional structure. Adjacent sheets are related to one another by an inversion centre. This produces straight 10-ring channels of elliptical shape with dimensions of 0.53 x 0.55 nm and perpendicularly arranged 10-ring channels of near circular cross-section with dimensions 0.53 x 0.56 nm. The latter channels link the straight channels to one another to form a 3-dimensional 10-ring sinusoidal channel system (as shown in Figure 2.3 d).

These materials find applications as an adsorbent for the removal of organic compounds from water [38]. Their importance as potential sorbents in a number of separation processes has been shown by Dessau et al. [39]. Above all, zeolite ZSM-5 is widely known for its shape selective catalysis, which mostly involves either (1) cracking of undesirable molecules to smaller, easily removable fragments or (2) avoiding undesirable competing reactions such as coking and transalkylation. Applications of ZSM-5 in such shape selective catalysis are distillate and lube oil dewaxing, the production of para-xylene, ethylbenzene and para-ethyl toluene and processes like methanol-to-gasoline, methanol-to-olefins and olefins-to-gasoline [40].

2.1.2 FAU

Another most important zeolite that has applications in catalysis and adsorption is zeolite Y. Zeolite Y is a synthetic form of the mineral faujasite with $n_{\text{Si}}/n_{\text{Al}}$ ratios from about 1.5 to 2.5. Therefore, IZA assigned a three letter code as “FAU” to zeolite Y. Zeolite Y consists of periodic building units of sodalite or β -cages. Each sodalite cage consists of 24 T- atoms (six 4-rings and eight 6-rings). These sodalite cages are tetrahedrally interconnected through a double six-ring into the hexagonal faujasite layer depicted in Figure 2.4. This creates a large cage called supercage or α -cage with a diameter of ca. 1.3 nm and a free aperture of 0.74 nm.

Due to the excess negative charge present at the AlO_2^- units, charge compensating cations are present to neutralize the negative framework charge. These cations are distributed all over the zeolite framework and the locations of these cations within the framework are shown in Figure 2.5 with the nomenclature established by Smith [41]. The locations of these sites are named as follows: SI – at the center of the hexagonal prism and octahedrally coordinated to the framework, SI' – on the face of the six-membered ring inside the sodalite cage and opposite to SI, SII – on the six-membered ring face of the sodalite cage on the supercage side, SII' – on the six-membered ring inside the sodalite cage and opposite to SII, SU - at the center of the sodalite cage and SIII – at the center of the square face of the sodalite cage on the supercage side.

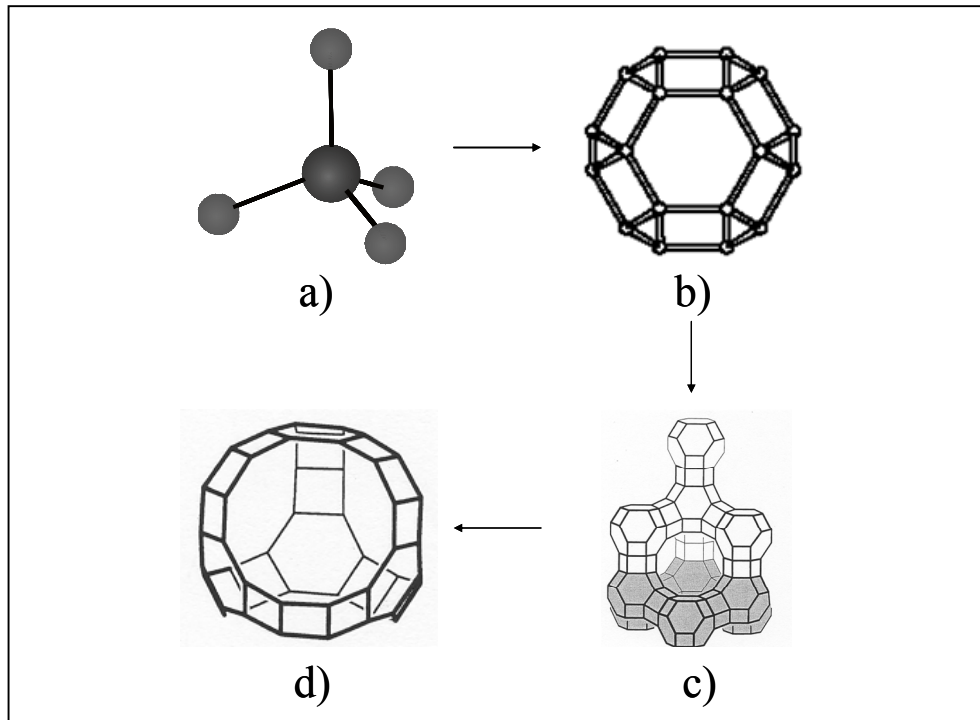


Figure 2.4: a) TO₄, Primary building unit, b) sodalite unit, 4⁶6⁸ c) faujasite framework type, one layer is highlighted in gray and d) supercage.

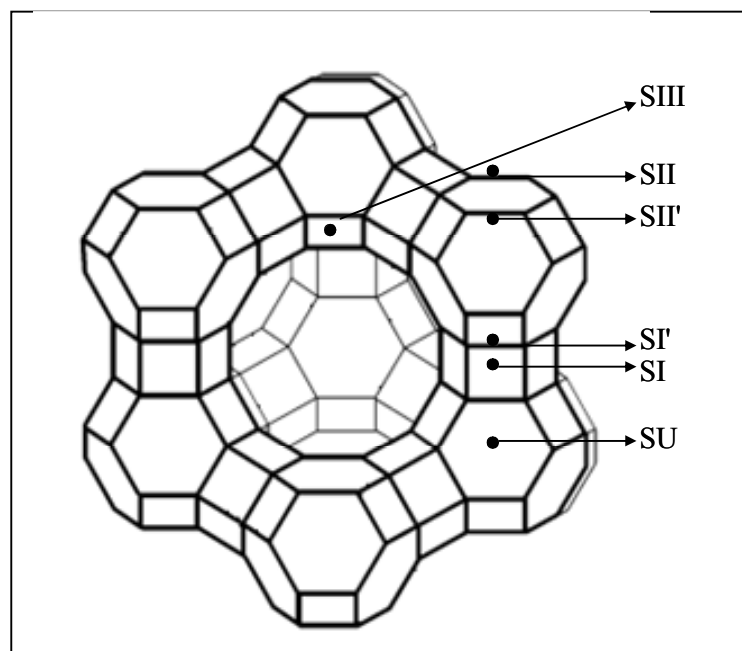


Figure 2.5: Topology of FAU structure, showing locations of the cation sites.

The Y-type zeolites are used in several catalytic applications. The most important one is its application in fluid catalytic cracking processes (FCC). FCC uses more than 90 % of zeolites that are applied in the field of catalysis. It is an example where zeolites have had a large impact on crude oil economy.

2.1.3 MWW

The high-silica zeolite MCM-22, having MWW topology, has a rather unusual framework structure. It was synthesized by Rubin et al. and described in a Mobil patent [42]. It is formed by stacking of double layer. Each individual layer consists of $[4^35^66^3]$ cages joined by sharing 4-ring faces and is attached to the second layer (mirror image of the first layer) via double 6-rings

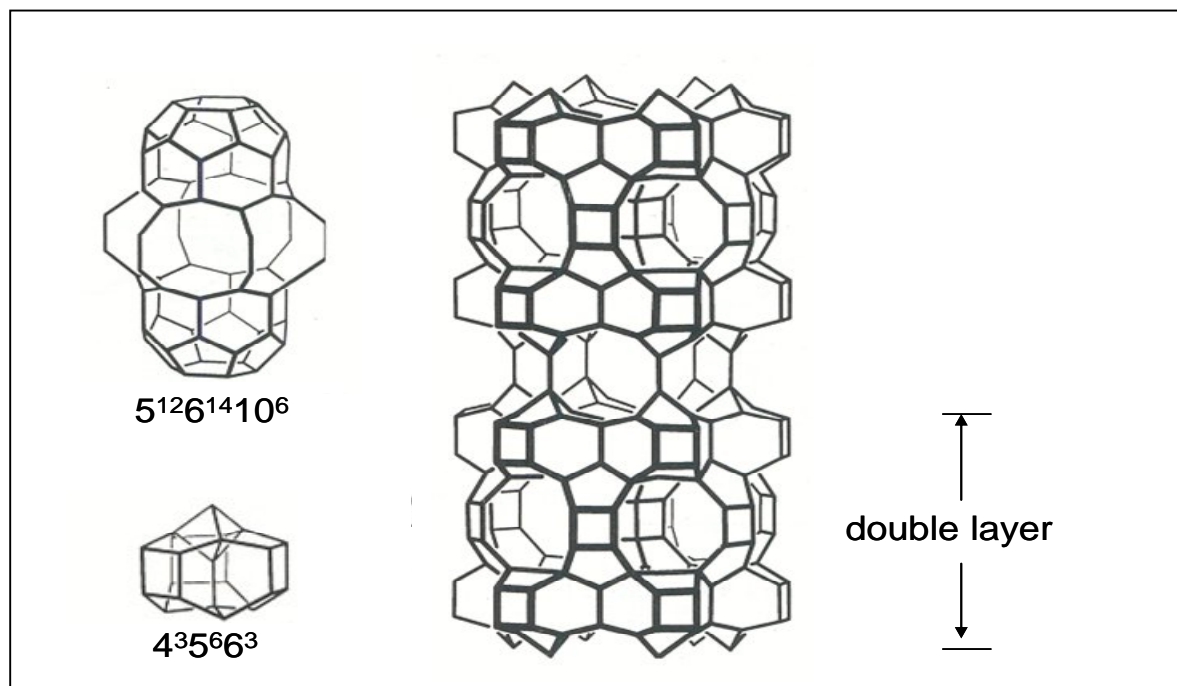


Figure 2.6: The MWW framework topology showing the double layer, the small $[4^35^66^3]$ cage and the side pockets at the channel intersection between double layers.

This produces two non-intersecting 2-dimensional, 10-membered ring channel systems. One of these lies within the double layer, and the second between the double layers. The latter also has two side pockets (12-ring access) at each channel intersections (see Figure 2.6 right).

Among these two independent 10-membered ring pore systems, one consists of two dimensional, sinusoidal intersecting 10-membered ring channels with an elliptical cross section of 0.41 x 0.51 nm and the small cage located along each sinusoidal channel has dimensions of 0.64 x 0.69 nm. The other pore system possesses large cylindrical supercages whose diameters are defined by a 12-membered ring, having interior dimensions of 0.71 x 0.71 x 1.8 nm and can be accessed by 10-membered ring windows with 0.45 x 0.55 nm. With this interesting properties it can be used e.g. for toluene alkylation with propylene to cymene or n-butene skeletal isomerization to *iso*-butene [43].

2.1.4 MOR

Zeolite mordenite possesses an aluminium content which is intermediate between faujasite and ZSM-5. Hence, with its relatively low n_{Si}/n_{Al} ratio (ca. 5) this material contains a larger number of counter cations balancing the negative charge of the framework than ZSM-5.

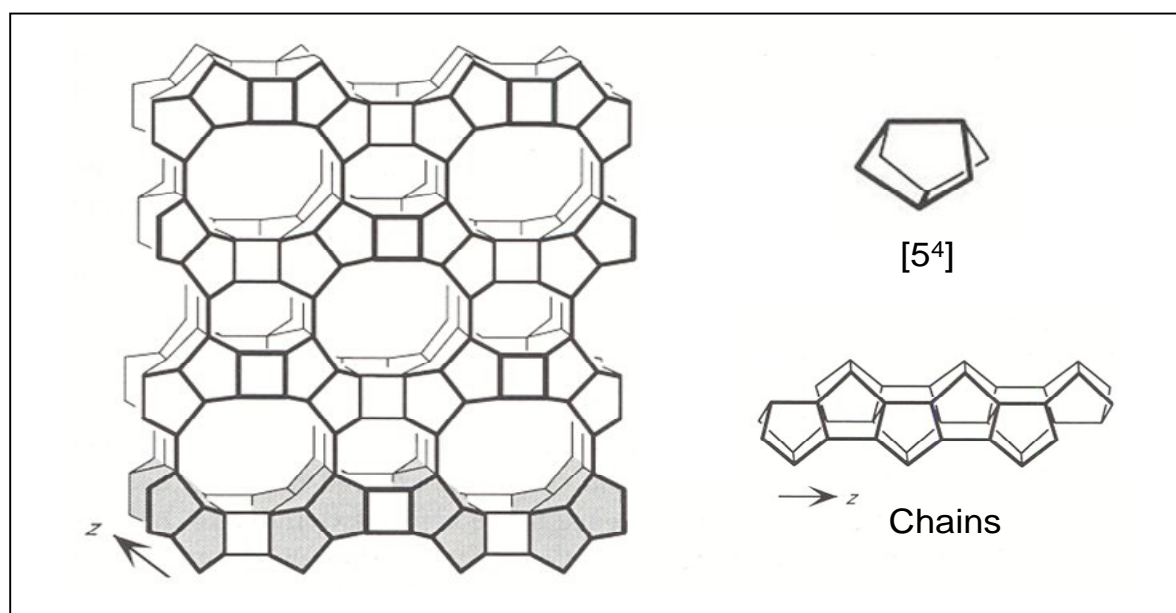


Figure 2.7: The MOR framework type (left) and the chain composed of edge-sharing [5⁴] units (right).

The framework contains units of four 5-rings [5⁴] joined to one another via common edges to form chains. Mirror images of these chains are connected via oxygen bridges to form corrugated sheets (arranged horizontally in Figure 2.7). These sheets, displaced by half a

translation in z, are then connected to one another to form oval 12- and 8-rings along the corrugations. The walls of the 12-ring channels contains 8-rings, but the 8-ring openings of adjacent 12-ring channels are displaced with respect to one another, so only very limited access from one channel to the next is possible. Consequently, the channel system is effectively one dimensional. The 12-membered ring with an elliptical shape has dimensions of 0.65 x 0.7 nm and the 8-membered ring window has dimensions of 0.26 x 0.57 nm. Mordenite is a very important material widely used in catalysis and adsorption in petroleum refining and the fine chemicals industry.

2.2 Techniques of characterization

The characterization of zeolites is an essential tool not only in understanding the chemical and physical properties of zeolites, but also in exploring the application of zeolites in adsorption and catalysis. An adequate characterization with appropriate analytical techniques should be able to describe the properties of adsorbents. X-ray diffraction, nitrogen adsorption isotherms, thermal and gravimetric analysis, vibrational spectroscopy, electron microscopy and atomic absorption spectroscopy are the techniques used to characterize the adsorbents used in this work.

2.2.1 Powder X-ray diffraction

The X-ray diffraction pattern is a “finger print” which allows us to confirm the structure of the zeolite. The peak positions in a powder pattern (usually measured in 2θ , diffraction angle) are related to the geometry of the unit cell. Each peak represents at least one reflection (and several that happen to have similar 2θ values). The 2θ value is related to the d-spacing of the corresponding reflection (spacing of the diffracting planes) by the Bragg Equation 2.1.

$$\lambda = 2d_{hkl}\sin\theta_{hkl} \quad (2.1)$$

Where λ is the wavelength of the X-rays, d is the spacing between the planes in the atomic lattice and hkl are the Miller indices of the planes.

Sample purity, degree of crystallinity, crystallite size and unit cell dimensions can be derived from several features of the XRD pattern of the zeolite. Damage to the zeolite structure by

post-synthesis processes like cation exchange, steaming or calcination can also be assessed using this technique and the corresponding equipment.

2.2.2 Scanning electron microscopy (SEM)

In scanning electron microscopy, a source of electrons is focussed on a very fine probe that is rastered over the surface by a scanning coil. A schematic diagram of the SEM principle is shown in Figure 2.8. When high energy incident electrons interact with atoms, they will be scattered elastically or inelastically. In an inelastic scattering event, a part of the incident energy is transferred to other electrons in atoms (if the energy transferred exceeds the work function of the crystal, secondary electrons can exit from the crystal) or produces light or X-rays induced by the transition between an excited state and the ground state. Several different kinds of outputs can be used including secondary electrons, back scattered electrons, X-rays, transmitted electrons, beam induced current and light cathodo-luminescence. Hereafter, the output of the SEM will be confined to secondary electrons. The output signal derived from secondary electrons can then be used to modulate the brightness of a cathode ray tube (CRT) as a function of the surface position where the electrons are focussed. The yield of secondary electrons increases with the decreasing glance angle of the incidence to the specimen surface, i.e. the yield depends on the surface topology. The superiority of the SEM over the optical microscope is the high spatial resolution and great depth of focus and therefore, surface topological information from a large specimen area can be observed at high resolution.

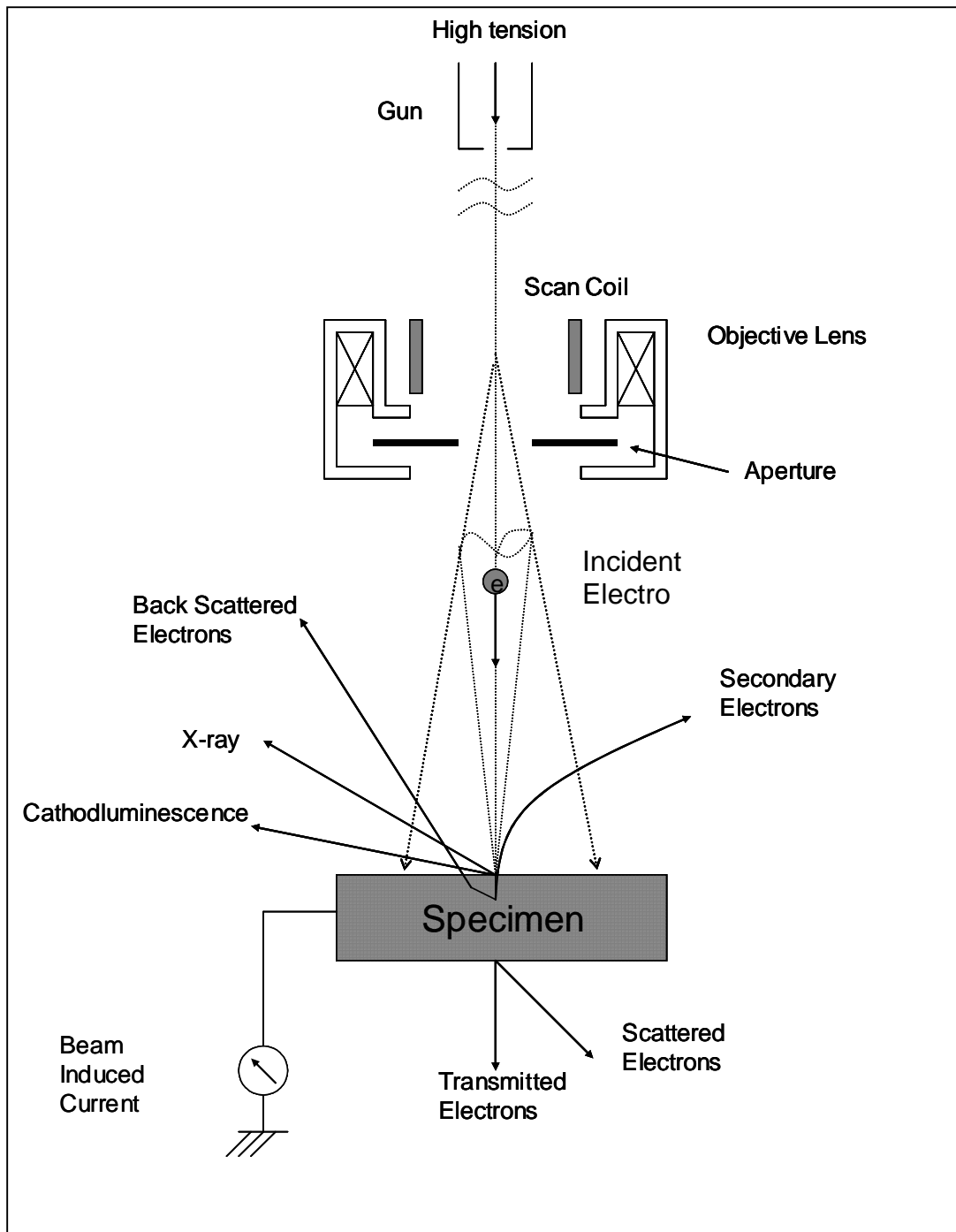


Figure 2.8: Schematic diagram of a scanning electron microscope (adapted from [44]).

2.2.3 Nitrogen adsorption isotherms

When the quantity of adsorbate on a surface is measured over a wide range of relative pressures at constant temperature, the result is an adsorption isotherm. Using the adsorption isotherms of small molecules (e.g., N₂), the total surface area, pore volume, pore size and pore size distribution can be determined. All adsorption isotherms can be grouped into 6 principal types [45] and are shown in Figure 2.8. The type of the adsorption isotherm reflects the size and shape of the pores. From type II to IV isotherms, the specific surface area of the adsorbents can be determined by applying the BET method. The BET method is the most widely used procedure for the determination of the specific surface area of porous solid materials and involves the use of the following Equation 2.2 [46].

$$\frac{1}{W((p_0/p)-1)} = \frac{1}{cW_{\text{mon}}} + \frac{(c-1)}{cW_{\text{mon}}} \left(\frac{p}{p_0} \right) \quad (2.2)$$

in which W is the mass of gas adsorbed, W_{mon} is the mass of the gas adsorbed for monolayer coverage of the surface, p_0 is the vapour pressure of the gas, p is the atmospheric pressure and c is proportional to $\exp(-(\Delta H_{\text{ads}} - H_{\text{vap}})/RT)$ in which ΔH_{ads} is the enthalpy of adsorption in the first layer and H_{vap} is the heat of vaporization of adsorbate. The term c , the so-called BET constant, is related to the energy of adsorption in the first adsorbed layer and consequently its value is an indication of the magnitude of the adsorbent/adsorbate interactions.

The mass of the gas adsorbed for monolayer coverage of the surface can be obtained from the slope s and intercept i of the linear region of the BET plot (i.e., a plot of $1/(W((p/p_0)-1))$ vs. p/p_0). The linear plot for the BET equation usually appears in the p/p_0 range of 0.05 to 0.35 when nitrogen is used as adsorbate.

The total surface area of the sample can be expressed as:

$$S_t = \frac{W_m N A_{\text{cs}}}{M} \quad (2.2)$$

Where N is the Avagadro number (6.023×10^{23} molecules/mol), A_{cs} is the molecular cross-sectional area (1.62 nm for nitrogen) and M is the molecular weight of the adsorbate.

The specific surface area S of the solid can be calculated from the total surface area S_t and the sample weight W according to the Equation 2.3.

$$S = S_t/W \quad (2.3)$$

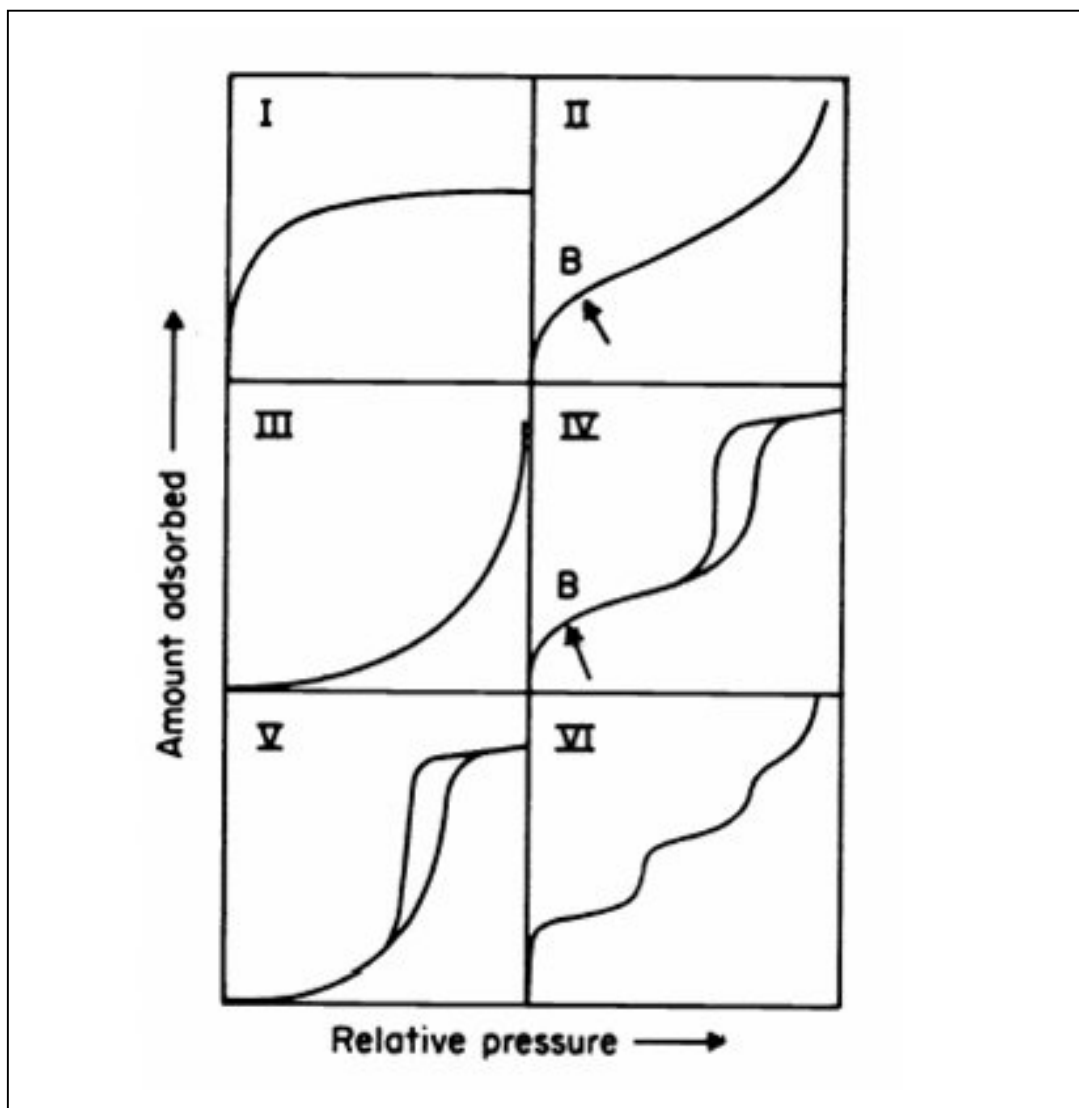


Figure 2.9: Types of adsorption isotherms according to the IUPAC classification

2.2.4 Thermogravimetric and differential thermal analysis (TG-DTA)

Thermogravimetric analysis and differential thermal analysis (TGA/DTA) are typically performed on zeolites in nitrogen or synthetic air environments to determine changes in sample weight and heat flow in dependence of the actual temperature. The commonly investigated processes are determination of water content, decomposition of template and other adsorbed products, desorption etc. The exothermic and endothermic changes in the sample can also be investigated in dependence of the actual temperature and gaseous environment.

2.2.5 Elemental analysis

2.2.5.1 Atomic absorption spectroscopy

Quantitative analysis of elements in a sample can be performed by atomic absorption spectroscopy. The ground state atom absorbs light energy of a specific wavelength as it enters the excited state. As the number of atoms in the light path increases, the amount of light absorbed also increases. The use of specific wavelengths allows the determination of individual elements. By measuring the amount of light absorbed, a quantitative determination of the amount of analyte can be made. These quantitative measurements are based on Beer's law, which states that the concentration of a given species is proportional to the absorbance ($c = kA$, where c is the concentration of a given species, k is a constant and A is the absorbance) and a linear relationship exists between concentration and absorbance at low concentrations.

2.2.5.2 Energy dispersive X-ray analysis (EDAX)

When the surface of the specimen is illuminated by an electron beam, it causes excitation of atoms near the sample surface. The excitation energy stored in the excited atoms is radiated as X-rays, which are characteristic for each element. By analysing the distribution and energy of the emitted X-rays, the content of different elements on the sample surface can be evaluated.

2.3 IR spectroscopic studies of thiophene adsorbed on zeolites.

The relationship between mid-infrared spectral features and structural properties of zeolites are described in a classical paper by Flanigen et al. [47]. As shown in Table 2.1, the bands observed in the mid-infrared region were classified into two main categories, viz. intra-tetrahedral bands (or structure insensitive bands) and inter-tetrahedral bands or structure

sensitive bands. Intra-tetrahedral bands of lattice vibrations are present in all zeolite structures and inter-tetrahedral bands of lattice vibrations occur selectively in some zeolite structures.

The bands observed in the ranges $1250-950\text{ cm}^{-1}$, $790-650\text{ cm}^{-1}$ and $500-420\text{ cm}^{-1}$ are tentatively assigned to the asymmetric stretching mode ($\leftarrow \text{OT} \rightarrow \leftarrow \text{O}$), the symmetric stretching mode ($\leftarrow \text{OTO} \rightarrow$) and the O-T-O bending mode of the $\text{TO}_{4/2}$ tetrahedra, respectively. The bands ranging from $650-500\text{ cm}^{-1}$, $420-300\text{ cm}^{-1}$, $820-750\text{ cm}^{-1}$ and $1150-1050\text{ cm}^{-1}$ were assigned to structure sensitive bands. Some of the bands in the range from 3500 cm^{-1} to 3800 cm^{-1} disappear during the activation of zeolites. These bands are assigned to the stretching vibration of hydroxyl groups. During activation, due to dehydration at above $300\text{ }^\circ\text{C}$, zeolite framework loses these hydroxyl groups whose vibrational bands and their assignments are summarized in Table 2.2.

Table 2.1: Assignments of zeolite lattice vibrations.

Tentative assignment	Wavenumber / cm^{-1}
Intra-tetrahedral bands (structure insensitive)	
Asymmetric stretch ($\leftarrow \text{OT} \rightarrow \leftarrow \text{O}$)	1250 - 950
Symmetric stretch ($\leftarrow \text{OTO} \rightarrow$)	720 - 650
O-T-O bending	500 - 420
Inter-tetrahedral bands (structure sensitive)	
Double ring	650 - 500
Pore opening	420 - 300
Symmetric stretch	820 - 750
Asymmetric stretch	1150 - 1050

Tentative assignment	Wavenumber / cm^{-1}
----------------------	-------------------------------

$\nu(\text{OH})$ of isolated Si-OH	3740
$\nu(\text{OH})$ of Al-OH	3680
$\nu(\text{OH})$ of hydroxyl groups in supercages	3640
$\nu(\text{OH})$ of hydroxyl groups in sodalite cages	3550

Table 2.2: Overview over bands observed during dehydration of metal-ion exchanged Y-type zeolite and their assignments.

Shifts in the characteristic vibrational wavenumbers of thiophene adsorbed on zeolites and of the zeolite framework when exposed to IR radiation are of great importance to characterize the type of interaction.

Table 2.3: Assignment of vibrational modes for thiophene vapour.

Tentative assignment	$\text{C}_4\text{H}_4\text{S}(\text{g})$ (band wavenumber / cm^{-1})
$\nu\text{CH}(\alpha)$	3126
$\nu\text{CH}(\beta)$	3098
$\nu(\text{C}=\text{C})_{\text{asym}}$	1507
$\nu(\text{C}=\text{C})_{\text{sym}}$	1409
$\nu(\text{ring})$	1360
$\nu(\text{ring})$	1256
$\delta(\text{CH})_{\text{asym}}$	1085
$\delta(\text{CH})_{\text{sym}}$	1083
$\nu(\text{ring})$	1036

(ν - stretching vibration; δ – in-plane bending vibration; α - α position; β - β position, asym. – asymmetric; sym.- symmetric)

The near-infrared region from 4000 cm⁻¹ to 400 cm⁻¹ is used to investigate the interaction of thiophene with metal species. The thorough understanding of all vibrations of the system can help in understanding the chemistry of adsorption. Some important vibration modes of thiophene are described in Table 2.3 [48, 49]. This information could be helpful to develop adsorbents with higher selectivities. An ideal adsorbent is believed to be one which removes sulphur-containing organic compounds by interacting with the S-atom. In this way, the competitive adsorption by other hydrocarbons (which do not contain an S atom), could be minimized.

2.4 UV-Vis spectroscopy

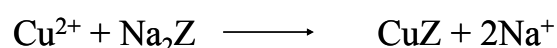
UV-Vis spectroscopy is most widely used in the determination of transition metal ions and oligomerized organic compounds in solutions and solid mixtures. It works on the principle of electronic transitions taking place in a molecule encountered with visible and ultraviolet light. The analysis of species absorbing UV or visible light is made based on the Beer-Lambert law:

$$A = -\log_{10} (I/I_0) \quad (2.4)$$

where A is the measured absorbance, I₀ is the intensity of the incident light at a given wavelength and I is the transmitted intensity.

2.5 Post-synthesis modification of FAU zeolites by ion-exchange

Ion-exchange operations are chemical reactions between an electrolyte in solution and an insoluble electrolyte with which the solution is contacted. As discussed earlier zeolites have an intrinsic ability to exchange cations (section 2.1). This is typically performed on the sodium form of zeolites suspended in dilute aqueous solutions of the cations to be exchanged as shown:



The objective of an ion-exchange is to change the surface properties of a solid by replacing the cations present in the as-synthesized form with the cations needed for the adsorption of the targeted compounds. The ion-exchange procedure used was the conventional liquid-phase ion-exchange.

The acid form of zeolites can be made by preparing ammonia form of zeolite and then calcinating it to release ammonia. The remaining proton is attached to the oxygen atom connected to neighbouring silicon and aluminium atoms, resulting in the so-called Brønsted acidity of zeolites. Theoretically, one proton should be introduced for each framework Al^{3+} and therefore the larger the number of framework aluminium atoms, the higher the number of acid sites would be in a given zeolite structure.

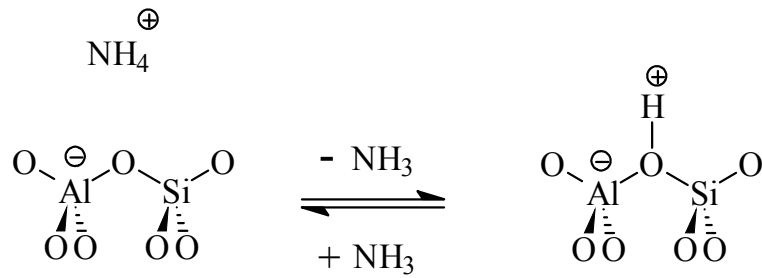


Figure 2.10: Schematic representation of the formation of Brønsted-acid sites in zeolite.

3 Experimental section

3.1 Materials

The characteristic data of the adsorbents applied in this work are summarized in Table 3.1.

Table 3.1: Characteristic data of the applied adsorbents.

No.	Adsorbent	n_{Si}/n_{Al}	Specific surface area (m ² /g)	Specific pore volume (cm ³ /g)	Water content (%)	Degree of ion-exchange (%)
1	H-ZSM-5	13	300	0.12	8.2	-
2	H-ZSM-5	19	401	0.18	6.3	-
3	H-ZSM-5	36	434	0.19	5.2	-
4	Silicalite-1	1280	284	0.12	0.6	-
5	H-MCM-22	20	593	0.24	7	-
6	H-MOR	5	422	0.17	12.8	-
7	Na ⁺ -Y	2.4	870	0.35	23	-
8	H ⁺ -Y	2.5	762	0.31	12.9	-
9	Cu ²⁺ -Y	2.5	698	0.28	24	92
10	Ni ²⁺ -Y	2.3	620	0.25	26	65
11	Ag ⁺ -Y	2.5	642	0.26	18.8	58
12	Ce ³⁺ -Y	2.4	700	0.28	21	99
13	La ³⁺ -Y	2.7	600	0.24	20	98
14	Y ³⁺ -Y	2.5	601	0.23	19	90

The chemicals used in this work for the synthesis and modification of zeolites are summarized in Table 3.2.

Table 3.2: Chemicals used and their suppliers.

Chemical	Supplier
Cab-osil M-5 (SiO ₂)	Riedel-de Haën
Tetrapropyl ammonium bromide	Alfa Aesar GmbH
Sodium aluminate	Riedel-de Haën
Ammonium nitrate	Merck
Aluminium nitrate nonahydrate	Merck
Ludox AS-40 (colloidal silica, 40 wt.-% suspension in water)	Sigma Aldrich
Ludox AM-30 (colloidal silica, 30 wt.-% suspension in water)	Sigma Aldrich
Ludox AS-30 (colloidal silica, 30 wt.-% suspension in water)	Sigma Aldrich
Hexamethyleneimine	Fluka
Aluminium(III) sulphate octadecahydrate	Riedal-de Haën
Silver(I) chloride	Fluka
Nickel(II) acetate tetrahydrate	Fluka
Copper(II) chloride	Riedal-de Haën
Cerium(III) acetate hydrate	Aldrich
Lanthanum(III) nitrate hexahydrate	Chempur
Yttrium(III) nitrate hexahydrate	Riedal-de Haën
Thiophene	Fluka
Benzothiophene	Fluka
Dibenzothiophene	Fluka
4,6-Dimethyl dibenzothiophene	Aldrich
Toluene	Merck
<i>n</i> -Heptane	Merck

The commercial zeolites applied in this work are summarised in Table 3.3.

Table 3.3: Commercial zeolites and their suppliers.

Zeolite	Supplier
LZ-Y54 (Na ⁺ -Y, $n_{Si}/n_{Al} = 4$)	UOP
LZ-M5 (MOR, $n_{Si}/n_{Al} = 5$)	UOP
SH-27 (H-ZSM-5, $n_{Si}/n_{Al} = 13$)	Süd-Chemie

3.2 Characterization of the adsorbents

3.2.1 Powder X-ray diffraction

Powder X-ray diffractograms were recorded on a Siemens D5005 X-ray diffractometer operated at 40 kV and 30 mA using monochromatic CuK α -radiation ($\lambda_{CuK\alpha} = 0.15405$ nm). The diffraction experiments were conducted at 2θ values from 3° to 50° with steps of 0.01°. The acquisition time was set to 10 seconds per step.

3.2.2 Scanning electron microscopy

Scanning electron micrographs were recorded using an analytical scanning electron microscope of the type JEOL JSM-6490LA equipped with a tungsten cathode. Prior to taking the micrographs, all samples were sputtered with gold using a JEOL JFC-1200 fine coater. Gold sputtering increases the conductivity of the samples and therefore a better resolution can be obtained.

3.2.3 Nitrogen adsorption

Nitrogen adsorption and desorption isotherms were recorded on a Quantachrome Autosorb 1 instrument at -196 °C. Before recording the isotherms, the samples were degassed at 250 °C for at least 5 hrs. The surface area of the zeolites was determined by using the BET equation as addressed in section 2.2.3.

3.2.4 Thermogravimetric and differential thermal analysis

Thermogravimetric and differential thermal analysis (TG-DTA) measurements with all samples were done on a SETARAM Setsys 16/MS instrument. The water content was determined by heating the sample in a flow of nitrogen from 20 °C to 550 °C with a temperature program of 5 °C/min and then cooling down to 20 °C. The regeneration of the adsorbents was also studied using TG-DTA analysis. For this purpose, the loaded acidic zeolites adsorbents were heated with the temperature program mentioned above in a flow of nitrogen and the desorbed products were determined by mass spectrometry. To observe the regeneration behaviour of metal-ion exchanged zeolites, they were heated from 20 °C to 500 °C with a temperature program of 5 °C/min while recording the loss in weight and heat flow.

3.2.5 Elemental analysis

Elemental analysis of the adsorbents was done by two methods: atomic absorption spectroscopy (AAS-300 from perkin elmer) and EDX analysis using a JEOL EX-54165 JMC module attached to the scanning electron microscope.

3.2.5.1 Atomic absorption spectroscopy

The contents of the elements silicon, aluminium, copper, nickel and silver were determined using atomic absorption spectroscopy. Samples of about 20 mg were dissolved with ca. 1 ml of 40 % hydrofluoric acid in a 50 ml polypropylene bottle and diluted with distilled water. The elements were analysed with a atomic absorption spectrometer type AAnalyst 300 from Perkin-Elmer using the conditions given in Table 3.4.

3.2.5.2 EDAX

Elemental analysis using EDAX was performed with a JEOL EX-54165 JMC module attached to the scanning electron microscope (JEOL JSM-6490LA) at a voltage of 70 kV.

Table 3.4: Standard conditions used for elemental analysis via atomic absorption spectroscopy.

Element	Flame gas	Wave length / nm	Slit size / nm
Si	Nitrous oxide/Acetylene	251.6	0.2
Al	Nitrous oxide/Acetylene	309.3	0.7
Cu	Air/Acetylene	324.8	0.7
Ni	Air/Acetylene	232.0	0.2
Ag (Emission)	Nitrous oxide/Acetylene	328.1	0.7

3.3 UV-Vis spectroscopy

UV-Vis spectroscopy was performed on a Perkin-Elmer Lambda 18 spectrometer equipped with an accessory (RSA-PE-19M) designed for diffuse reflectance measurements of powder or rough surface samples. Detection wavelengths from 300 to 900 nm were used.

3.4 Infrared spectroscopy

Infrared spectra of the zeolites were measured by the diffuse reflectance technique on a Nicolet-Nexus FT-IR Spectrometer. This spectrometer is equipped with a high temperature and pressure cell (SpectraTech) containing a ZnSe crystal window. This allows to measure the IR spectra of samples between 4000 cm^{-1} and 700 cm^{-1} . The sample was placed as a thick layer (ca. 5 mm) and the spectrum was collected after performing 220 scans with a resolution of 4 cm^{-1} .

As a background correction, the spectrum of dried KBr was used. Prior to the measurement, the adsorbent mixed with KBr was activated in-situ at $400\text{ }^{\circ}\text{C}$ under a nitrogen flow for 1 hour to remove water adsorbed on the zeolite surface. The adsorbent was brought to $20\text{ }^{\circ}\text{C}$ and the IR spectrum was collected. Thiophene vapours are admitted into the cell by N_2 stream with 20 ml/min via a saturator maintained at $20\text{ }^{\circ}\text{C}$ and filled with thiophene ($p_{\text{Thiophene}} = 0.81\text{ kPa}$). After admitting thiophene vapours for 30 min, the unadsorbed thiophene was flushed out in a nitrogen flow ($\dot{V}_{\text{N}_2} = 20\text{ ml/min}$) for 1 hour and the IR spectrum was collected.

3.5 Applied zeolites

The X-ray diffraction patterns and scanning electron micrographs of the applied zeolites are shown in Figures 3.1 to 3.28. The similarity was observed in the X-ray diffraction pattern of the ion-exchanged Na^+ -Y zeolites to the parent Na^+ -Y zeolite. This indicates that the original zeolite structure was retained after ion-exchange and heat treatment. From the morphology of the crystals shown by scanning electron micrographs, it can be confirmed that the ion-exchange procedure will not alter the original form of the zeolite crystals.

3.5.1 H-ZSM-5 ($n_{\text{Si}}/n_{\text{Al}} = 13$)

This material was a commercial sample from Süd-Chemie (designated as SH-27).

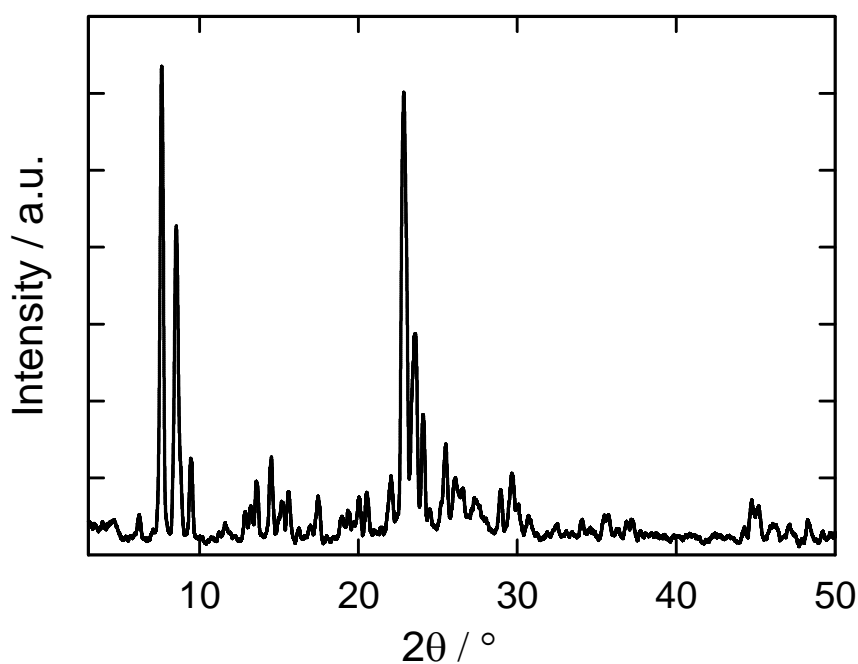


Figure 3.1: Powder X-ray diffraction pattern of zeolite H-ZSM-5 ($n_{\text{Si}}/n_{\text{Al}} = 13$).

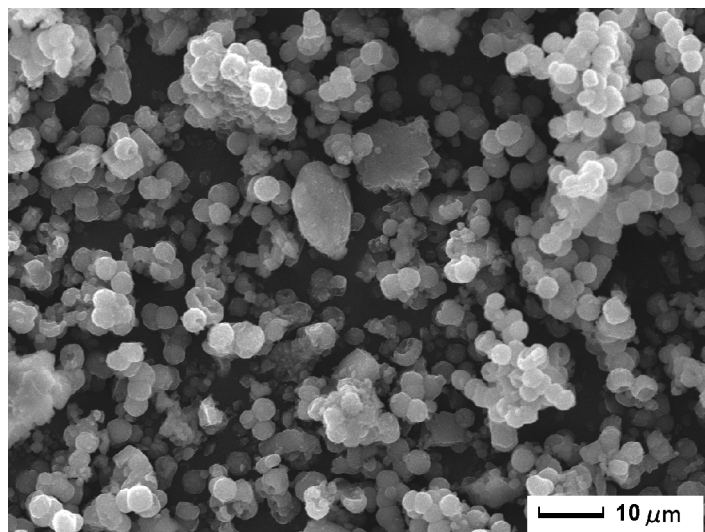


Figure 3.2: Scanning electron micrograph of zeolite H-ZSM-5 ($n_{\text{Si}}/n_{\text{Al}} = 13$).

3.5.2 H-ZSM-5 ($n_{\text{Si}}/n_{\text{Al}} = 20$)

The zeolite Na-ZSM-5 with $n_{\text{Si}}/n_{\text{Al}} = 20$ was synthesized according to the procedure described in [50]. Cab-osil M-5 (13.26 g) and sodium hydroxide (1.91 g) dissolved in water (38.5 ml) were added to a solution of tetrapropyl ammonium bromide (3.001 g) dissolved in water (94 ml) under stirring. Then, a solution of NaAlO_2 (1.016 g) in water (12 ml) was added. The pH value was brought to 11 with concentrated sulphuric acid under stirring. The resulting mixture was crystallized in a stainless steel autoclave at 180 °C for 3 days under rotation. The product was filtered and washed thoroughly with distilled water. The product was then dried at 100 °C for 24 hours and afterwards calcined at 540 °C for 24 hours. The calcined product was pulverized in an agate mortar.

To obtain NH_4 -ZSM-5 from Na-ZSM-5, 2 g of Na-ZSM-5 were stirred in 500 ml of an aqueous solution containing 1 g of $\text{NH}_4\text{NO}_3 \cdot 9 \text{H}_2\text{O}$ at 80 °C. After stirring for 8 hours, the solid material was recovered by filtration, washed thoroughly with ca. 1 litre of water and dried at 100 °C. This ion-exchange procedure was repeated for three times along with drying in between. The obtained NH_4 -ZSM-5 was calcined in air at 450 °C to convert it to H-ZSM-5.

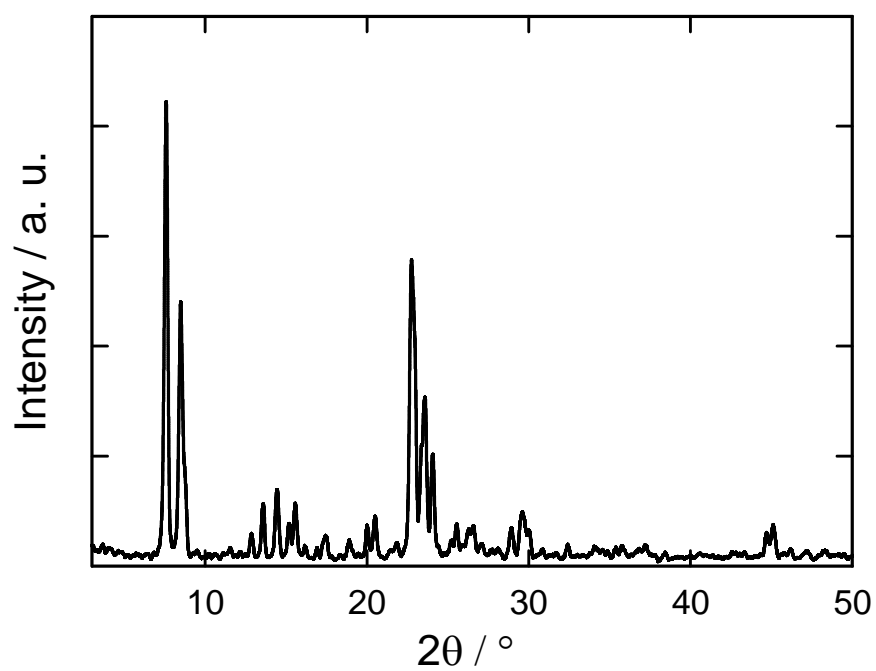


Figure 3.3: Powder X-ray diffraction pattern of zeolite H-ZSM-5 ($n_{\text{Si}}/n_{\text{Al}} = 20$).

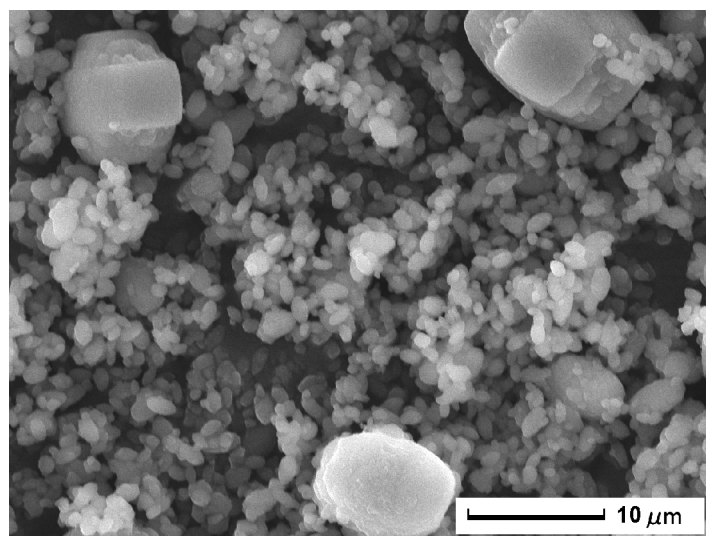


Figure 3.4: Scanning electron micrograph of zeolite H-ZSM-5 ($n_{\text{Si}}/n_{\text{Al}} = 20$).

3.5.3 H-ZSM-5 ($n_{\text{Si}}/n_{\text{Al}} = 40$)

The synthesis of H-ZSM-5 ($n_{\text{Si}}/n_{\text{Al}} = 40$) was performed as described in the literature [51]: $\text{Al}(\text{NO}_3)_3 \cdot 9\text{H}_2\text{O}$ (2.0 g) and tetrapropyl ammonium bromide (4.6 g) were dissolved in water (32 ml). Then, Ludox AS-40 (32 g) and ammonium hydroxide solution (43.6 ml, 25%) were added to the above aqueous solution. The product was crystallised in a stainless autoclave at 180 °C for 5 days under rotation. The mixture was filtered and washed thoroughly with distilled water. The solid was then dried at 100 °C for 24 hours and calcined in air at 540 °C for 24 hours. The calcinated product was pulverized in an agate mortar.

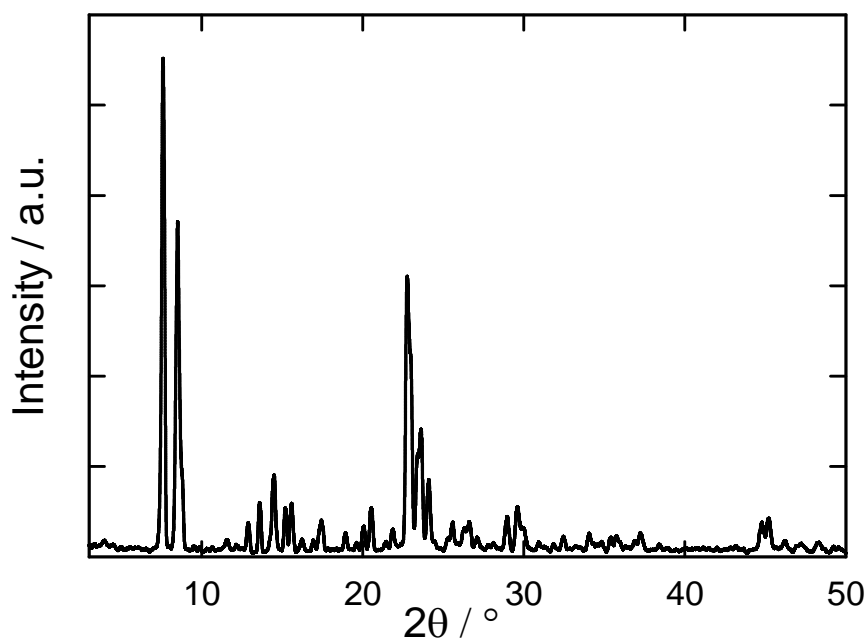


Figure 3.5: Powder X-ray diffraction pattern of zeolite H-ZSM-5 ($n_{\text{Si}}/n_{\text{Al}} = 40$).

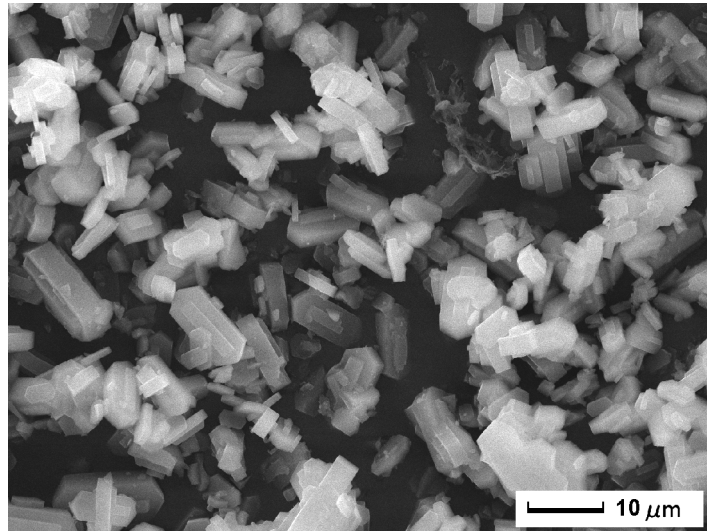


Figure 3.6: Scanning electron micrograph of zeolite H-ZSM-5 ($n_{\text{Si}}/n_{\text{Al}} = 40$).

3.5.4 Silicalite-1

Silicalite-1 was synthesized according to the procedure described in the literature [52]. Ludox AS-30 (333 g; 30 % SiO_2 in water) and ammonium hydroxide solution (340 ml, 25 %) were added to a solution of tetrapropyl ammonium bromide (4.6 g) in water (167 g) under stirring. The resulting mixture was crystallized in a stainless steel autoclave at 180 °C for 36 hours under rotation. The mixture was filtered and washed thoroughly with distilled water. The solid was dried at 100 °C for 24 hours and calcined at 540 °C in air for 24 hours. The calcined product was pulverized in an agate mortar.

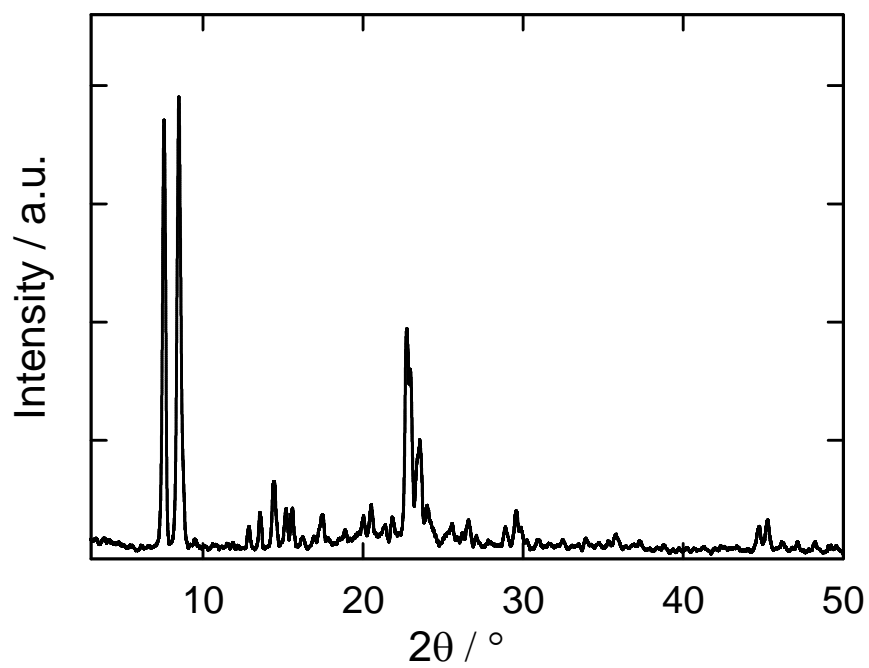


Figure 3.7: Powder X-ray diffraction pattern of zeolite Silicalite-1.

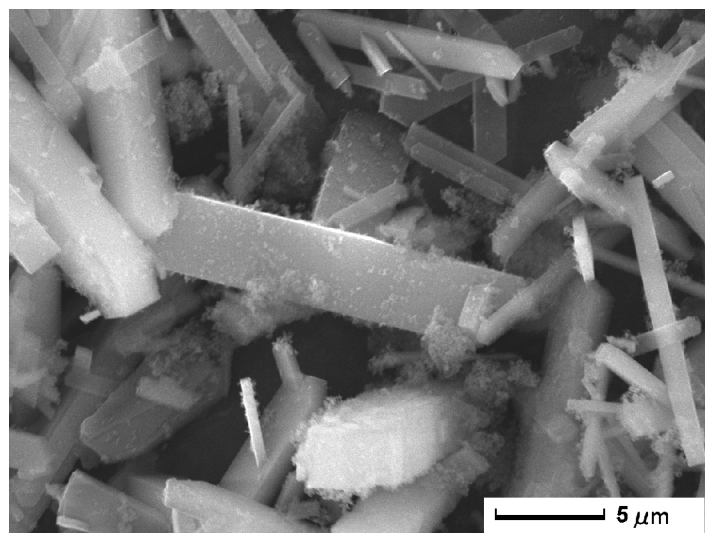


Figure 3.8: Scanning electron micrograph of zeolite Silicalite-1.

3.5.5 H-MCM-22

The synthesis of MCM-22 was achieved by following the procedure described in the literature [53]. In a solution of 6.0 g of sodium hydroxide, 12.4 g of hexamethyleneimine and 60.5 g of water, 50.7 g of Ludox AM-30 (30 wt.-% SiO₂) was dissolved. The obtained solution was then dissolved in a solution containing 3.5 g aluminiumsulphate octadecahydrate and 87.5 g of water. At the end, 4.5 g of sulphuric acid (96 wt.-%) was added drop wise under vigorous stirring. The product was crystallized in an autoclave after rotating for 4 days at 150 °C. The product was filtered, washed with distilled water and dried at 100 °C.

2 g of the above obtained Na-MCM-22 were ion-exchanged with 1 g of ammonium nitrate nonahydrate at 80 °C for 8 hours. After ion-exchange, the product was recovered by filtration, washed thoroughly with distilled water and dried at 100 °C. This ion-exchange procedure was repeated for 3 times including washing and drying. Finally, the product was calcined in air at 450 °C to obtain H-MCM-22.

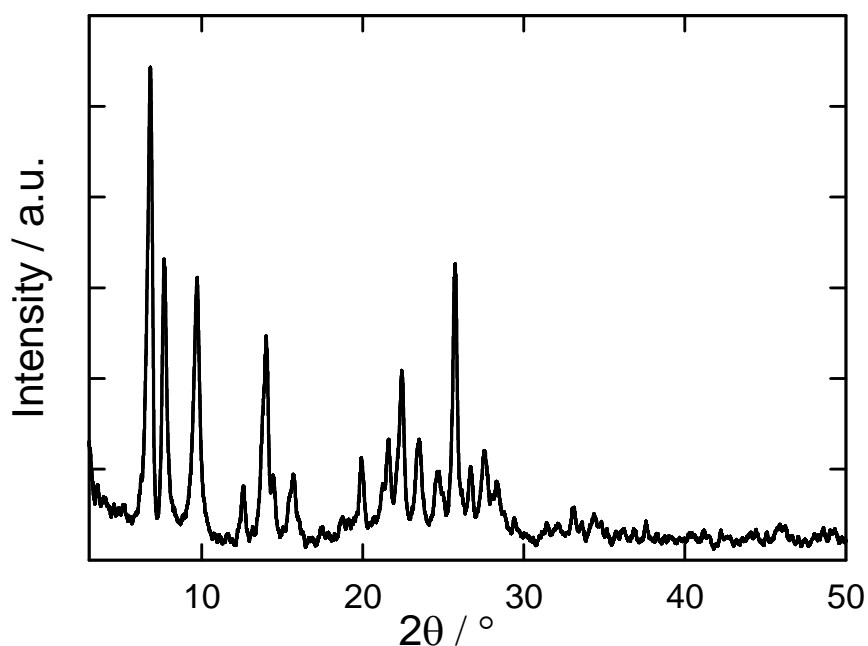


Figure 3.9: Powder X-ray diffraction pattern of zeolite H-MCM-22.

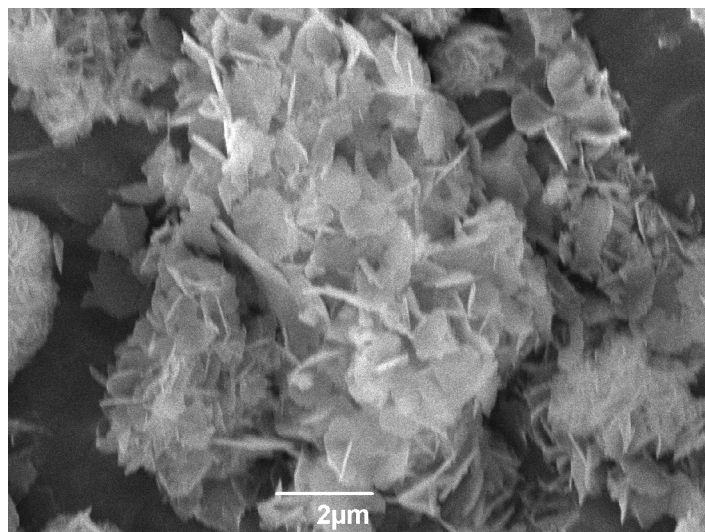


Figure 3.10: Scanning electron micrograph of zeolite H-MCM-22.

3.5.6 H-MOR

Zeolite Na-MOR was obtained from UOP, the commercial name of this product is LZ-M5. The ammonium form of mordenite, i.e. $\text{NH}_4\text{-MOR}$, was generated by stirring 2 g of Na-MOR in 500 ml of an aqueous solution containing 1 g of $\text{NH}_4\text{NO}_3 \cdot 9 \text{H}_2\text{O}$ at 80 °C. After stirring for 8 hours, the solid material was recovered by filtration, washed thoroughly with ca. 1 litre of water and dried at 100 °C. This ion-exchange procedure was repeated for three times along with drying. The obtained $\text{NH}_4\text{-MOR}$ was calcined in air at 450 °C to convert it to H-MOR.

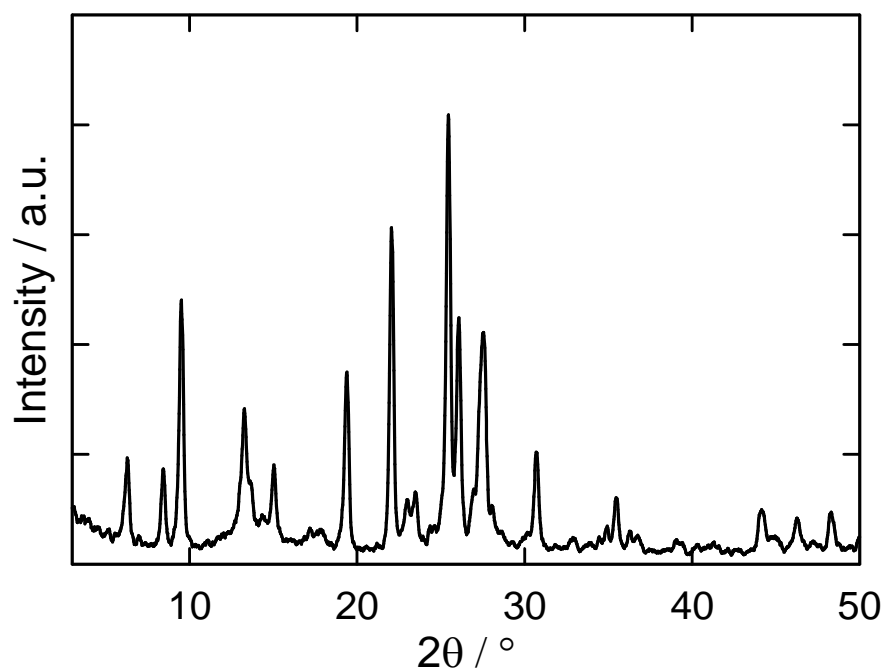


Figure 3.11: Powder X-ray diffraction pattern of zeolite H-MOR.

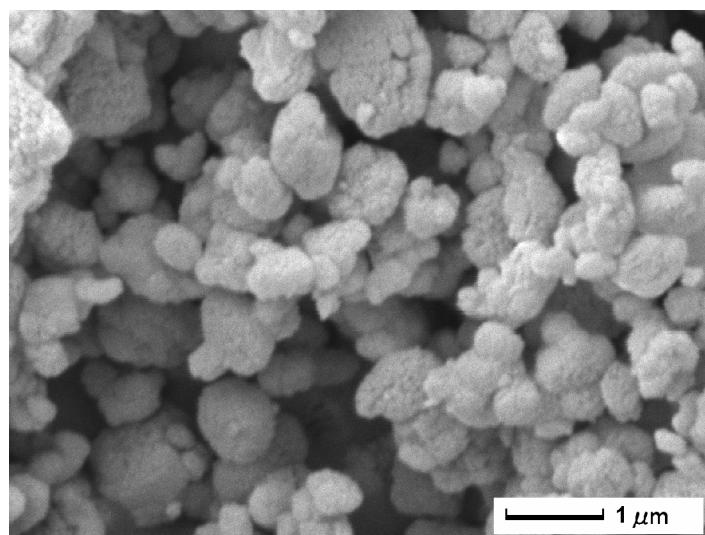


Figure 3.12: Scanning electron micrograph of zeolite H-MOR.

3.5.7 Na⁺-Y

In this work, a Na⁺-Y zeolite with a silicon to aluminium ratio of 2.43 from Union Carbide was used.

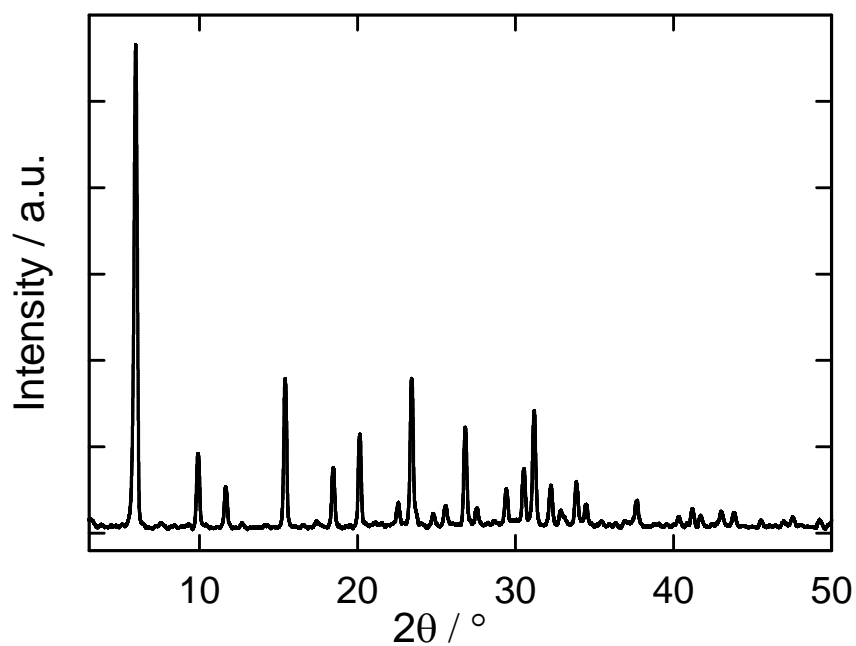


Figure 3.13: Powder X-ray diffraction pattern of zeolite Na⁺-Y.

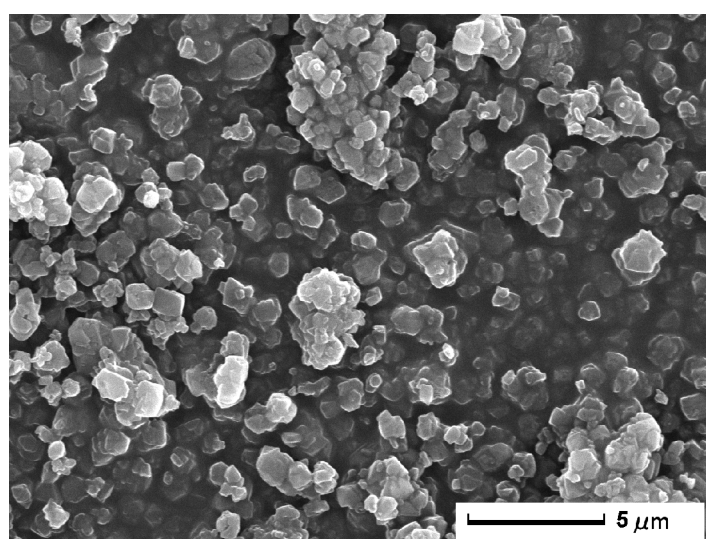


Figure 3.14: Scanning electron micrograph of zeolite Na⁺-Y.

3.5.8 H⁺-Y

2 g of zeolite Na⁺-Y was ion-exchanged with 1 g NH₄NO₃ · 9 H₂O dissolved in 500 ml of water at 80 °C to obtain the corresponding NH₄⁺-form. The solid was recovered by filtration and washed thoroughly with ca. 1 litre of distilled water to remove excess ammonium nitrate.

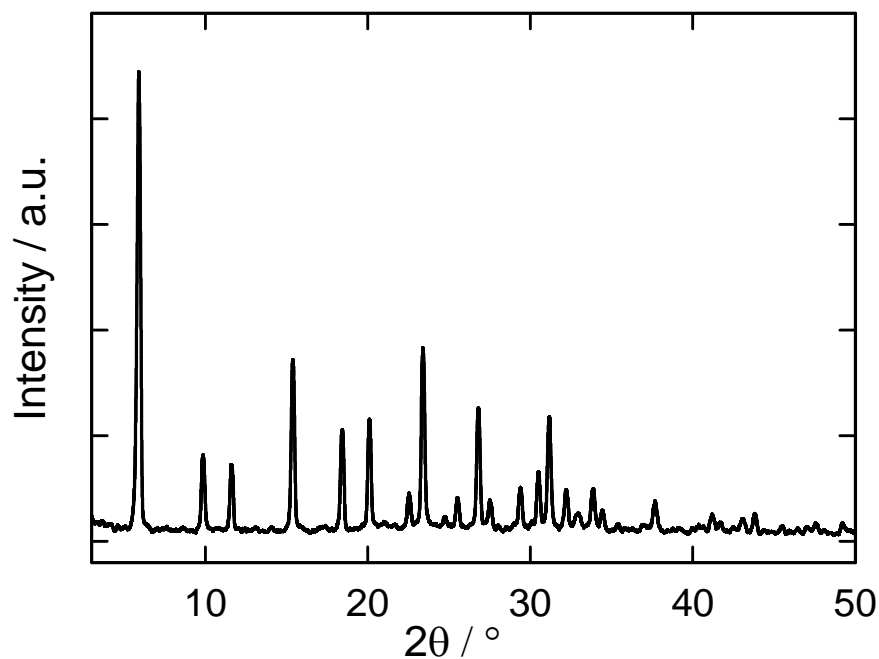


Figure 3.15: Powder X-ray diffraction pattern of zeolite H⁺-Y.

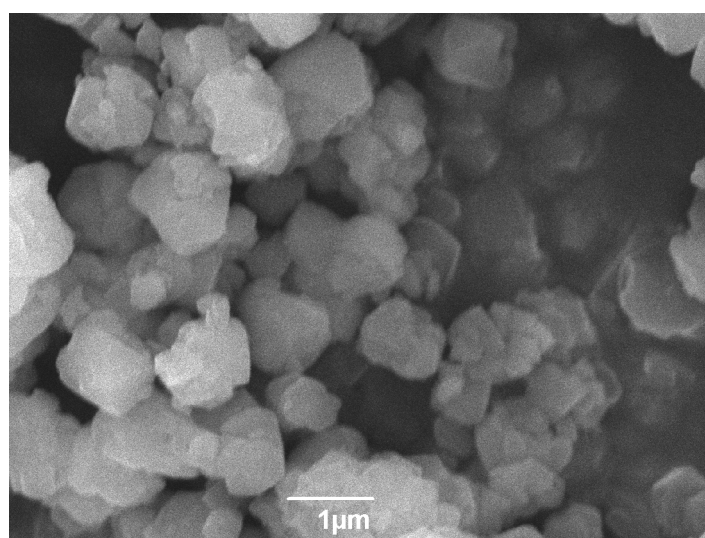


Figure 3.16: Scanning electron micrograph of zeolite H⁺-Y.

Then the sample was dried overnight at 100 °C. This procedure was repeated for 3 times including filtering, washing and drying to obtain a high degree of ion-exchange. NH_4^+ -Y was then calcined in air at 450 °C to prepare acid form of zeolite Y (H^+ -Y).

3.5.9 Ag^+ -exchanged Na^+ -Y

Ag^+ -Y zeolite was prepared by ion-exchange of Na^+ -Y with 500 ml of aqueous solution containing 1 g of AgCl . The ion-exchange was done at room temperature in the absence of light. This ion-exchange procedure was repeated for 3 times to obtain a maximum degree of exchange. After each ion-exchange procedure, the material was recovered by filtration, washed thoroughly with ca. 1 litre of water and dried at 100 °C.

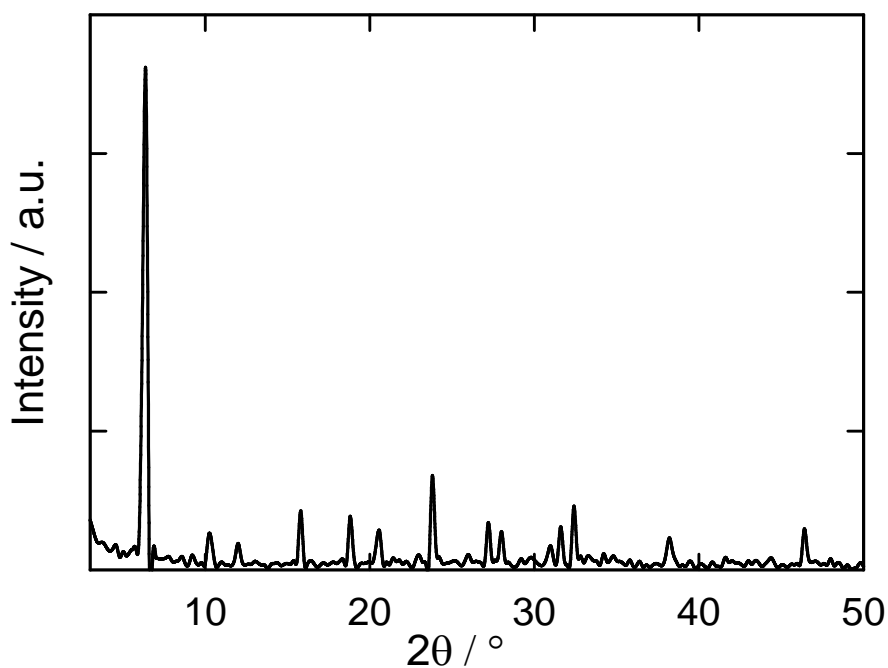


Figure 3.17: Powder X-ray diffraction pattern of zeolite Ag^+ -Y.

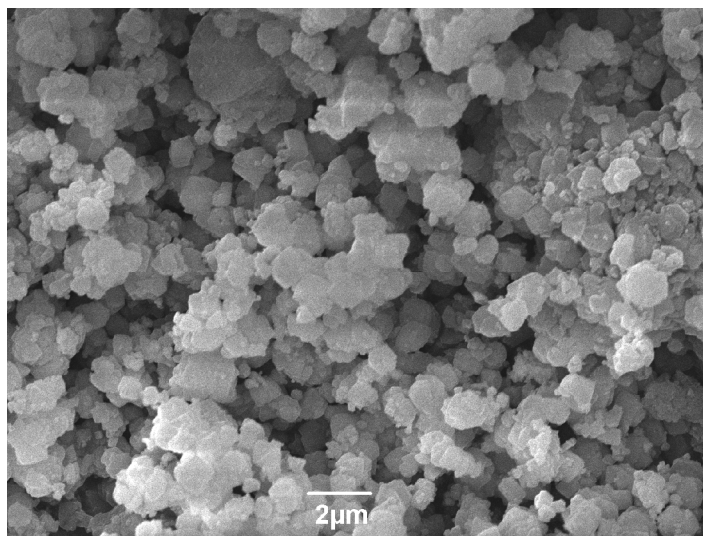


Figure 3.18: Scanning electron micrograph of zeolite Ag^+ -Y.

3.5.10 Ni^{2+} -exchanged Na-Y

Ni^{2+} -Y was prepared by ion-exchange of Na^+ -Y (2 g) at 80 °C with an aqueous solution of nickel (II) acetate tetrahydrate (1 g) dissolved in 500 ml of water. The product was recovered by filtration, washed thoroughly with ca. 1 litre of water and dried at 100 °C. The ion-exchange procedure was repeated for 3 times. After each ion-exchange step, the product was recovered by filtration, washed thoroughly and dried for 12 hours before proceeding to another ion-exchange step.

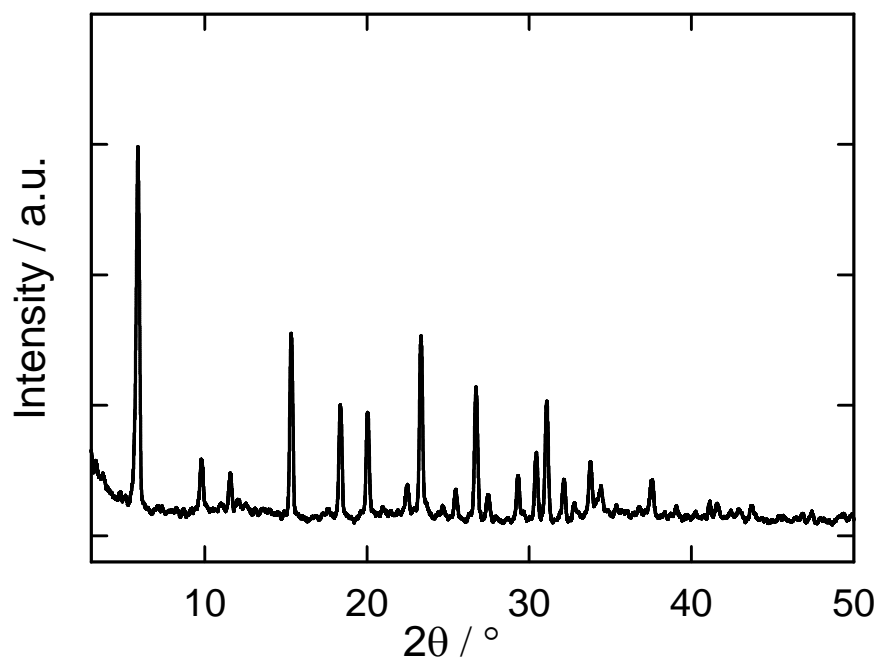


Figure 3.19: Powder X-ray diffraction pattern of zeolite Ni^{2+} -Y.

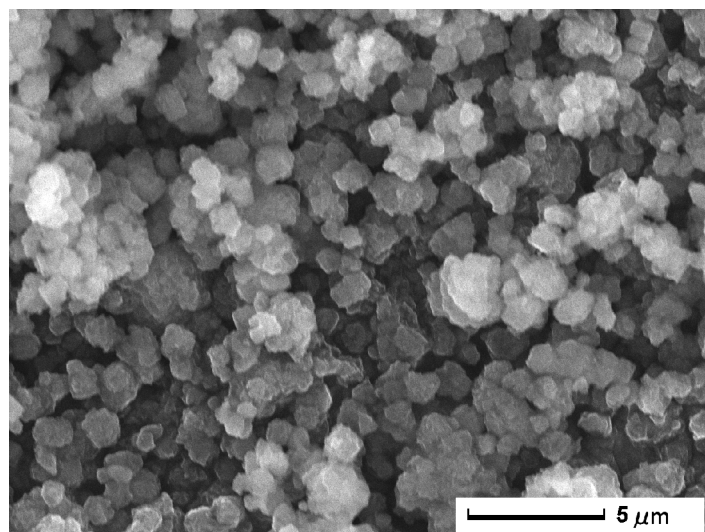


Figure 3.20: Scanning electron micrograph of zeolite Ni^{2+} -Y.

3.5.11 Cu^{2+} -exchanged Na^+ -Y

Cu^{2+} -Y was prepared by ion-exchanging Na^+ -Y at room temperature with an aqueous solution of CuCl_2 . Degree of ion-exchange of 20 % was obtained by ion-exchanging 2 g of Na-Y with 0.3 g of CuCl_2 dissolved in 500 ml of distilled water. Similarly, ion-exchange degrees of 46 and 72 % were obtained with 0.1 and 0.3 g of CuCl_2 in 500 ml distilled water, respectively. Ion exchange degrees of 82 and 92 % were obtained by ion-exchanging 0.662 g of CuCl_2 with 2 g of zeolite twice and thrice, respectively. While repeating the ion-exchange steps, the product was filtered, washed thoroughly and dried at 100 °C for at least 12 hours. Figures 3.21 and 3.22 show the powder XRD pattern and the scanning electron micrograph of zeolite Cu^{2+} -Y with 92 % degree of ion-exchange, respectively.

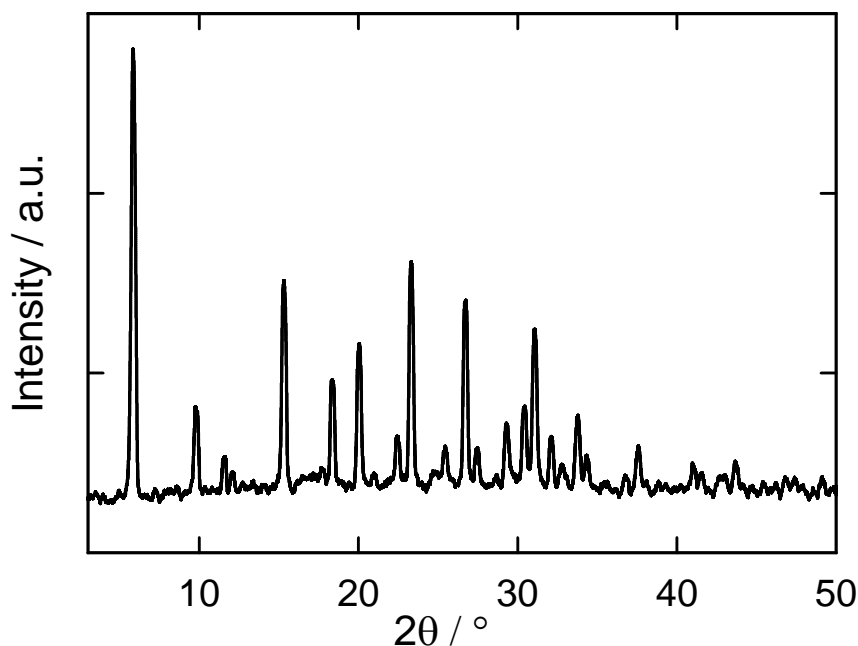


Figure 3.21: Powder X-ray diffraction pattern of zeolite Cu^{2+} -Y.

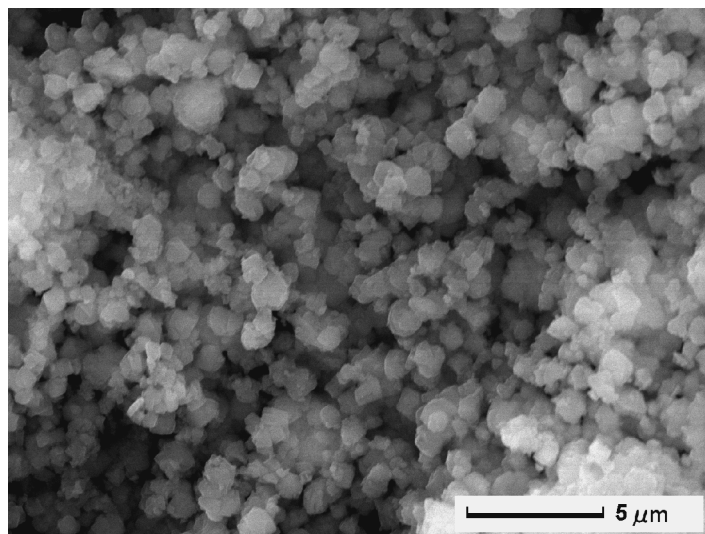


Figure 3.22: Scanning electron micrograph of zeolite Cu^{2+} -Y.

3.5.12 Ce^{3+} - and Ce^{4+} - exchanged Na^{+} -Y

Ce^{3+} -Y was prepared by ion-exchanging 2 g of Na-Y with 1 g of cerium(III) acetate hydrate salt dissolved in 500 ml of distilled water at room temperature.

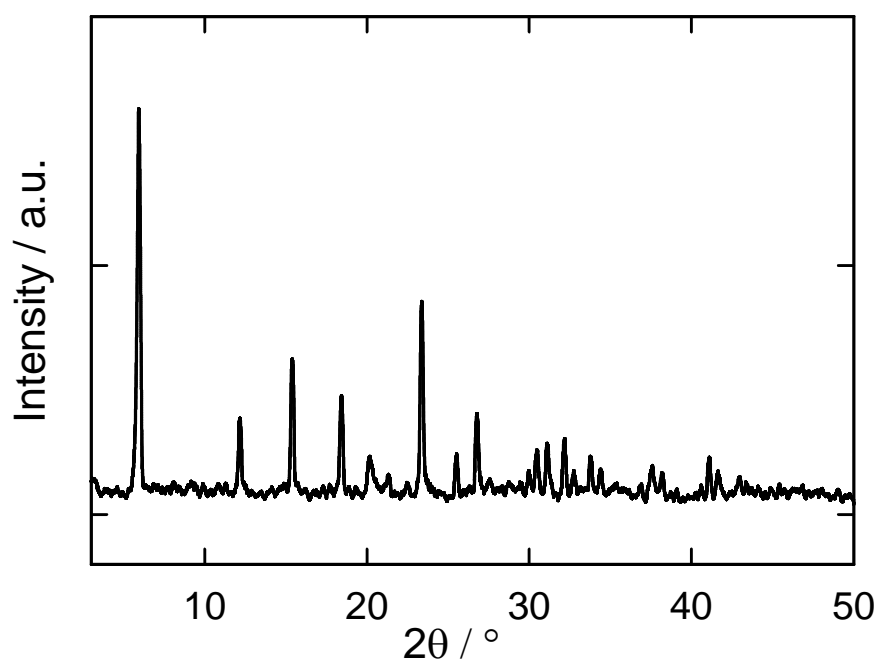


Figure 3.23: Powder X-ray diffraction pattern of zeolite Ce^{3+} -Y.

The ion-exchange was repeated for three times, the product was recovered by filtration, washed thoroughly with water and dried at 100 °C after each ion-exchange step. Ce^{3+} -Y was oxidized to Ce^{4+} -Y by heating Ce^{3+} -Y in the presence of air at 400 °C. The oxidation was also indicated by the change of colour of the sample from white to yellow.

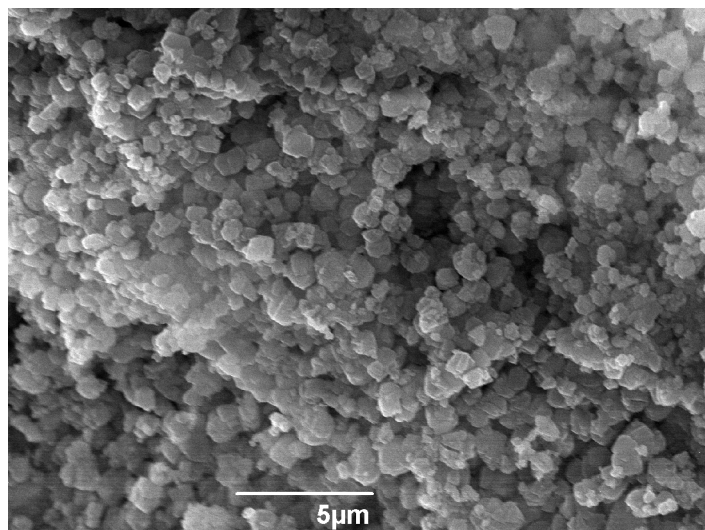


Figure 3.24: Scanning electron micrograph of zeolite Ce^{3+} -Y.

3.5.13 La^{3+} -exchanged Na^{+} -Y

Preparation of La^{3+} -Y by conventional liquid ion-exchange was done by stirring 2 g of zeolite Na^{+} -Y (LZ-Y 54 obtained from Union Carbide) and 1 g of $\text{La}(\text{NO}_3)_3 \cdot 6 \text{H}_2\text{O}$ in 500 ml of distilled water at room temperature. The ion-exchange procedure was repeated for 3 times and the product was subsequently recovered by filtration after washing with water. Before proceeding to the next ion-exchange step, the product was dried at 100 °C.

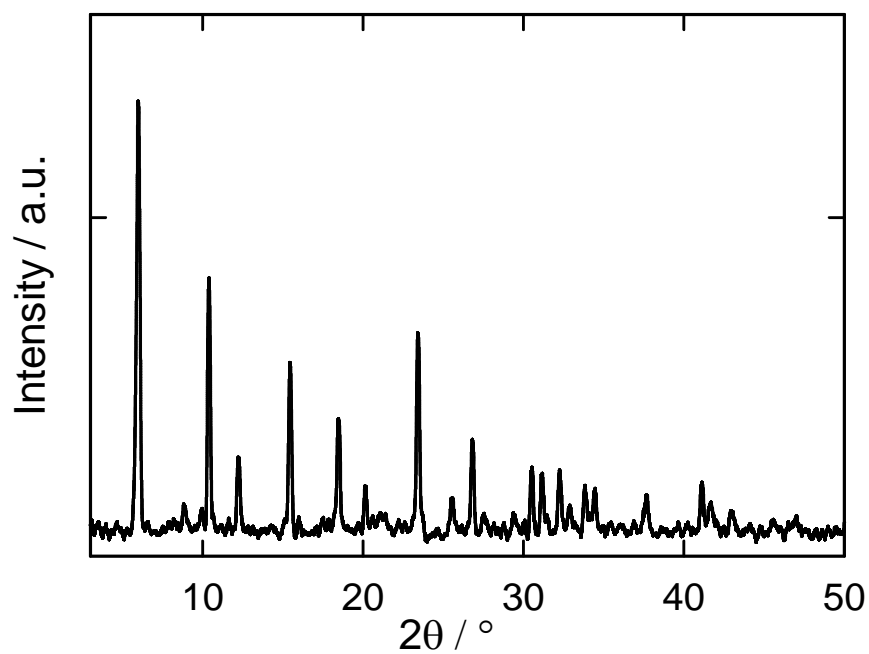


Figure 3.25: Powder X-ray diffraction pattern of zeolite La³⁺-Y.

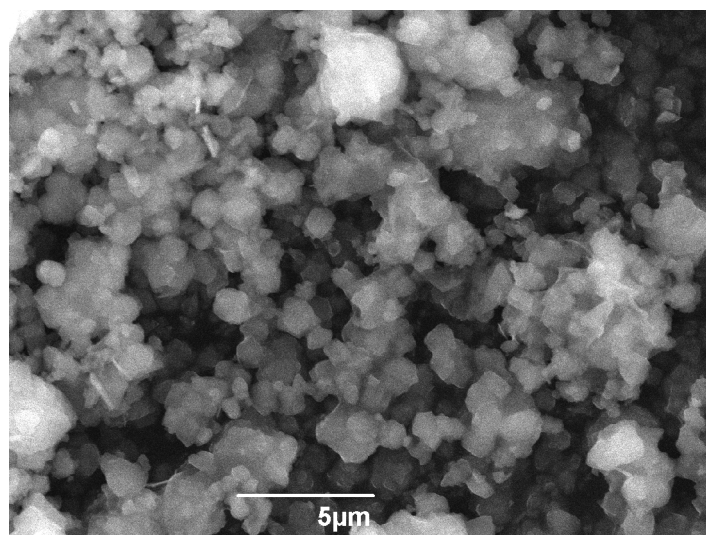


Figure 3.26: Scanning electron micrograph of zeolite La³⁺-Y.

3.5.14 Y^{3+} -exchanged Na^+ -Y

Zeolite Y^{3+} -Y was prepared by exchanging 2 g of Na-Y with 1 g of yttrium(III) nitrate hexahydrate (99.9 %) in 500 ml of water at room temperature.

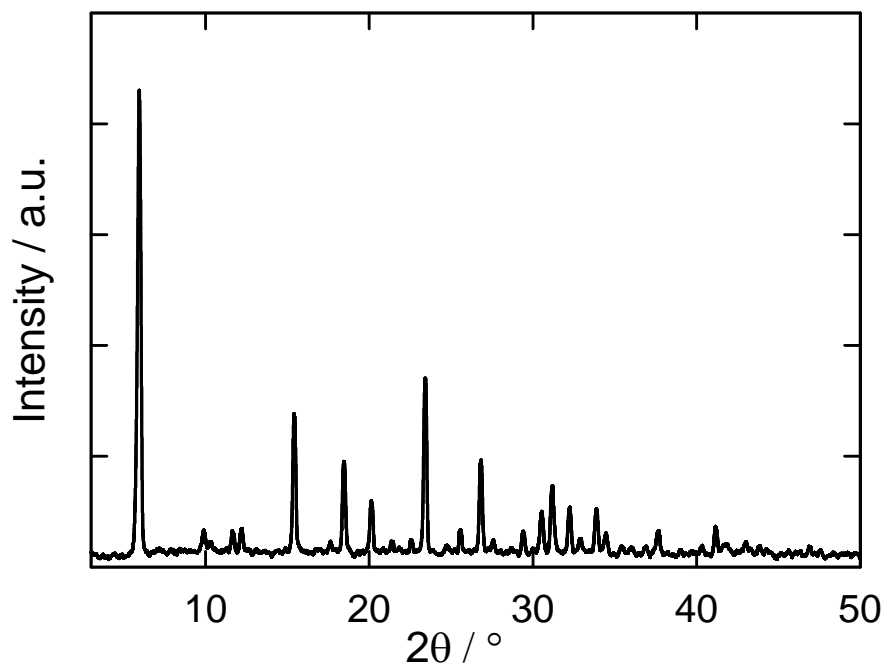


Figure 3.27: Powder X-ray diffraction pattern of zeolite Y^{3+} -Y.

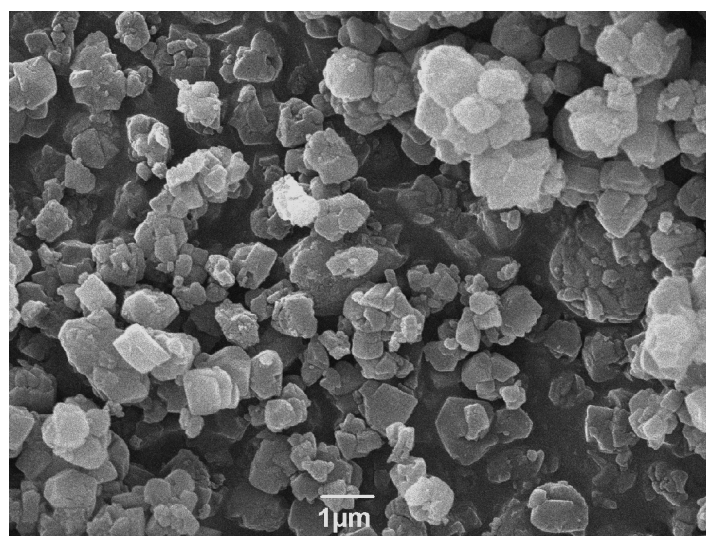


Figure 3.28: Scanning electron micrograph of zeolite Y^{3+} -Y.

The ion-exchange procedure was repeated for 3 times. After each ion-exchange procedure, the material was recovered by filtration and washed thoroughly with ca. 1 litre of distilled water and dried at 100 °C.

3.6 Batch adsorption experiments

Y-type zeolites ion-exchanged with different metal ions, H-ZSM-5 zeolites with various n_{Si}/n_{Al} ratios and the acid zeolites H-Y, H-MOR and H-MCM-22 were screened for their ability to adsorb thiophene in batch experiments. The screening tests were done using either toluene or *n*-heptane as solvent to represent aromatic and aliphatic compounds found in the pyrolysis oil. Prior to the experiments, the zeolite samples were pretreated at 400-450 °C under a nitrogen flow ($\dot{V}_{N_2} = 20$ ml/min) for 12 hours to remove the adsorbed water. After cooling down to 20 °C, 500 mg of activated zeolite was introduced into a vial containing ca. 10 ml of a solution of 0.5 wt.-% thiophene in toluene or 0.5 wt.-% thiophene in *n*-heptane. The zeolite was contacted with the solution using a glove bag containing a dry nitrogen atmosphere in order to avoid the adsorption of moisture from the air. The vials were then kept under stirring. The change in the concentration of thiophene as a function of the contact time of the solution with the zeolite was determined. The change in concentration of thiophene was analyzed by gas chromatography using a Chrompack WCOT fused silica capillary column (50 m x 0.25 mm, film thickness = 0.2 µm) coated with CP-Sil 88 and a flame ionization detector (FID).

The adsorbed amount per mass of dry adsorbent after a given adsorption time q_t is calculated as:

$$q_t = \frac{\left(1 - \frac{C_{ts}}{C_{is}}\right) \left(\frac{C_{is}}{100} m_{\text{Solution}}\right)}{m_{\text{Adsorbent}}} \quad (3.1)$$

The adsorption capacity q_s after reaching equilibrium is calculated as

$$q_s = \frac{\left(1 - \frac{C_{es}}{C_{is}}\right) \left(\frac{C_{is}}{100} m_{\text{Solution}}\right)}{m_{\text{Adsorbent}}} \quad (3.2)$$

Where, C_{is} is the initial concentration of the sulphur-containing compounds in the solution in wt.-%, C_{ts} is the concentration of the sulphur-containing compounds in the solution after time t in wt.-%, m_{solution} is the total amount of model solution in mg, C_{es} is the concentration of the sulphur-containing compounds in the solution after reaching equilibrium in wt.-%, $m_{\text{Adsorbent}}$ is the mass of adsorbent in mg.

The total amount of sulphur-containing compounds in the solution is given by the expression $(C_{is}/100) \times m_{\text{Solution}}$. The expression C_{ts}/C_{is} gives the fraction of residual sulphur-containing compounds left in the solution after time t and $(1 - (C_{ts}/C_{is}))$ is the fraction of sulphur-containing compounds adsorbed on the adsorbent. Therefore, the amount of sulphur-containing compounds adsorbed on the adsorbent per unit mass of adsorbent is given by Equation 3.1. Similarly, the amount of sulphur-containing compounds adsorbed after the system has reached the equilibrium is given by the equation 3.2.

3.7 Continuous flow fixed-bed adsorption experiments

Zeolite pellets of 355-250 μm in size were activated as described in the chapter on batch adsorption experiments to remove previously adsorbed water. The pellets were slowly transferred into a fixed-bed column (length 100 mm, inner diameter 4 mm). The reason for using pellets is to avoid a high pressure drop in the column. The experimental set-up used to perform continuous fixed-bed adsorption in order to measure breakthrough curves is shown in Figure.3.29. The set-up consisted of a low-flow pump, three feed tanks, a fixed-bed column and an auto-sampler. Prior to contacting the adsorbent with the model solution, the bed was wetted with the solvent. The model solution was pumped into the fixed-bed adsorption column at a rate of 0.5 cm^3/min . The samples were then collected using an autosampler for every 0.25 or 0.5 minutes. The collected samples were analysed by gas-chromatography using the conditions described in Tables 3.5 to 3.11.

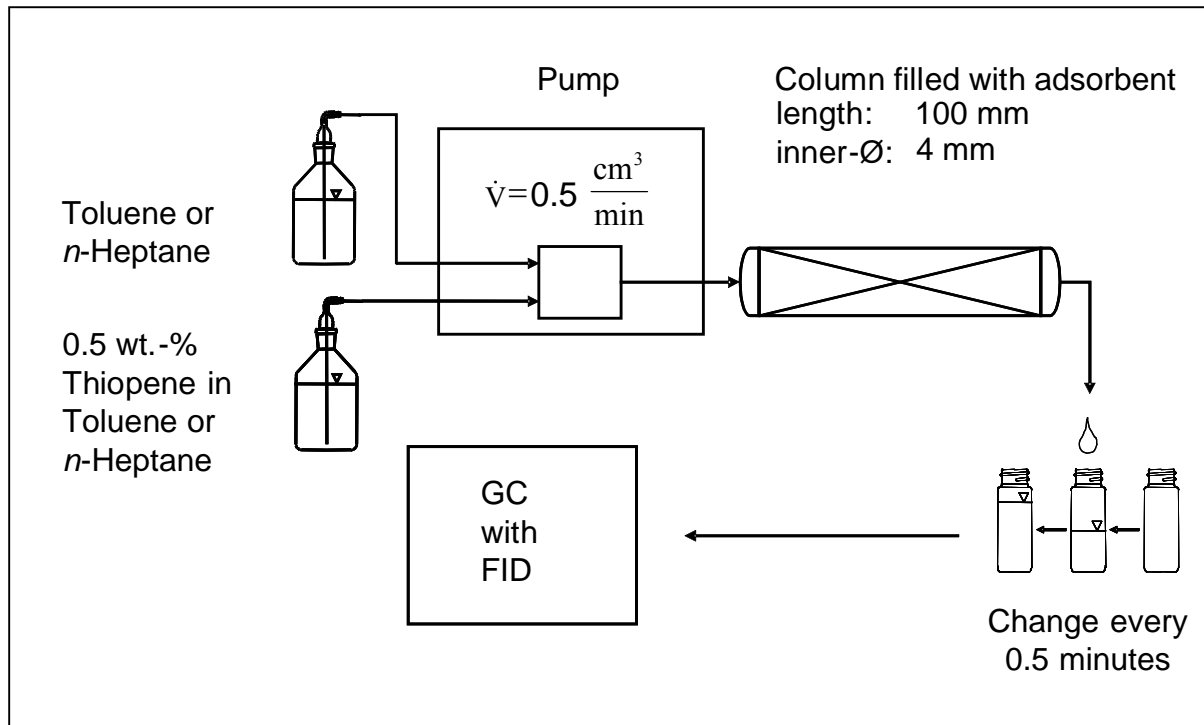


Figure 3.29: Experimental set-up for continuous fixed-bed adsorption.

A breakthrough curve is represented as shown in Figure 3.30. As the feed with the initial concentration of sulphur-containing compounds, viz. C_{is} , was pumped into the bed at the inlet side, the samples of the purified solution were collected at the outlet side and the concentration of sulphur-containing compounds at time t (viz. C_{ts}) was determined at regular time intervals using gas chromatography. The samples at the outlet side were collected until the concentrations of sulphur-containing compounds at the inlet and the outlet sides are equal i.e., when C_{ts}/C_{is} equals to 1. The integral part of the equation 3.3 is the area above the breakthrough curve indicated by the shaded region in Figure 3.30

The adsorption capacity per mass of adsorbent was obtained after solving the following Equation 3.3.

$$q_t = \left(\frac{\dot{V}}{m_{\text{Ads.}}} \right) \rho_{\text{solution}} \int_0^t \left(1 - \frac{C_{ts}}{C_{is}} \right) dt \quad (3.3)$$

Where q_t is the amount of sulphur-containing compounds adsorbed per unit mass of adsorbent in mg/g, \dot{V} is the volumetric flow rate of the feed in cm^3/min , ρ_{solution} is the density of the

model solution in g/cm^3 at $20\text{ }^\circ\text{C}$, C_{is} is the initial concentration of sulphur-containing compounds in the feed in wt.-%, C_{ts} is the concentration of sulphur-containing compounds in wt.-% at time t , $m_{\text{Ads.}}$ is the weight of the dry adsorbent in g and $V_{\text{Effl.}}$ is the cumulative effluent volume in cm^3 .

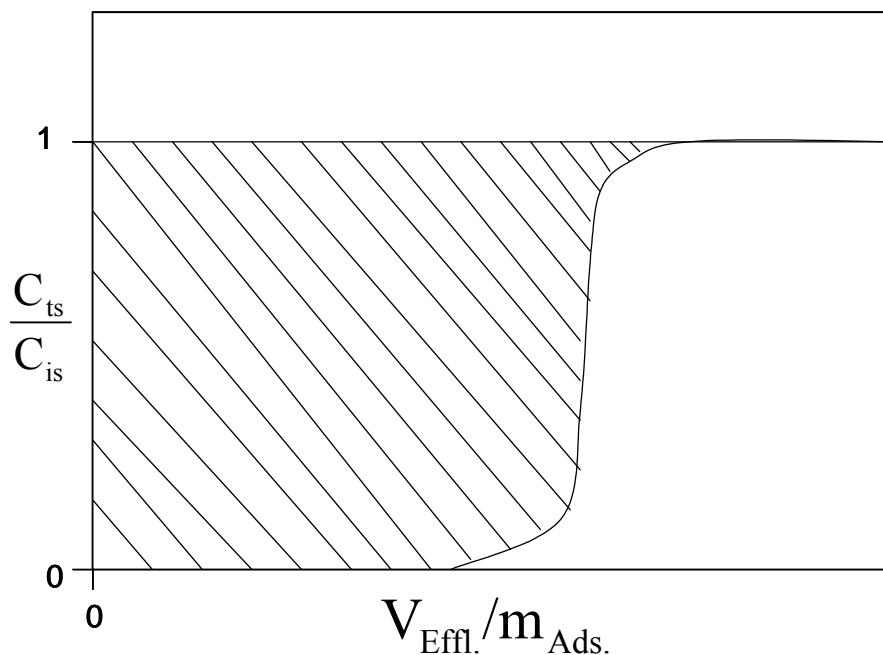


Figure 3.30: Graphical representation of a breakthrough curve.

Tables 3.5 to 3.11 describe the conditions and settings of gas chromatographic analysis applied for the analysis of collected samples with sulphur-containing compounds.

Table 3.5: GC-column used for the separation of sulphur-containing compounds from toluene and/or *n*-heptane.

Column	Chrompack, WCOT fused silica column
Stationary phase	CP-SIL 88
Length	50 m
Inner diameter	250 μm
Film thickness	0.20 μm
Maximum temperature	250 $^\circ\text{C}$

Table 3.6: Detector and the conditions used for the detection of sulphur-containing compounds.

Detector	FID
\dot{V}_{H_2}	40 ml/min
\dot{V}_{Air}	450 ml/min
Make-up gas, \dot{V}_{N_2}	40 ml/min
Temperature	250 °C

Table 3.7: Conditions used for separating thiophene from toluene.

Inlet type	Split inlet
Temperature	250 °C
Amount injected	6 μ l
Split	50:1
Column flow (H ₂)	10 ml/min
Oven temperature	30 °C , 5 min

Table 3.8: Conditions used for separating thiophene from *n*-heptane.

Inlet type	Split inlet
Temperature	250 °C
Amount injected	6 μ l
Split	50:1
Column flow (H ₂)	7 ml/min
Oven temperature	60 °C , 5 min

Table 3.9: Conditions used for separating benzothiophene and thiophene from toluene.

Inlet type	Split inlet
Temperature	250 °C
Amount injected	6 µl
Split	50:1
Column flow (H ₂)	7 ml/min
Oven temperature	100 °C , 10 min

Table 3.10: Conditions used for separating dibenzothiophene, benzothiophene and thiophene from toluene.

Inlet type	Split inlet
Temperature	250 °C
Amount injected	6 µl
Split	50:1
Column flow (H ₂)	7 ml/min
Oven temperature	100 °C , 10 min

Table 3.11: Conditions used for separating 4,6 dimethyl dibenzothiophene from toluene.

Type	Split inlet
Temperature	250 °C
Amount injected	6 µl
Split	50:1
Column flow (H ₂)	7 ml/min
Oven temperature	200 °C , 10 min

4 Results and discussion

4.1 Kinetics of thiophene adsorption: Batch experiments

4.1.1 Acid zeolites

The acid zeolites used through out this work were either synthesized directly or prepared by post-synthesis modification of their Na^+ -form. The thiophene adsorption capability of these zeolites was explored using two different model solutions. One contained 0.5 wt.-% thiophene in toluene (model solution 1) and the other 0.5 wt.-% thiophene in *n*-heptane (model solution 2). The reason behind selecting these two model solutions is to investigate the competition effect of polar (toluene) and non-polar (*n*-heptane) compounds with thiophene in adsorbing on zeolites.

The H-ZSM-5 materials with different $n_{\text{Si}}/n_{\text{Al}}$ ratios were synthesized as mentioned in section 3.5. Batch experiments were performed in the liquid phase to explore the removal of thiophene from non-polar and polar solvents. H-ZSM-5 materials with $n_{\text{Si}}/n_{\text{Al}}$ ratios of 13, 19, 36 and Silicalite-1 ($n_{\text{Si}}/n_{\text{Al}} = 1280$), containing 8.3, 6.3, 5.2 and 0.6 wt.-% of water, respectively, were pre-activated at 400 °C prior to the experiment to remove the adsorbed water. The adsorption of thiophene from model solution 2 on H-ZSM-5 zeolites is shown in Figure 4.1. The thiophene adsorption capacities of H-ZSM-5 zeolites containing different $n_{\text{Si}}/n_{\text{Al}}$ ratios (13, 19, 36) and of Silicalite-1 amount to 47, 10, 5 and 1.5 mg/g, respectively. Obviously, the Al-content has a large influence on the adsorption of thiophene on H-ZSM-5. The thiophene adsorption capacity increases with decreasing $n_{\text{Si}}/n_{\text{Al}}$ ratio. The $n_{\text{Si}}/n_{\text{Al}}$ ratio is an indication of the polarity of the zeolite; the lower it is, the more aluminium and, hence, more charge compensating cations are present, and the more polar the framework will be. Highly polar zeolites show a strong physical interaction with polar compounds. Thiophene is a polar compound and *n*-heptane is a non-polar compound and therefore, the thiophene adsorption capacity in *n*-heptane solution increased with decreasing $n_{\text{Si}}/n_{\text{Al}}$ ratio. Moreover, thiophene may react on acid sites to form oligomers which can be detected through UV-Vis spectroscopy. These oligomers adhere to the acid sites and therefore the chemisorption of thiophene through oligomerization also increases with decreasing $n_{\text{Si}}/n_{\text{Al}}$ ratio of zeolite H-ZSM-5, due to an increase in the number of acid sites.

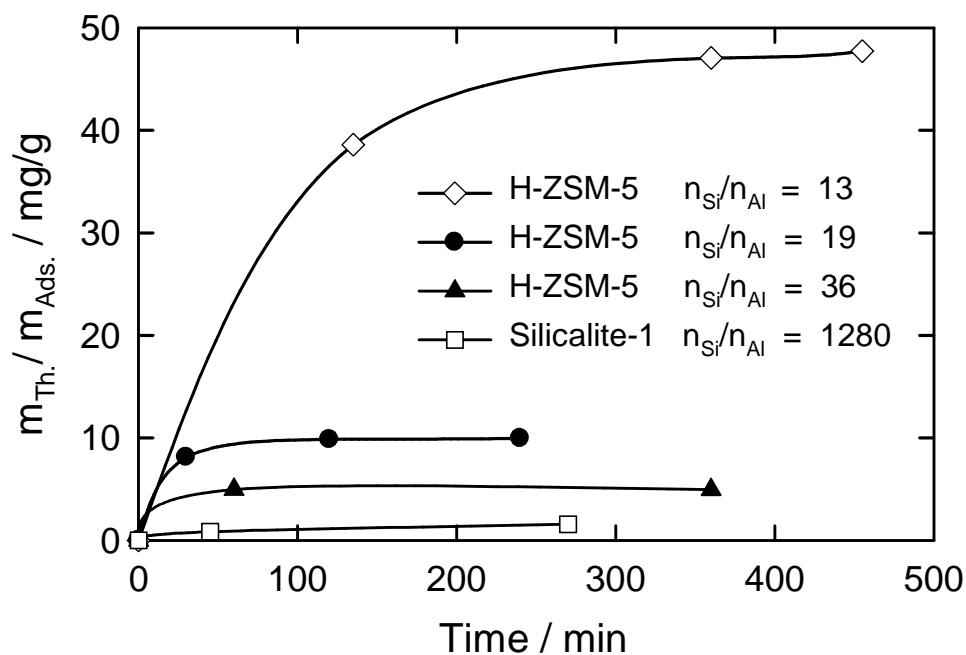


Figure 4.1: Adsorption of thiophene at 20 °C from model solution 2 on H-ZSM-5-type zeolites.

In case of model solution 1 (of Figure 4.2), the adsorption capacity of H-ZSM-5 for thiophene with n_{Si}/n_{Al} ratios 13, 19, 36 and of Silicalite-1 ($n_{Si}/n_{Al} = 1280$) were measured to be 36, 14, 17, 22 mg/g, respectively. The polarity of toluene is more than that of thiophene and the polar zeolites adsorbs the compounds in the order of decreasing polarities. Therefore the thiophene adsorption capacity from model solution 1 should decrease with decreasing n_{Si}/n_{Al} ratio since the polarity of the zeolite framework increases with Al-content. The above explanation is in agreement with the H-ZSM-5 zeolites having n_{Si}/n_{Al} ratios 19 and 36 and with silicalite-1 (thiophene adsorption capacities 14, 17 and 22 mg/g, respectively). H-ZSM-5 with n_{Si}/n_{Al} ratio 13 is an exception where a maximum adsorption capacity of 36 mg/g was observed. This might be due to a domination of the reaction of thiophene over Brønsted-acid sites.

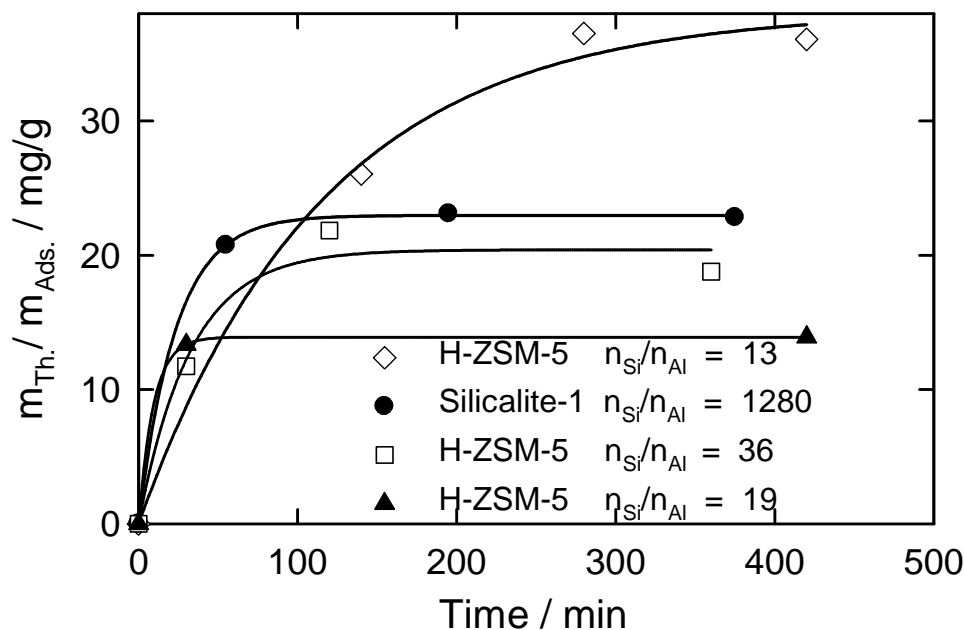


Figure 4.2: Adsorption of thiophene at 20 °C from model solution 1 on H-ZSM-5-type zeolites.

After the batch experiments, the spent adsorbents were recovered by filtration and dried at 100 °C under a flow of nitrogen ($\dot{V}_{N_2} = 20$ ml/min) to purge the unadsorbed components and UV-Vis spectrum was recorded. Figure 4.3 shows the spectrum of the products formed on H-ZSM-5 samples containing different amounts of aluminium. The intensity of oligomerization increased with the decreasing n_{Si}/n_{Al} ratio. That means, as the number of acid sites increases in the channels of the H-ZSM-5 framework, the intensity of oligomerization also increases. It was also found that the colour of the adsorbent changes from pale yellow, after immediate contact with solution, to intense red after 6 hours of contact. A similar colour change was observed by Geobaldo et al. [54] during their studies of the adsorption of thiophene on zeolite H-Y. It is important to remark at this point that thiophene is known to easily undergo electrophilic attack in acidic solutions like phosphoric acid [55, 56] with the formation of stable oligomeric compounds, the structure of which is strongly dependent upon the presence or absence of oxygen in the surrounding medium. It is also known that acid zeolites can induce protonation of unsaturated species through electrophilic attack of the Brønsted-acid sites on the π -systems with formation of carbocation monomers, and that these monomeric carbocations can further react with excess monomers to produce an oligomer [54, 57-66]. The mechanism of oligomerization of thiophene can be tentatively assumed to proceed as shown in schemes 4.1 and 4.2: A protonated monomer $C_4H_5S^+$ is formed following the mechanism

shown in scheme 4.1 (reaction 2). This species ($C_4H_5S^+$), in the presence of excess thiophene, can further react to give positively charged oligomers (scheme 2, reaction 3) whose tentative structure is shown in schemes 4.2 (b), (c), (d).

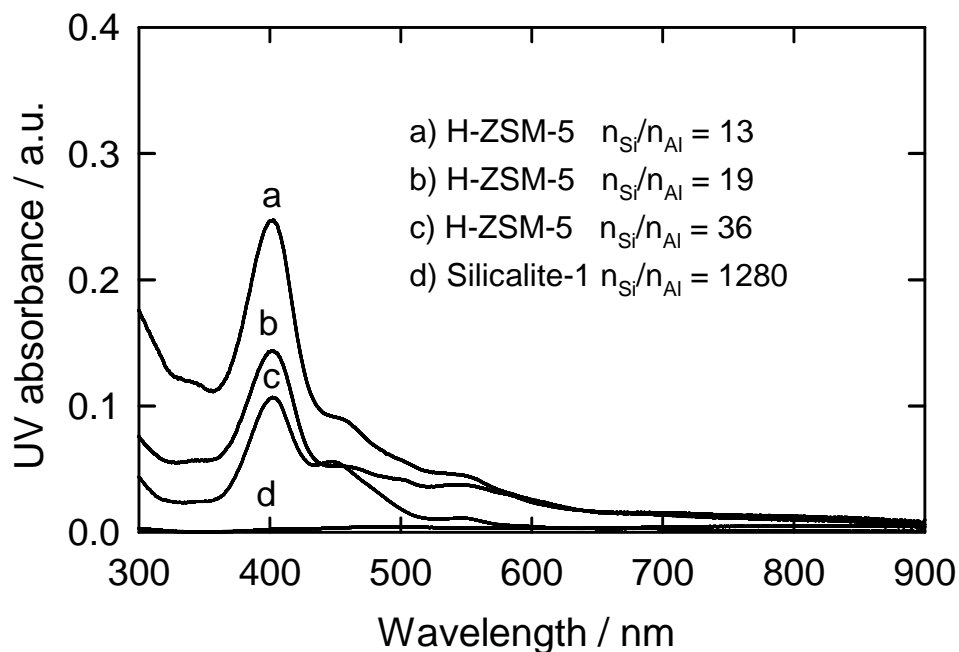
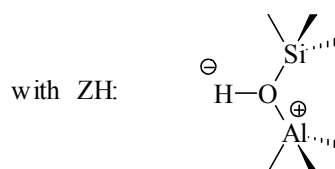
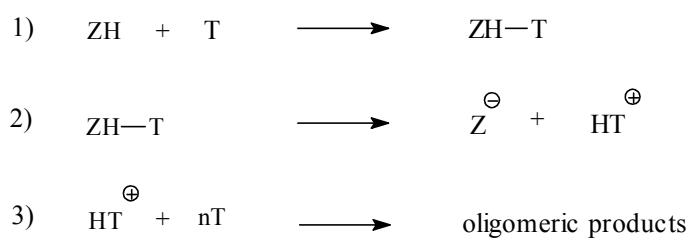
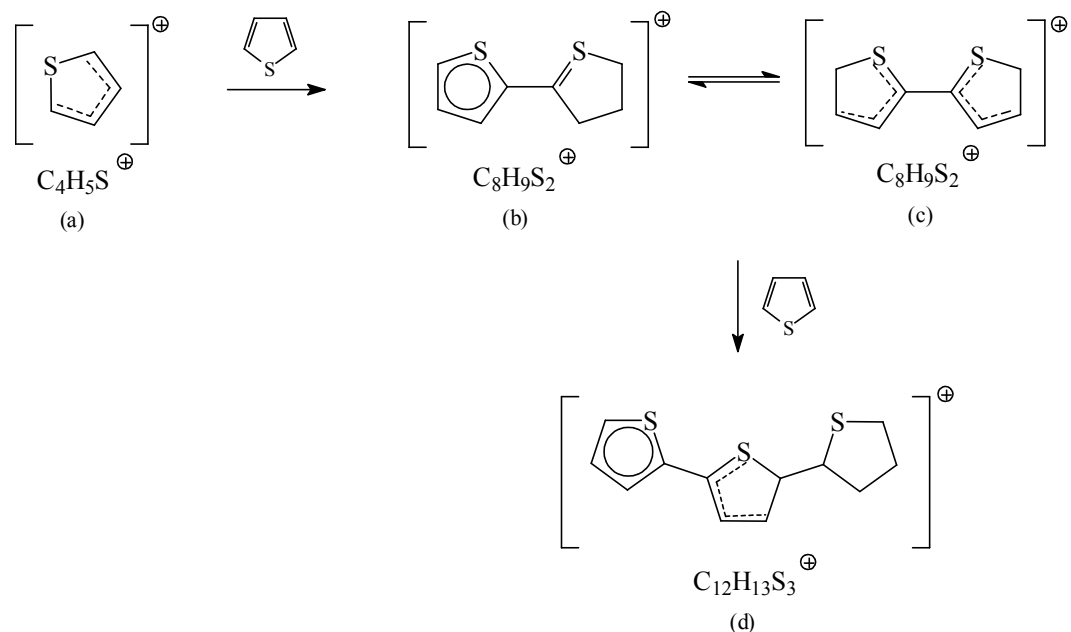


Figure 4.3: UV-Vis spectra showing the presence of other products on spent adsorbent MFI.



Scheme 4.1: Schematic representation of the adsorption of thiophene on acidic zeolites.



Scheme 4.2: Schematic representation of the oligomerization of thiophene; (a) is protonated thiophene, (b),(c),(d) are positively charged oligomers

Adsorption experiments for benzothiophene on ZSM-5 revealed that benzothiophene did not adsorb on ZSM-5. Zeolite ZSM-5 contains 10-ring channels with dimensions 0.51 x 0.56 nm when viewed along [100] and 0.53 x 0.56 nm when viewed along [010] and the molecular size of benzothiophene is larger than the pore apertures of MFI-type zeolites. Obviously, the bulkier sulphur-containing compounds e.g., dibenzothiophene and alkyldibenzothiophenes are hindered from entering the pores of ZSM-5.

The thiophene adsorption capacities of other acid zeolites, viz. H-Y, H-MOR and H-MCM-22 from model solution 1 are 3.5, 9.5 and 38 mg/g, respectively and from model solution 2 they amount to 30, 42, and 48 mg/g, respectively. Figures 4.4 and 4.5 describe the behaviour of zeolites H-Y, H-MOR and H-MCM-22 in adsorbing thiophene from model solution 1 and 2, respectively. The adsorption reaches equilibrium after ca. 6 hours of stirring like H-ZSM-5 zeolites. The higher adsorption capacities of these acid zeolites (H-Y, H-MOR and H-MCM-22) for thiophene from *n*-heptane as compared to toluene as solvent can be attributed to the differences in polarities of the solvents. The effect of polarity in removing thiophene from solvents was already discussed.

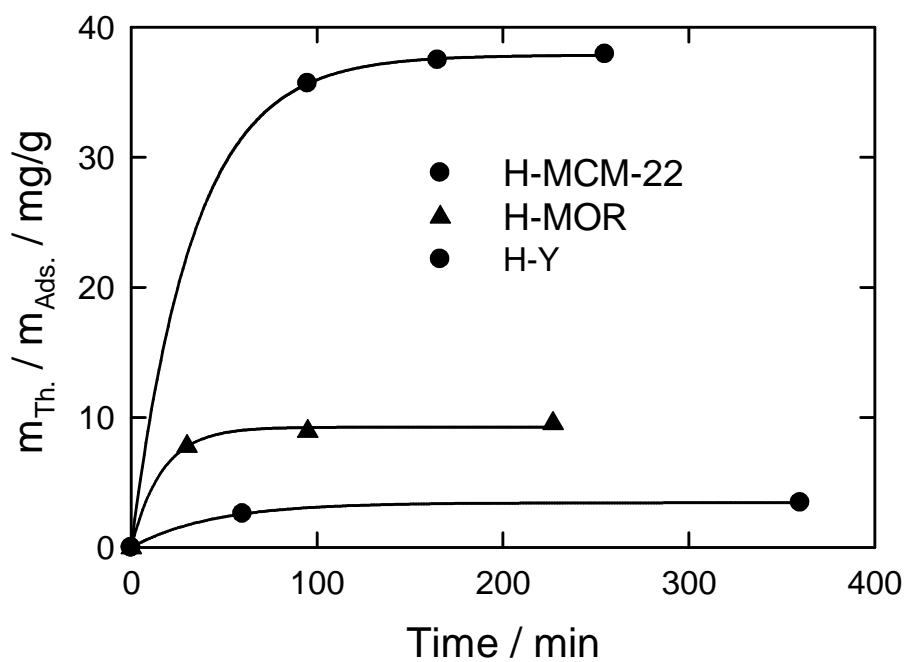


Figure 4.4: Adsorption of thiophene at 20 °C from model solution 1 on the acid zeolites H-MCM-22, H-MOR and H-Y.

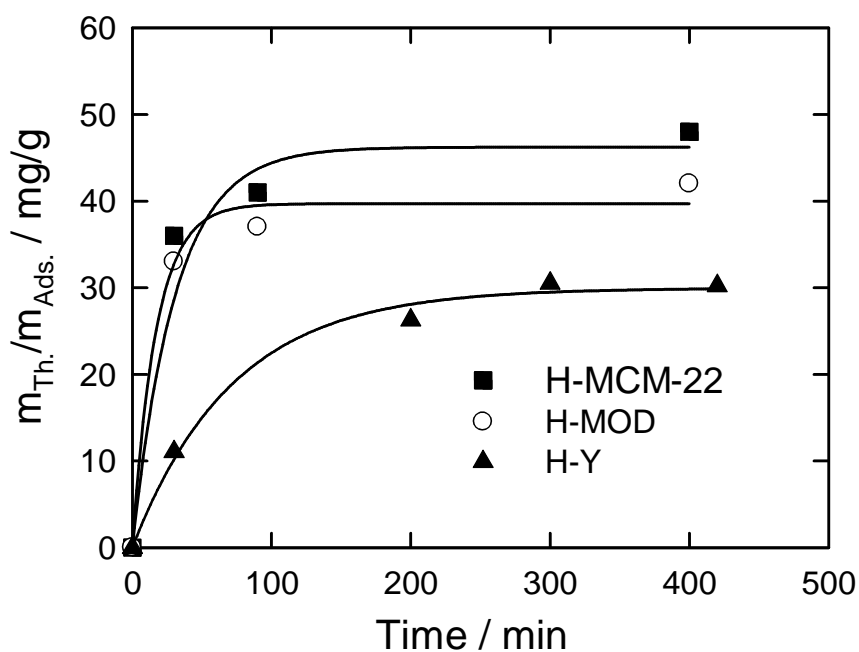


Figure 4.5: Adsorption of thiophene at 20 °C from model solution 2 on the acid zeolites H-MCM-22, H-MOR and H-Y.

The intensity of thiophene oligomerization on acid zeolites decreases in the order H-MCM-22 > H-ZSM-5 > H-MOR > H-Y. It was claimed that distances and bond angles in the Al-OH-Si groups of the zeolite can affect the acidity of the hydroxyl group [67] and that strongly acidic zeolites have a range of T-O-T angles (ZSM-5, 137-177°; Mordenite, 143-180°) larger than other less acidic ones (HY, 138-147°). The higher contribution of oligomerization might therefore be due to a higher strength of acid sites of the adsorbents.

In the work of propene oligomerization by Geobaldo et al. [64] it was found that despite of a higher proton density, the intensity of oligomerization is lower on mordenite as compared to H-ZSM-5. Their experimental evidences indicate that the oligomerization occurs immediately at the entrance of the channels. The oligomers formed by the reaction might block the entrance of the pores and prevent further diffusion of monomers to reach the internal Brønsted- acid sites. This hypothesis probably also applies to H-Y zeolite.

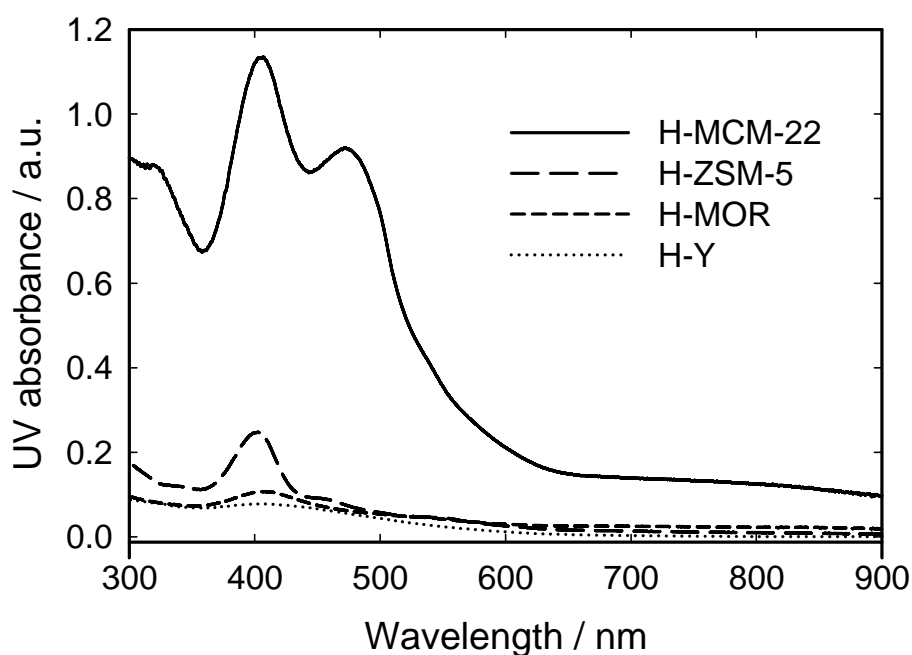


Figure 4.6: UV-Vis spectra showing the presence of other products on H-MCM-22, H-ZSM-5, H-MOR and H-Y.

From Figures 4.6 and 4.3 and the calculated thiophene adsorption capacities, it can be concluded that H-MCM-22 with lowest acid site density has proven to be the best acid zeolite for the oligomerization of thiophene. In contrast, in H-ZSM-5 zeolites the amount of

oligomers formed from thiophene increases with decreasing $n_{\text{Si}}/n_{\text{Al}}$ ratio. All these results suggest that the geometry of the zeolite pore system and strength of the acid site plays a critical role with respect to oligomerizing thiophene inside the channels of the adsorbents.

4.1.2 Ion-exchanged Na^+ -Y zeolites

The adsorption of thiophene on zeolites Na^+ -Y, Ag^+ -Y, Cu^+ -Y and Ni^{2+} -Y was investigated at 20 °C in a stirred batch system. 500 mg of zeolites Ag^+ -Y and Na^+ -Y were pretreated at 400 °C for 12 hours under nitrogen flow ($\dot{V}_{\text{N}_2} = 20$ ml/min) to remove the previously adsorbed water. The degree of ion-exchange, the water content and the $n_{\text{Si}}/n_{\text{Al}}$ ratios were mentioned in Table 3.1. Unlike the former adsorbents, Cu^{2+} -Y and Ni^{2+} -Y were pretreated at different temperatures. Cu^{2+} -Y was treated at 450 °C under a nitrogen flow for 12 hours to achieve a maximum degree of auto-reduction of Cu^{2+} -Y to Cu^+ -Y. Cu^+ -Y was proven to be a better π -complexation adsorbent than Cu^{2+} -Y due to the presence of an empty s-orbital in Cu^+ ($1s^2 2s^2 2p^6 3s^2 3p^6 3d^{10} 4s^0$). Ni^{2+} -Y was pretreated at 350 °C to avoid auto-reduction of Ni^{2+} to Ni^+ , as Ni^{2+} contains already an empty s-orbital and, hence, π -complexation of thiophene is favourable with Ni^{2+} . The thiophene adsorption capacities of Cu^+ -Y, Ni^{2+} -Y, Ag^+ -Y and Na^+ -Y in removing thiophene from model solutions 1 and 2 are shown in Figure 4.7 and 4.8. The thiophene adsorption capacities of Cu^+ -Y, Ni^{2+} -Y, Ag^+ -Y and Na^+ -Y in toluene as solvent are 11, 10, 6.4 and 2 mg/g, respectively, whereas with *n*-heptane as solvent the adsorption capacities amount to 69, 58, 52 and 53 mg/g, respectively.

It was already shown that π -electrons of the thiophene ring will take part in interaction with the metal cation [21]. As toluene also contains π -electrons, the low thiophene adsorption capacities of the metal-ion exchanged zeolites in model solution 1 can be attributed to the competition of toluene with thiophene for π -complexation with the metal cation. This can also be confirmed by the results shown in Figures 4.7 and 4.8, which indicate higher thiophene adsorption capacities in the presence of *n*-heptane as solvent which contains no π -electrons.

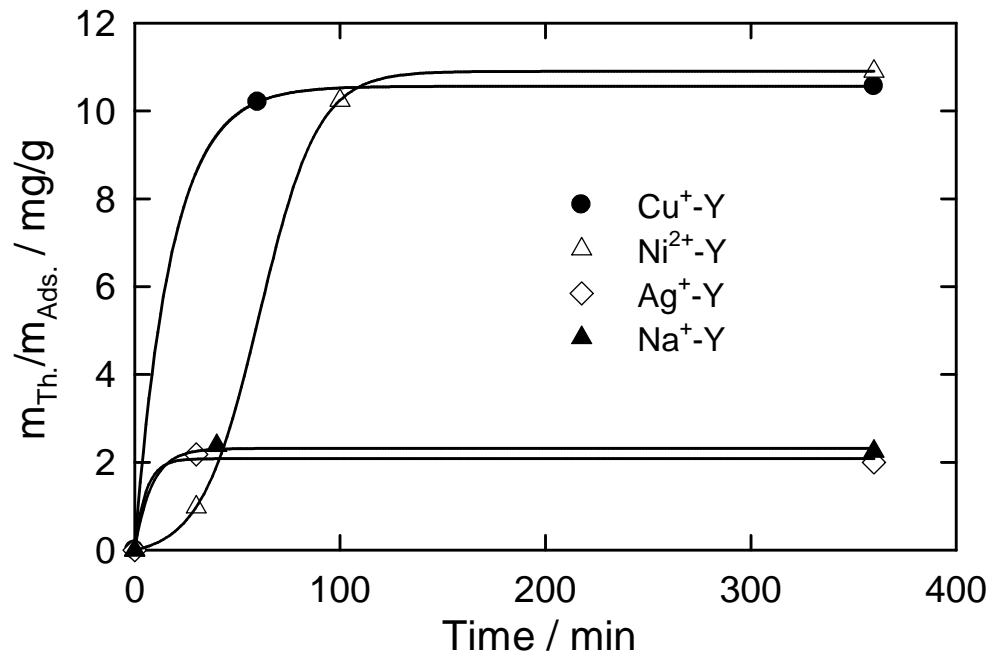


Figure 4.7: Adsorption of thiophene at 20 °C from model solution 1 on Cu^+ -, Ni^{2+} - and Ag^+ -ion-exchanged Na^+ -Y zeolites and of the parent Na^+ -Y zeolite.

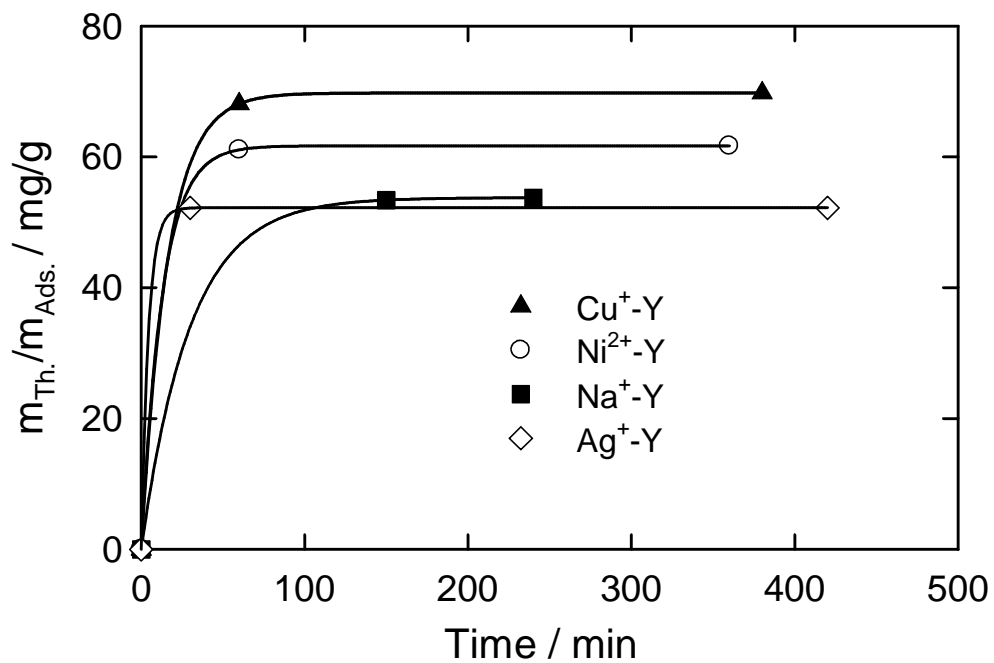
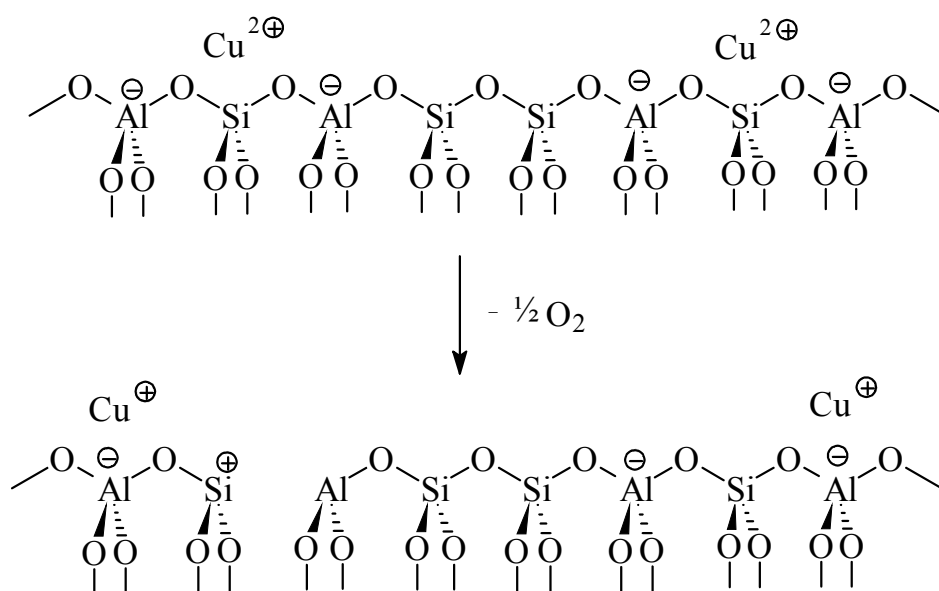


Figure 4.8: Adsorption of thiophene at 20 °C from model solution 2 on Cu^+ -, Ni^{2+} - and Ag^+ -ion-exchanged Na^+ -Y zeolites and of the parent Na^+ -Y zeolite.

4.1.3 Cu^{2+} -exchanged Na^+ -Y zeolite

Cu^{2+} -Y adsorbents with different copper contents were prepared by ion-exchange as described in chapter 3.5.11. The degrees of ion-exchange and the thiophene adsorption capacities of these adsorbents are given in Table 4.1. All these adsorbents were pretreated at 450 °C to auto-reduce Cu^{2+} -Y to Cu^+ -Y as shown in scheme 4.3 [68]. The specific surface area and the pore volume of the samples decreased as the degree of ion-exchange increased. Moreover, the XRD pattern show that the intensity of the peaks decrease by exchanging Na^+ -Y with Cu^{2+} cations. This might be due to the disturbance of the zeolite structure by the replacement of monovalent cations with divalent cations. In this context, disturbance of the zeolite structure essentially means slight changes in the unit cell parameters.



Scheme 4.3: Schematic representation of the auto-reduction of Cu^{2+} -Y to Cu^+ -Y (adapted from [68]).

Figure 4.9 shows a plot of the number of thiophene molecules adsorbed per unit cell of zeolite as a function of cation content of the adsorbents Cu^{2+} -Y (1) to Cu^{2+} -Y (5) (Table 4.12). It is observed that the thiophene loading increases with increasing ion-change level of Cu^{2+} cations in Cu^{2+} -Y up to ion-exchange degrees of ca. 70 % and the further increase observed in the adsorption for ion-exchange degrees of 70 % (ca. 20 Cu^{2+} cations / unit cell) and above is inconsiderable. Thiophene can enter only into the supercage of Cu^+ -Y zeolite and the cation sites exposed to this cage are site S(II) and site S(III). Obviously, the adsorption of thiophene

through the interaction with Cu^+ cation can only occurs at these sites. Therefore it can be concluded that the Cu^+ cation population at the sites exposed to supercage might not have increased after ion-exchange degree of 70 % with Na^+ -Y zeolite using the ion-exchange procedure described in section 3.5.11. And therefore, no increase in the adsorption capacity of Cu^+ -Y for thiophene was observed even after increasing the Cu^+ content in Cu^+ -Y.

Table 4.1: Cu^{2+} -Y zeolites with different degrees of ion-exchange and their thiophene adsorption capacities at 20 °C.

Zeolite	Degree of ion-exchange / %	Adsorption capacity / mg/g
Cu^{2+} -Y (1)	20	5.7
Cu^{2+} -Y (2)	40	7.0
Cu^{2+} -Y (3)	71	11.2
Cu^{2+} -Y (4)	82	10
Cu^{2+} -Y (5)	92	10.8

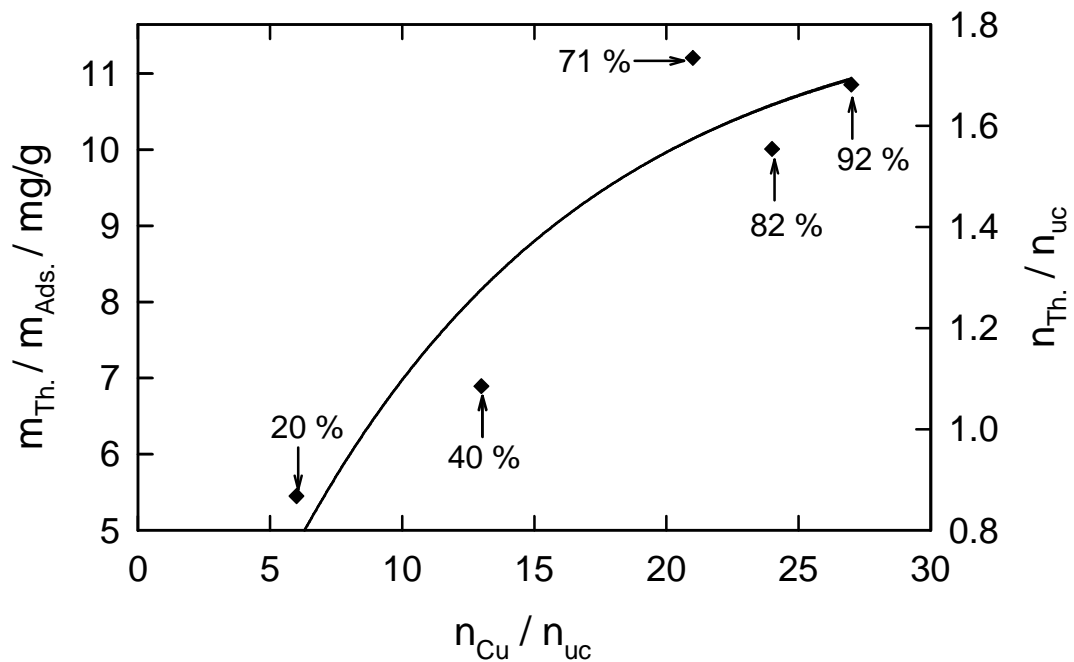


Figure 4.9: Thiophene adsorption capacities for Cu^{2+} -exchanged Na-Y zeolites at 20 °C per mass of adsorbent and unit cell of the zeolite, respectively.

4.1.4 Ce³⁺-, La³⁺- and Y³⁺- exchanged Na⁺-Y zeolites

Ce³⁺-Y, La³⁺-Y, Y³⁺-Y were prepared by ion-exchange methods as described in sections 3.5.12 to 3.5.14. The $n_{\text{Si}}/n_{\text{Al}}$ ratios and the degrees of ion-exchange obtained from the elemental analysis are shown in Table 3.1. The thiophene adsorption capability of these zeolites was investigated in batch experiments after a pretreatment at 400 °C under nitrogen flow ($\dot{V} = 20$ ml/min) and the results are shown in Figures 4.10 and 4.11. The thiophene adsorption capacities of Ce³⁺-Y, La³⁺-Y and Y³⁺-Y from model solution 1 are 60, 83 and 60 mg/g and from model solution 2 are 64, 102 and 96 mg/g, respectively. It is evident from Figures 4.10 and 4.11 that the equilibrium adsorption of thiophene from toluene as solvent on Ce³⁺-Y, La³⁺-Y and Y³⁺-Y zeolites was reached in ca. 20 hours whereas it took 10 hours for the equilibrium adsorption of thiophene from *n*-heptane as solvent on the preceding adsorbents. It can be expected that the rate of adsorption of thiophene is limited by the rate of adsorption of toluene at the adsorption sites.

The performance of Ce³⁺-, La³⁺- and Y³⁺-exchanged Na⁺-Y adsorbents is found to be better than with the parent Na⁺-Y and Ag⁺, Cu⁺, Ni²⁺-exchanged Na⁺-Y adsorbents. This leads to the tentative conclusion that thiophene interacts with Ce³⁺, La³⁺ and Y³⁺ in a different way. Thermogravimetric analysis of the loaded adsorbents as well as IR spectroscopic studies shown in later sections confirm two different types of metal-thiophene interactions. One is direct interaction of metal ions with the sulphur atom (M-S interaction) and the other is the interaction through π -complexation with π -electrons of the thiophene ring and the metal ion. There is a significant increase in the amount of adsorption of thiophene on zeolites La³⁺-Y and Y³⁺-Y when *n*-heptane was used as solvent whereas a very little increase is observed in case of zeolite Ce³⁺-Y. From this it can be expected that the adsorption of thiophene through M-S interaction is predominant on Ce³⁺-Y then followed by Y³⁺-Y and La³⁺-Y zeolites. And therefore the effect of competition of toluene to adsorb on Ce³⁺-Y might not be as significant as on La³⁺-Y and Y³⁺-Y zeolites.

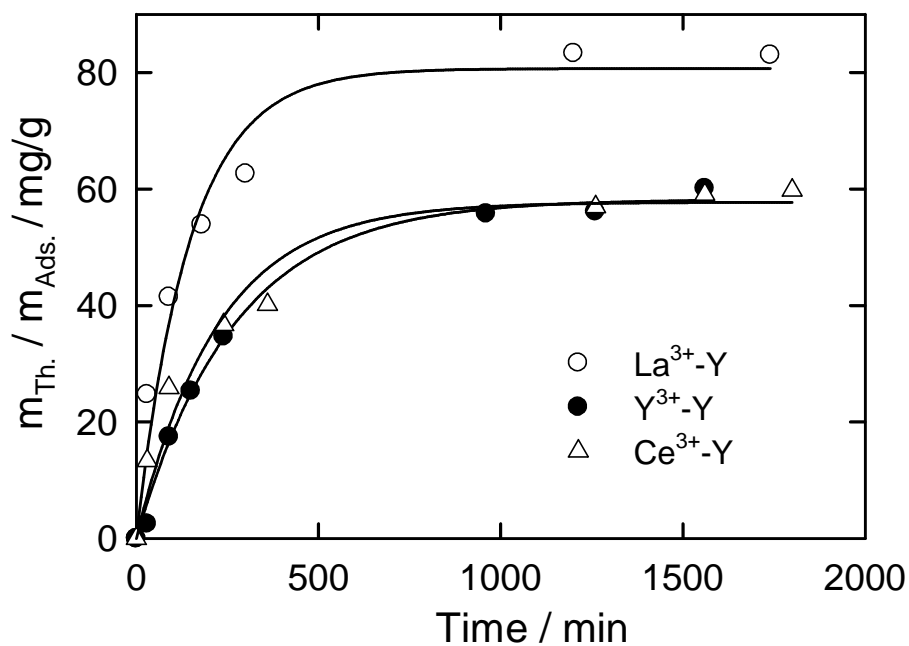


Figure 4.10: Adsorption of thiophene at 20 °C from model solution 1 on Ce³⁺-, La³⁺-, and Y³⁺-exchanged Na⁺-Y zeolites.

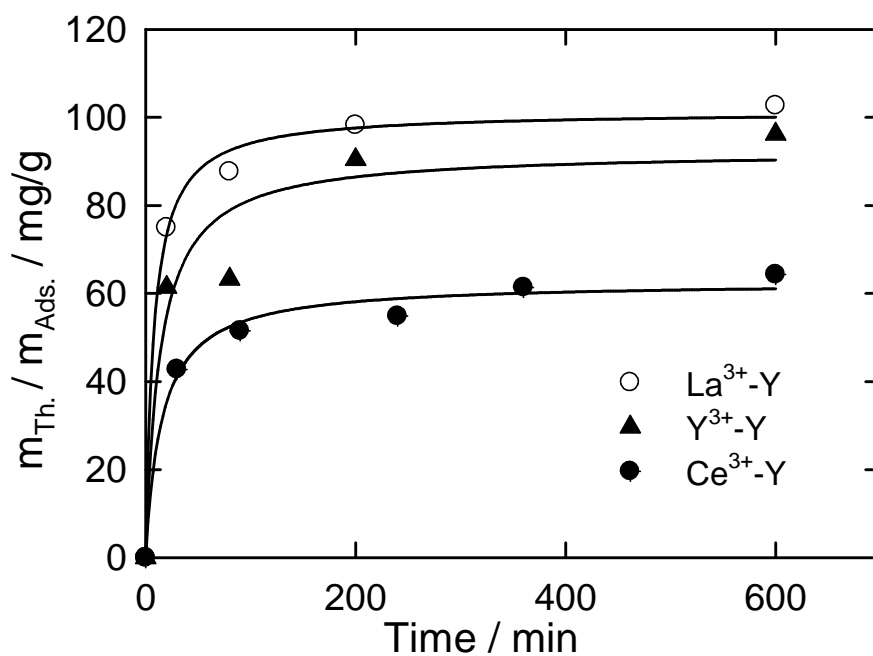


Figure 4.11: Adsorption of thiophene at 20 °C from model solution 2 on Ce³⁺-, La³⁺-, and Y³⁺-exchanged Na⁺-Y zeolites.

4.1.5 Ce^{4+} -Y zeolite

A Ce^{4+} -containing Y-type zeolite was obtained by calcination of zeolite Ce^{3+} -Y at 450 °C in air. The oxidation of the adsorbent was indicated by the change in colour from white to yellow. The adsorption performance as screened by batch adsorption experiment is found to be comparable to Ce^{3+} -Y zeolite and the behaviour of both adsorbents is shown in Figure 4.12.

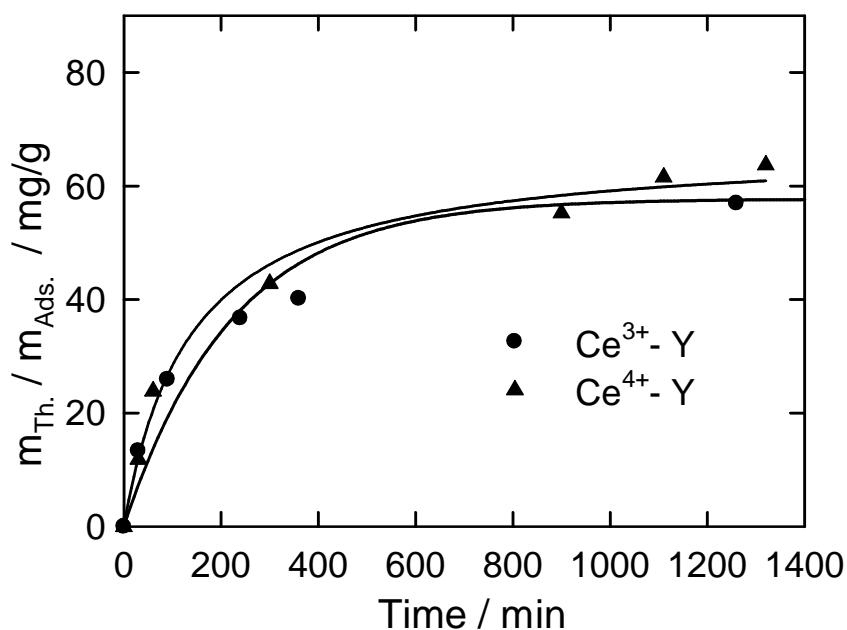


Figure 4.12: Adsorption of thiophene at 20 °C from model solution 1 on Ce^{3+} -Y and Ce^{4+} -Y zeolites.

4.2 Continuous flow fixed-bed adsorption of sulphur-containing compounds

4.2.1 Breakthrough curves for sulphur-containing compounds on Cu^+ - and Ni^{2+} -exchanged Na^+ -Y zeolites as adsorbents.

Breakthrough curves for the adsorption of thiophene from model solutions 1 and 2 on zeolite Cu^+ -Y were determined at different temperatures. Figures 4.13 and 4.14 show the obtained breakthrough curves on Cu^+ -Y at 20 °C. 1 g of Cu^+ -Y zeolite is capable of desulphurizing 1.7 ml of model solution 1 at ambient temperature. This corresponds to a breakthrough adsorption capacity of 7.1 mg/g and a saturation adsorption capacity of 10.9 mg/g. Hence, Cu^+ -Y is

capable of adsorbing 1.7 molecules of thiophene from toluene per unit cell of zeolite. The unit cell composition of zeolite $\text{Cu}^{2+}\text{-Y}$ as determined by elemental analysis is $\text{Na}_4\text{Cu}_{27}[\text{Al}_{58}\text{Si}_{134}\text{O}_{384}] \cdot 24 \text{H}_2\text{O}$. Based on the unit cell composition, it was found that only 6 % of the total Cu^+ -cations underwent π -complexation with thiophene molecules from model solution 1. The thiophene adsorption capacity of $\text{Cu}^+\text{-Y}$ at saturation from model solution 2 amounts to 86 mg/g, which corresponds to 13 molecules per unit cell, i.e., almost 48 % of the total available Cu^+ -cations undergo π -complexation with thiophene and these many are therefore accessible to thiophene. The increase in adsorption capacity for thiophene from *n*-heptane solution is tentatively due to less competition from aliphatic compounds (viz. the solvent *n*-heptane) as compared to aromatic species to undergo π -complexation with the transition metal ions. As mentioned in the literature, the adsorption of thiophene over transition metals is due to π -complexation between the metal-ion and thiophene [21, 24-26, 30]. The π -complexation capacity of thiophene, toluene and *n*-heptane is of the order thiophene > toluene >> *n*-heptane[30].

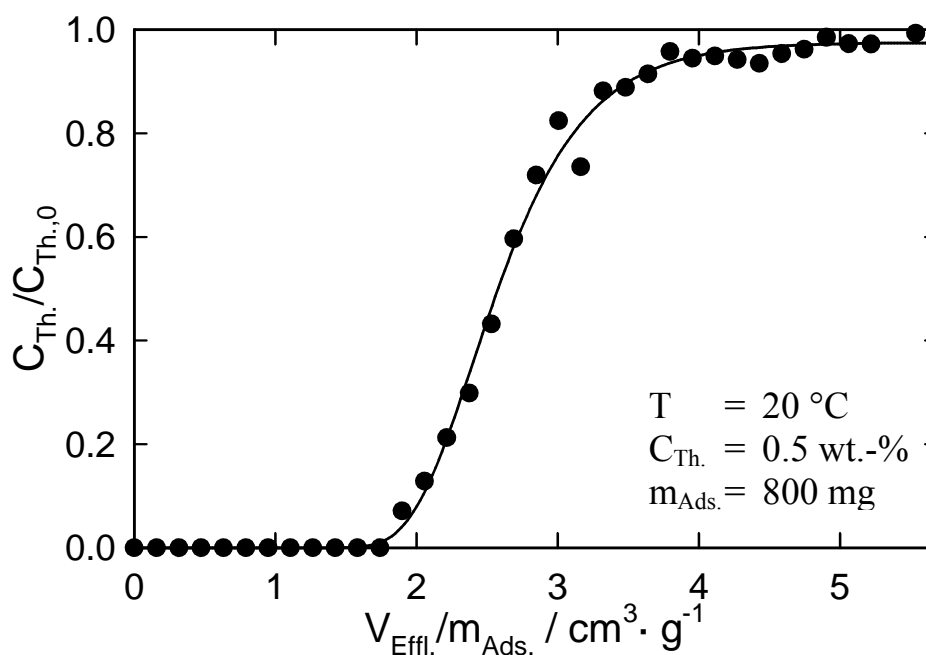


Figure 4.13: Breakthrough curve for the adsorption of thiophene from model solution 1 on zeolite $\text{Cu}^+\text{-Y}$.

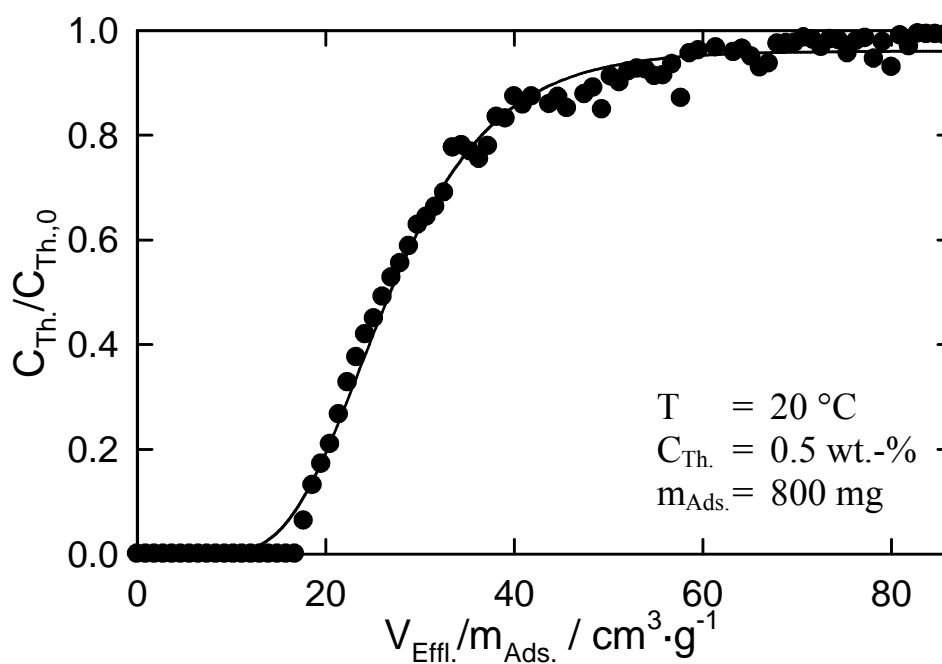


Figure 4.14: Breakthrough curve for the adsorption of thiophene from model solution 2 on zeolite $\text{Cu}^+\text{-Y}$.

For benzothiophene as sulphur containing compound it was found that $\text{Cu}^+\text{-Y}$ can remove 1.7 molecules of benzothiophene from a solution of 0.5 wt.-% benzothiophene in toluene at 20 °C. This is nearly equal to that observed for the removal of thiophene from the similar solvent and concentration level by $\text{Cu}^+\text{-Y}$. The mutual competition between different sulphur-containing compounds was studied with the following experiments: The breakthrough curves for a mixture containing 0.24 wt.-% of thiophene and 0.36 wt.-% of benzothiophene (total of 0.6 wt.-% of sulphur-containing compounds) in toluene were determined with zeolite $\text{Cu}^+\text{-Y}$ as adsorbent. The results are depicted in Figure 4.15 On a molar basis, the sum of 0.24 wt.-% of thiophene and 0.36 wt.-% of benzothiophene corresponds to 0.5 wt.-% of thiophene used in the single component measurements. The molar ratio of thiophene to benzothiophene in the feed is 1.045. The molar adsorption ratio on the adsorbent is found to be 1.043. This means that thiophene and benzothiophene compete equally in toluene solution to adsorb on $\text{Cu}^+\text{-Y}$. For a feed mixture consisting of thiophene, benzothiophene and dibenzothiophene in a molar ratio of 2.53:1:0.85 in toluene, the adsorption of thiophene, benzothiophene and dibenzothiophene on the adsorbent is found to be in the molar ratio of 0.83:1:0.86 and the corresponding breakthrough curves are shown in Figure 4.16 This indicates that the combined presence of bulkier thiophenic molecules like benzothiophene or dibenzothiophene may obstruct the diffusion of thiophene into the pore system of the adsorbent. These bulkier

thiophenic molecules may also compete with thiophene to adsorb on $\text{Cu}^+\text{-Y}$. The lower adsorption of thiophene when benzothiophene and dibenzothiophene were present might be the effect of above mentioned reasons.

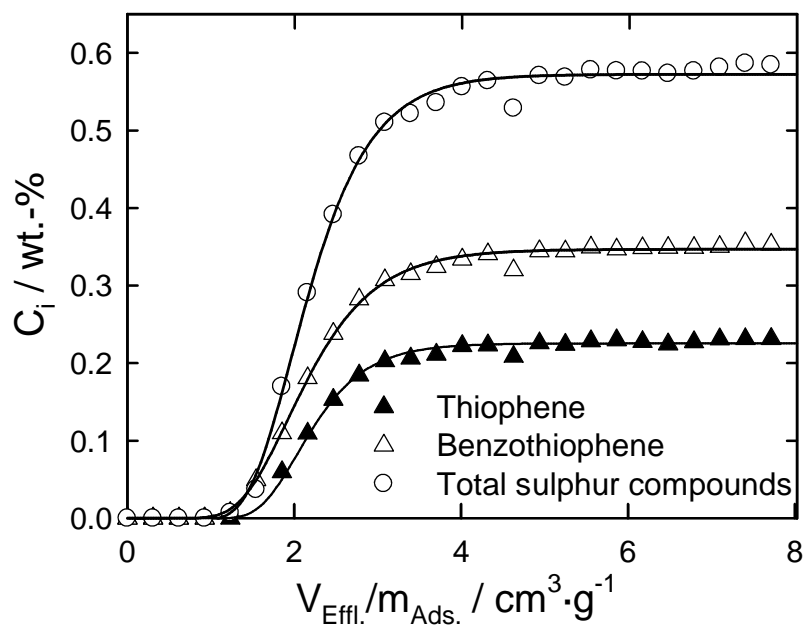


Figure 4.15 Breakthrough curves for the adsorption of thiophene and benzothiophene (0.24 wt.-% thiophene and 0.36 wt.-% benzothiophene) at 20 °C from toluene on zeolite $\text{Cu}^+\text{-Y}$.

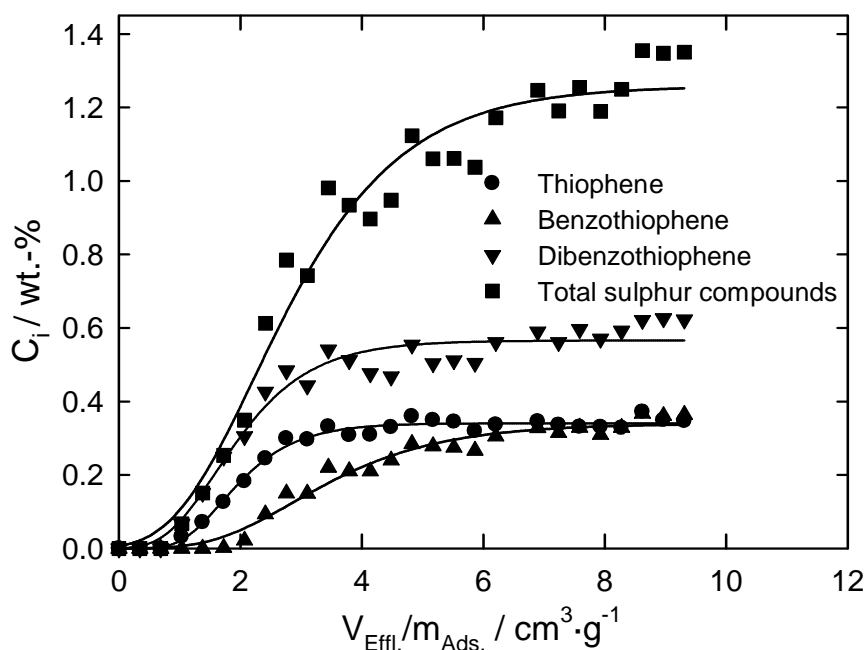


Figure 4.16 Breakthrough curves for the adsorption of thiophene, benzothiophene and dibenzothiophene (0.35 wt.-% thiophene, 0.36 wt.-% benzothiophene and 0.62 wt.-% dibenzothiophene) at 20 °C from toluene on zeolite Cu^+ -Y.

The breakthrough curves obtained with Ni^{2+} -Y with model solutions 1 and 2 at 20 °C are shown in Figures 4.17 and 4.18, respectively. The saturation adsorption capacities are found to be 9.2 mg/g and 63.6 mg/g from model solutions 1 and 2, respectively. By elemental analysis the composition of the unit cell of zeolite Ni^{2+} -Y has been estimated at $\text{Ni}_{17}\text{Na}_{18}[\text{Al}_{58}\text{Si}_{134}\text{O}_{384} \cdot 24 \text{H}_2\text{O}]$. Hence, ca. 1.4 molecules of thiophene per unit cell of the zeolite are adsorbed from model solution 1 (toluene), while 9.6 molecules were adsorbed per unit cell from *n*-heptane (model solution 2). It means that ca. 8 % and 56 % of the total available Ni^{2+} -cations underwent π -complexation with thiophene molecules from model solution 1 and model solution 2, respectively where as 6 % and 48 % of Cu^+ -cations underwent π -complexation from model solution 1 and model solution 2, respectively. It can be concluded that Ni^{2+} -cations in zeolite Ni^{2+} -Y occupies the sites exposed to supercages more preferably than Cu^+ -cations in zeolite Cu^+ -Y

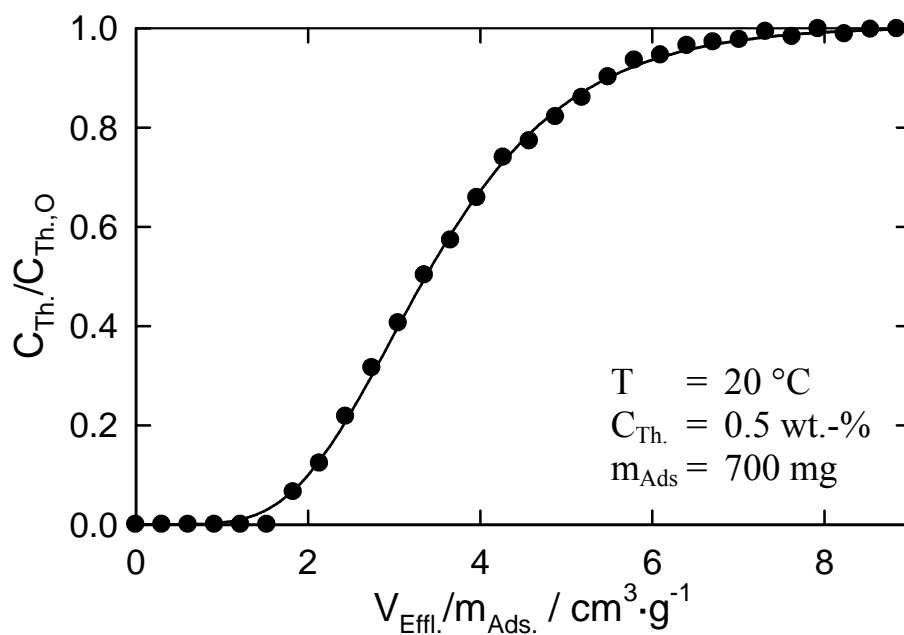


Figure 4.17: Breakthrough curve for the adsorption of thiophene from model solution 1 on zeolite Ni²⁺-Y.

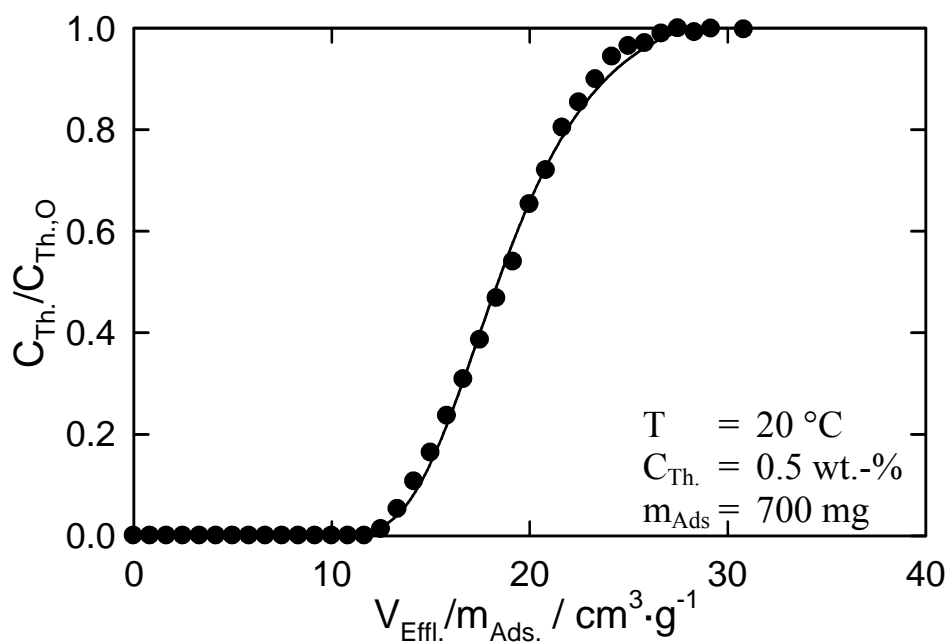


Figure 4.18: Breakthrough curves for the adsorption of thiophene from model solution 2 on zeolite Ni²⁺-Y.

4.2.2 Breakthrough curves for the adsorption of thiophene on Ce^{3+} -, La^{3+} - and Y^{3+} -exchanged Na^+ -Y zeolites.

The breakthrough curves for the adsorption of thiophene on Ce^{3+} -, La^{3+} - and Y^{3+} -exchanged Na^+ -Y zeolites from model solutions 1 and 2 have been measured at 20 °C. Figures 4.19 and 4.20 show the collected breakthrough curves with Ce^{3+} -Y. The obtained data indicate that the performance of zeolite Ce^{3+} -Y is equally good for removing thiophene from both the model solutions. Around 10 ml of model solution can be completely desulphurized by Ce^{3+} -Y before the breakthrough of thiophene starts. The adsorption capacities of Ce^{3+} -Y for thiophene are 61 and 67 mg/g from model solutions 1 and 2, respectively. This corresponds to the adsorption of 10.7 and 11.8 molecules per unit cell of zeolite or 0.38 and 0.42 molecules per cation. These calculations are based on the zeolite composition obtained from elemental analysis as $\text{Ce}_{18.42}\text{Na}_{0.58}[\text{Al}_{58}\text{Si}_{134}\text{O}_{348}]$. The complete utilisation of cations for the adsorption of thiophene is obviously not possible. As discussed earlier, not all the cations located in the zeolite framework are accessible to thiophene molecules. Only the cations exposed to the supercage, i.e., site II (SII) and site III S (III) can contribute in adsorbing thiophene. Moreover, in the case of model solution 1, toluene competes with thiophene by interacting with cations present

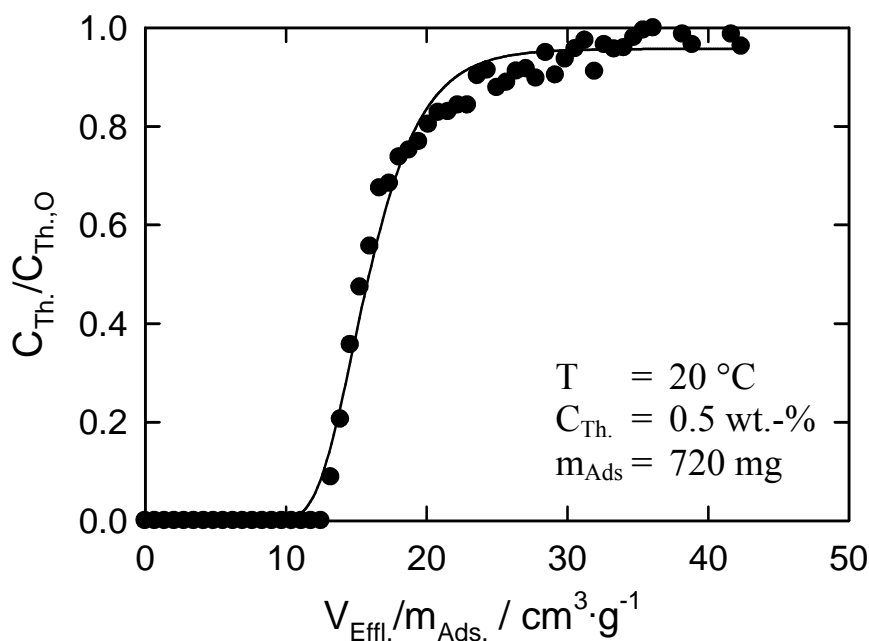


Figure 4.19: Breakthrough curve for the adsorption of thiophene from model solution 1 on zeolite Ce^{3+} -Y.

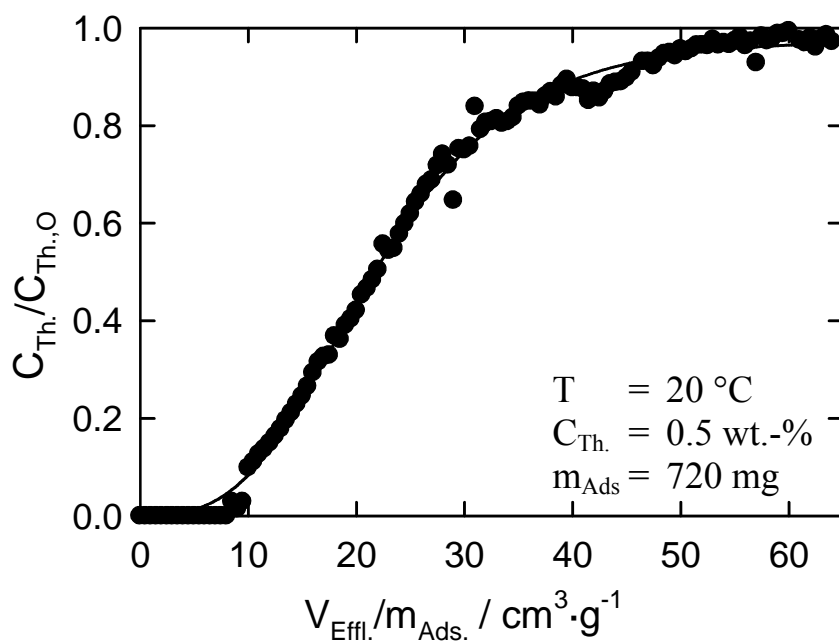


Figure 4.20: Breakthrough curves for the adsorption of thiophene from model solution 2 on zeolite Ce^{3+} -Y.

on these sites through π -complexation. However, the experimental results suggest that Ce^{3+} -Y, La^{3+} -Y and Y^{3+} -Y zeolites favours direct M-S bond with thiophene.

Figures 4.21 and 4.22 shows the breakthrough curves measured for the adsorption of thiophene from model solution 1 on La^{3+} -Y and Y^{3+} -Y zeolites, respectively. The adsorption capacities of La^{3+} -Y and Y^{3+} -Y for thiophene are 75 mg/g and 54 mg/g, respectively, which are nearly equal to the values obtained for batch experiments. The adsorption capacities were found to increase to 100 mg/g and 90 mg/g, respectively, when toluene is replaced by *n*-heptane as solvent. The possible reasons were discussed in section 4.1.4.

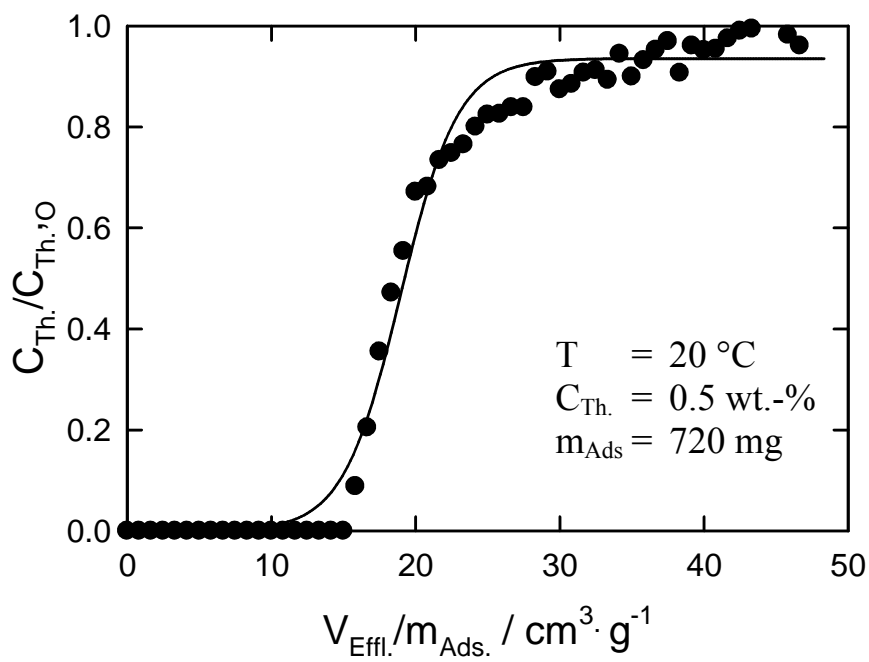


Figure 4.21 Breakthrough curve for the adsorption of thiophene from model solution 1 on La³⁺-Y zeolite.

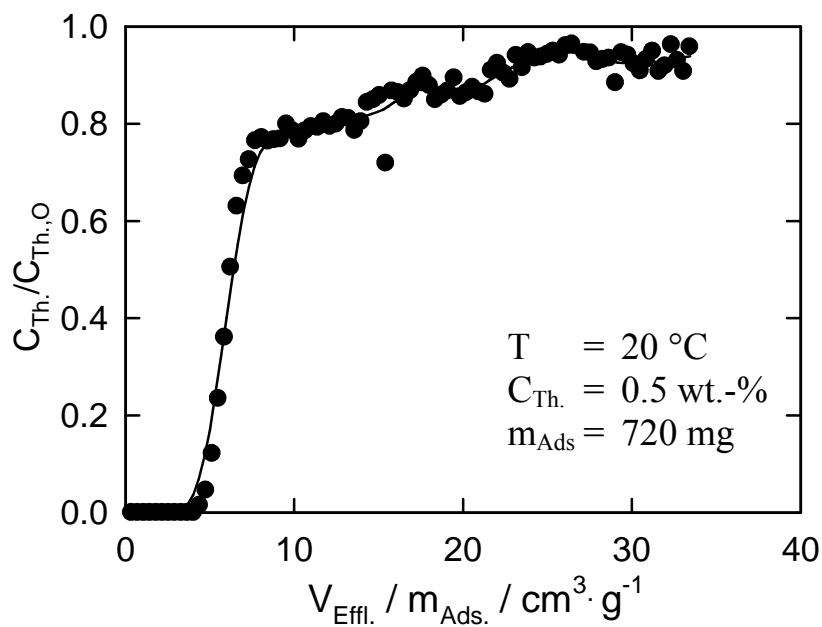


Figure 4.22: Breakthrough curve for the adsorption of thiophene from model solution 1 on Y³⁺-Y zeolite.

4.3 IR spectroscopic studies on the adsorption of thiophene on metal ion-exchanged zeolites

Curves a and b in Figure 4.23 represent IR spectra of zeolite Na⁺-Y and thiophene adsorbed on Na⁺-Y, respectively. In the IR spectra taken after the adsorption of thiophene on Na⁺-Y and subsequent flushing with nitrogen, 3 peaks are observed at wavenumbers 1396 cm⁻¹, 1633 cm⁻¹ and 3104 cm⁻¹. The peak at 1396 cm⁻¹ can be assigned to the shift in the $\nu(\text{C}=\text{C})_{\text{sym}}$ stretching vibration of the thiophene molecule. When compared with free thiophene ($\nu(\text{C}=\text{C})_{\text{sym}}$ stretching vibration at 1409 cm⁻¹) the peak has shifted about 13 cm⁻¹ to lower wavenumbers for adsorbed thiophene. The shift to lower wavenumbers indicates the decrease in electron density of the entire ring and thus confirms the interaction of thiophene with Na⁺ cation by π -complexation. A band at 1633 cm⁻¹, which occurs at a higher wavenumber than the corresponding value (1586 cm⁻¹) of free thiophene, is tentatively attributed to an out-of-plane mode. The presence of an adsorption band at around ca. 3110 cm⁻¹ (at ca. 3104 cm⁻¹ in Figure 4.23) characterizes the valence vibrations of the CH bonds.

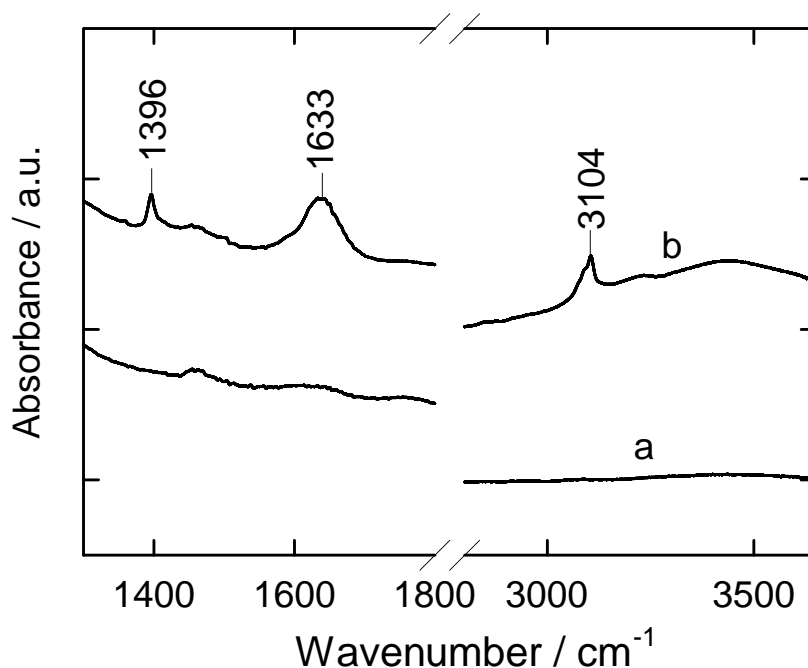


Figure 4.23: IR spectra of a) Na⁺-Y activated at 400 °C in N₂ and cooled down to 20 °C, b) thiophene adsorbed onto Na⁺-Y followed by flushing in N₂ at 20 °C.

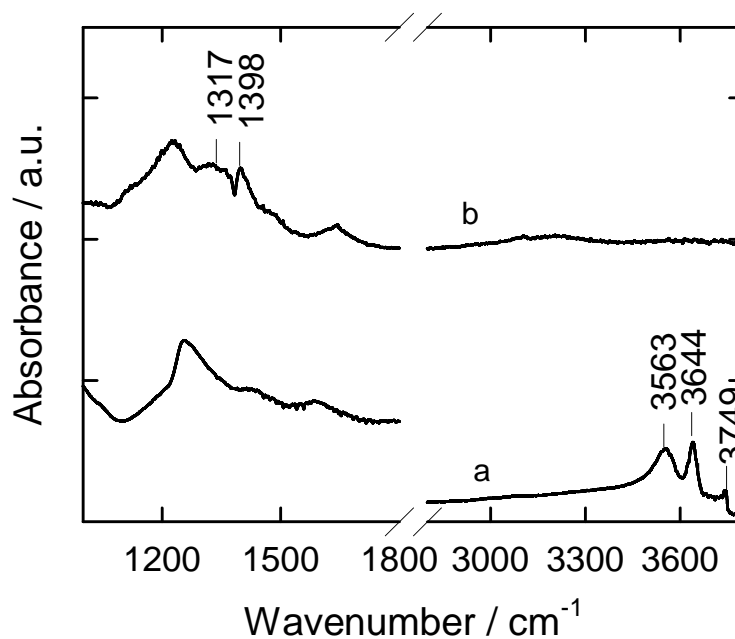


Figure 4.24: IR spectra of a) Cu⁺-Y activated at 450 °C in N₂ and cooled down to 20 °C, b) thiophene adsorbed onto Cu⁺-Y followed by flushing in N₂ at 20 °C.

The IR spectra of zeolite Cu⁺-Y and of thiophene adsorbed on Cu⁺-Y followed by flushing with nitrogen at 20 °C are shown in Figure. 4.24. For the thiophene-loaded sample, two extra peaks are observed at 1317 cm⁻¹ and 1398 cm⁻¹. Moreover, three peaks, observed for Cu⁺-Y zeolite at 3563 cm⁻¹, 3644 cm⁻¹ and 3749 cm⁻¹, disappeared upon thiophene adsorption. The appearance of two extra peaks at 1317 cm⁻¹ and 1398 cm⁻¹ can be attributed to shifts in the $\nu(\text{C}=\text{C})_{\text{sym}}$ stretching vibration of the thiophene molecule. Free thiophene shows a stretching vibration at 1409 cm⁻¹ which, after adsorbing on Cu⁺-Y, might have shifted by 9 cm⁻¹ and 11 cm⁻¹ to lower wavenumbers and resulted in the appearance of peaks at 1317 and 1398 cm⁻¹, respectively. The negative shifts indicate a decrease in electron density of the entire thiophene ring which implies that thiophene is adsorbed at Cu⁺-cation by π -complexation.

In previous studies on the dehydration of Cu²⁺-exchanged Na⁺-Y zeolites, bands in the 3650 cm⁻¹ to 3500 cm⁻¹ were assigned to the presence of [Cu(OH)]⁺[69]. These bands disappeared on heating the samples above 300 °C. In the present investigation, vibrations are observed at 3563 cm⁻¹, 3644 cm⁻¹ and 3749 cm⁻¹ even after heating the sample at 450 °C. Therefore, it is unlikely that these peaks resulted from copper hydroxyl species, which would have decomposed at above 300 °C. By contrast, these bands can be assigned to structural hydroxyl groups. The disappearance of these peaks after thiophene adsorption indicates that the corresponding sites (OH groups) act as adsorption sites for thiophene. The disappearance of

C-H stretching bands (2900 cm^{-1} to 3100 cm^{-1}) can be attributed to tentative adsorption of thiophene on the structural hydroxyl groups via hydrogen bond.

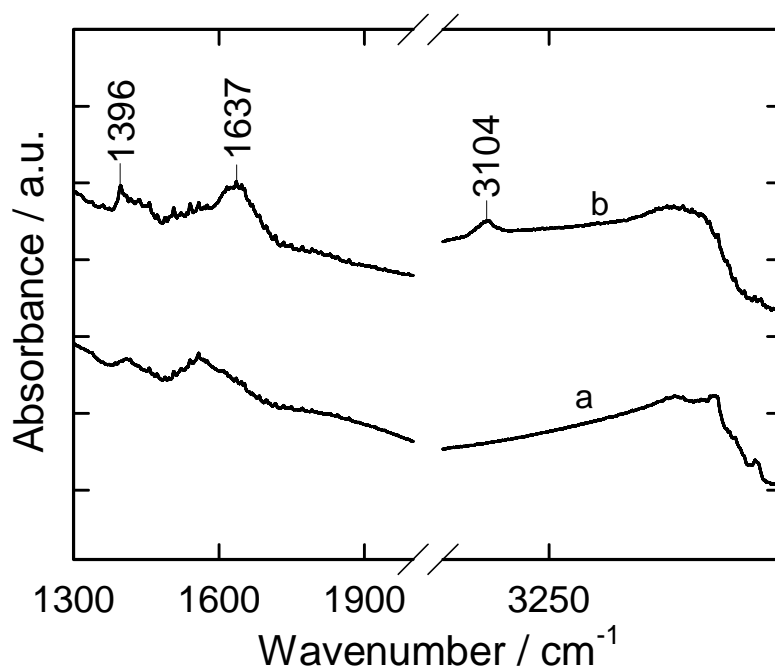


Figure 4.25: IR spectra of a) Ni^{2+} -Y activated at $400\text{ }^{\circ}\text{C}$ in N_2 and cooled down to $20\text{ }^{\circ}\text{C}$, b) Thiophene adsorbed onto Ni^{2+} -Y followed by flushing in N_2 at $20\text{ }^{\circ}\text{C}$.

Figure 4.25 shows IR spectra of zeolite Ni^{2+} -Y and of thiophene-loaded zeolite Ni^{2+} -Y. In the IR spectra taken after the adsorption of thiophene on Ni^{2+} -Y and subsequent flushing with nitrogen, the observed peaks at wavenumbers 1396 cm^{-1} , 1637 cm^{-1} and 3104 cm^{-1} are comparable to those peaks observed in the IR spectra for thiophene loaded Na^+ -Y zeolite (Figure 4.24). The type of interaction of thiophene with Ni^{2+} -cation is obviously the same as with Na^+ -cation and the peak assignments are comparable to those already given above.

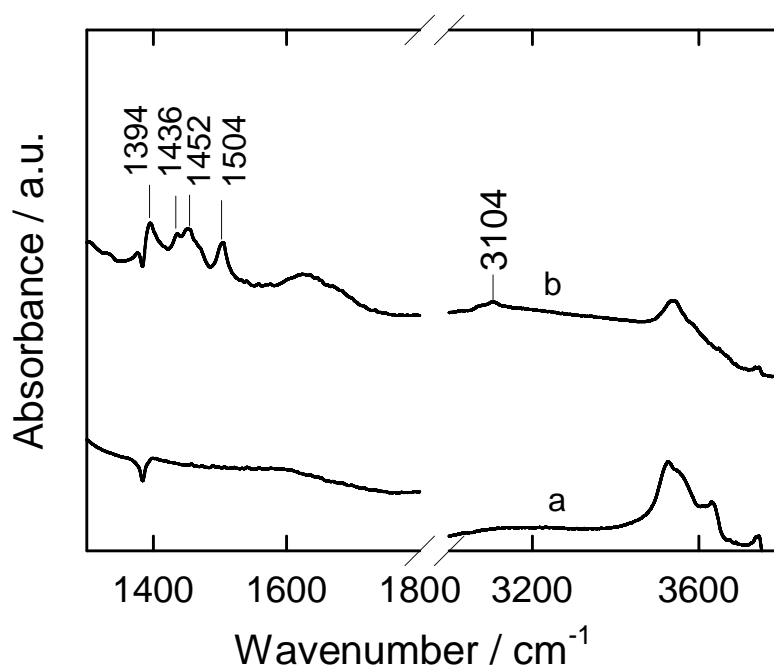


Figure 4.26: IR spectra of a) Ce^{3+} -Y activated at 400 °C in N_2 and cooled down to 20 °C, b) thiophene adsorbed onto Ce^{3+} -Y followed by flushing in N_2 at 20 °C.

The IR spectrum of thiophene adsorbed on zolite Ce^{3+} -Y followed by flushing at 20 °C is shown in Figure 4.26 (b). The absorption frequencies of 1394 cm^{-1} , 1436 cm^{-1} , 1452 cm^{-1} , 1504 cm^{-1} shown in curve b are very close to those of thiophene in the vapour phase. When compared to free thiophene, the $\nu(\text{C}=\text{C})_{\text{sym}}$ stretching vibration of the thiophene ring at 1409 cm^{-1} is shifted by 15 cm^{-1} to lower wavenumbers and 27 cm^{-1} to higher wavenumbers resulting in the appearance of peaks at 1396 cm^{-1} and 1436 cm^{-1} . The shift to lower wavenumbers by a decrease in the electron density of the entire ring indicates that thiophene is adsorbed at Ce^{3+} -cations by π -complexation. The shift to higher wavenumbers is tentatively attributed to a higher electron density within the thiophene ring and can be regarded as evidence for the interaction of thiophene with Ce^{3+} -ions directly via the S-atom. The band at 1504 cm^{-1} , which is more clearly visible for thiophene adsorbed on Ce^{3+} -Y than on Na^+ -Y and Cu^+ -Y, is due to asymmetric stretching of C=C double bond. The appearance of this band is a tentative consequence of a shift in the stretching vibration of C=C as a result of an interaction of S-atoms of thiophene with Ce^{3+} ions.

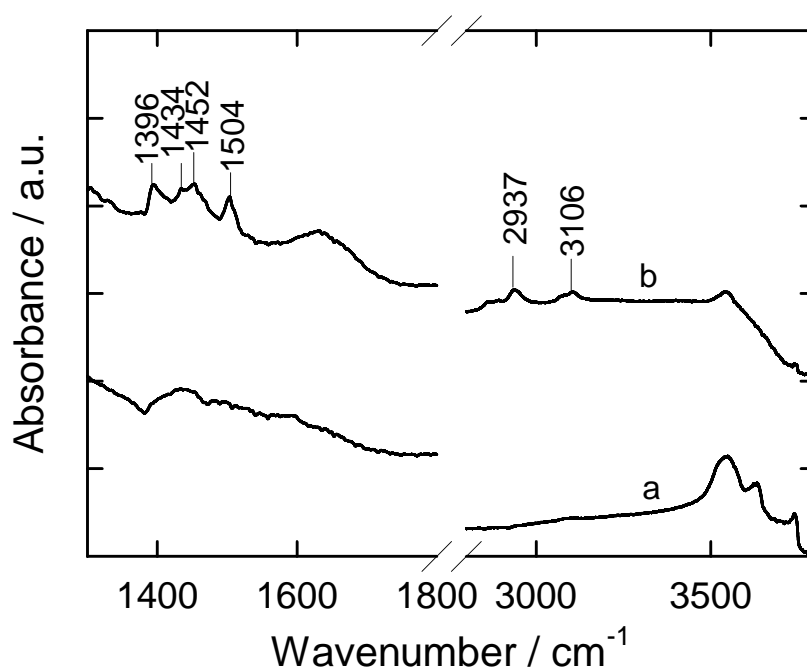


Figure 4.27: IR spectra of a) Ce⁴⁺-Y activated at 400 °C in N₂ and cooled down to 20 °C, b) thiophene adsorbed onto Ce⁴⁺-Y followed by flushing in N₂ at 20 °C.

The absorption bands observed on Ce⁴⁺-Y of Figure 4.27 below wavenumbers of 1600 cm⁻¹, which are due to the adsorption of thiophene (viz. 1396 cm⁻¹, 1434 cm⁻¹, 1452 cm⁻¹ and 1504 cm⁻¹) are quite similar to the absorption bands of thiophene adsorbed on Ce³⁺-Y. With this result, it is evident that thiophene interacts in a comparable mode with Ce³⁺ and Ce⁴⁺ cations. The two peaks observed between 2900-3110 cm⁻¹ can be attributed to C-H stretching bands of the physically adsorbed thiophene.

The IR spectra for the adsorption of thiophene on Y³⁺-Y are shown in Figure 4.28. The spectrum observed below 1600 cm⁻¹ is quite complex. Apart from the peaks observed in the previous adsorbents (1396 cm⁻¹, 1436 cm⁻¹, 1456 cm⁻¹, 1506 cm⁻¹), two extra peaks are found at 1488 cm⁻¹ and 1540 cm⁻¹. The band at 1488 cm⁻¹ can be tentatively ascribed to the $\nu(\text{C}=\text{C})_{\text{sym}}$ of thiophene adsorbed onto Y³⁺-Y via the S-atom and the band at 1540 cm⁻¹ can be attributed to $\nu(\text{C}=\text{C})_{\text{asym}}$ of thiophene interacting with Y³⁺-ions through the S-atom.

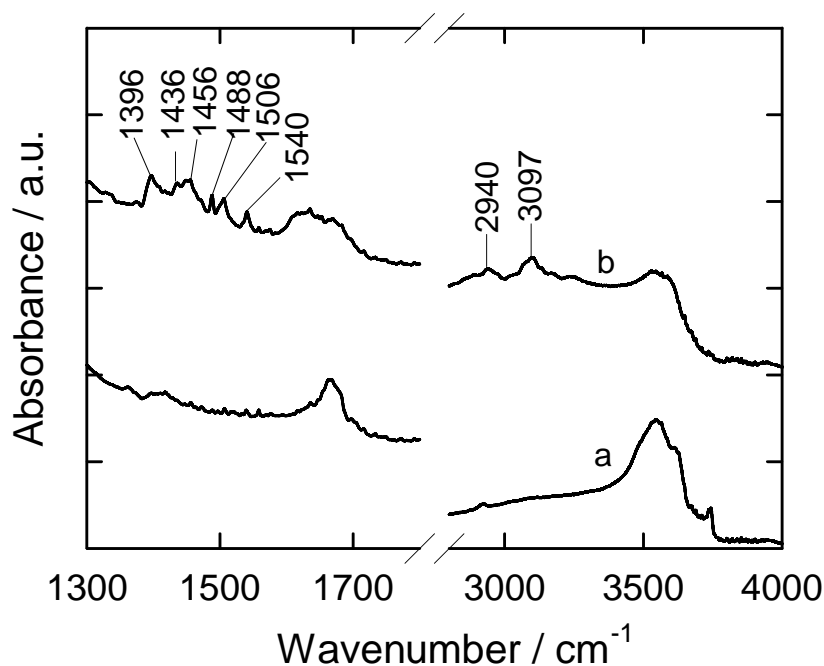


Figure 4.28: IR spectra of a) Y^{3+} -Y activated at 400 °C in N_2 and cooled down to 20 °C, b) thiophene adsorbed onto Y^{3+} -Y followed by flushing in N_2 at 20 °C.

The IR spectra for the adsorption of thiophene on La^{3+} -Y are depicted in Figure 4.29. A very intensive and broad peak is observed in the range from 1350 cm^{-1} to 1450 cm^{-1} . This could be due to the overlapping of several peaks previously observed on Ce^{3+} -Y and Y^{3+} -Y. Upon close inspection, 3 peaks can be identified in this range, i.e., at 1398 cm^{-1} , 1403 cm^{-1} and 1428 cm^{-1} . The peaks at 1398 cm^{-1} and 1403 cm^{-1} can be attributed to the $\nu(\text{C}=\text{C})_{\text{sym}}$ stretching vibrations of thiophene that have resulted as a consequence of shift by about 11 cm^{-1} and 6 cm^{-1} to lower wavenumbers when compared with the $\nu(\text{C}=\text{C})_{\text{sym}}$ stretching vibration of thiophene vapours. The peak at 1428 cm^{-1} could be interpreted as a result of a shift to higher wavenumbers that has occurred with the increase in the electron density within the thiophene ring as a consequence of the adsorption of thiophene via an S-atom on an La^{3+} -ion. The peaks observed between 3000 cm^{-1} and 3200 cm^{-1} are attributed to the valence vibrations of CH bonds.

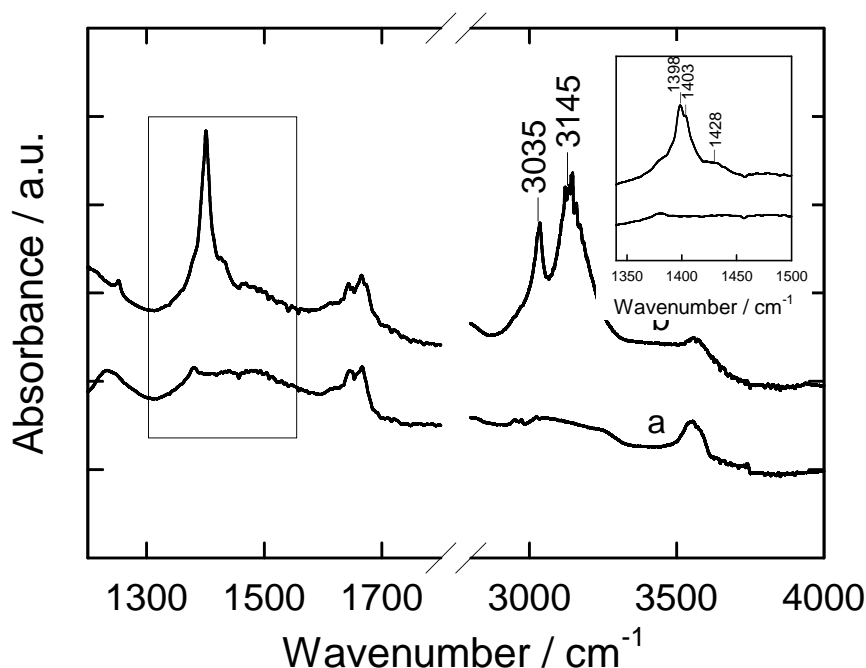


Figure 4.29: IR spectra of a) La³⁺-Y activated at 400 °C in N₂ and cooled down to 20 °C, b) thiophene adsorbed onto La³⁺-Y followed by flushing in N₂ at 20 °C.

4.4 Regeneration of used adsorbents

4.4.1 Regeneration of acidic zeolites

The possibility of a regeneration of acid zeolites after their use as thiophene adsorbents has been explored using a TGA-MS system. For this purpose, the used (and, hence, thiophene-loaded) zeolite was removed from the fixed-bed flow-type adsorber and dried at 100 °C for 12 hours in nitrogen. The material was then heated in the TGA-MS system from 50 °C to 550 °C under a nitrogen flow. The desorbing components (thiophene and toluene) were detected by a mass spectrometer coupled to TGA. The desorption profiles of thiophene from H-Na-Y and H-ZSM-5 were shown in Figures 4.30 and 4.31. Thiophene desorption starts at ca. 200 °C and ends at ca. 400 °C as detected by the mass-spectrometer coupled to the TGA.

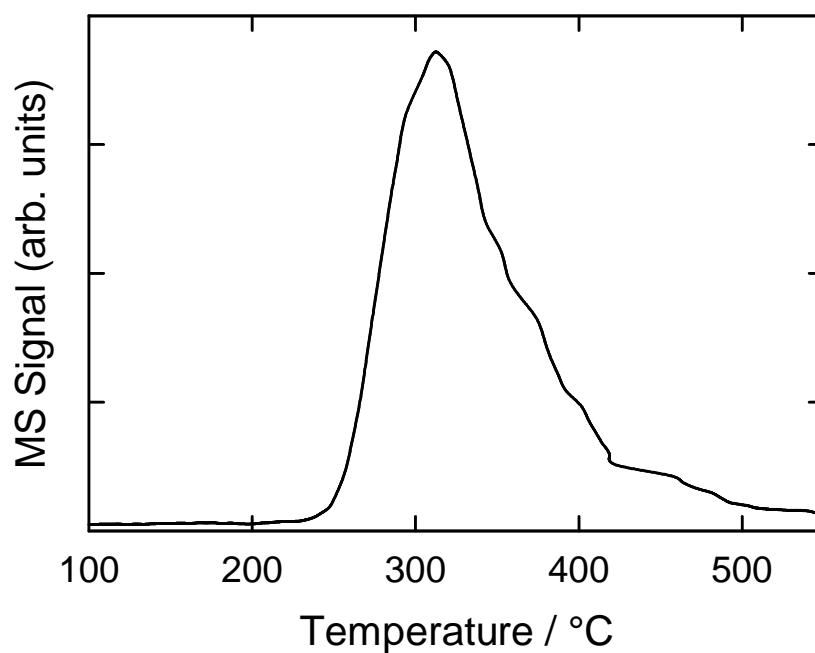


Figure 4.30: Regeneration of thiophene-loaded zeolite H-Y by heating under a nitrogen flow.

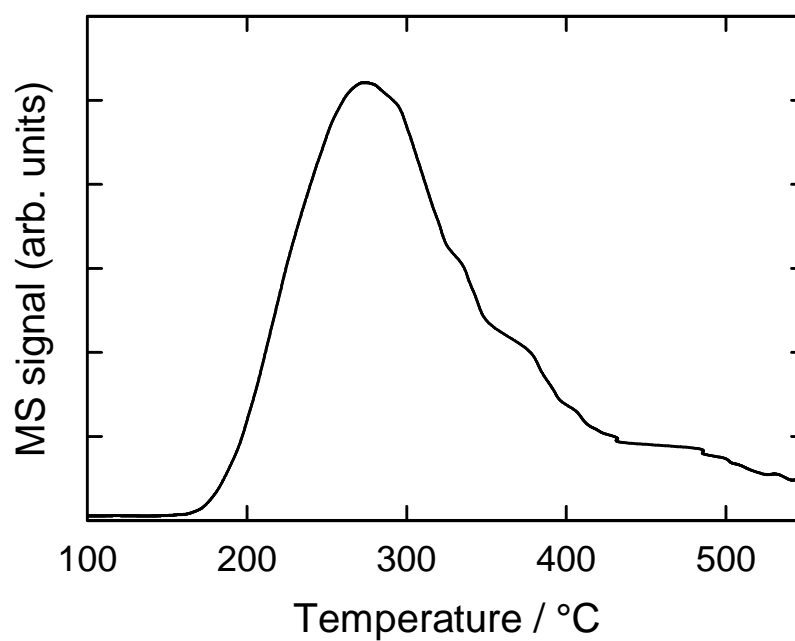


Figure 4.31: Regeneration of thiophene-loaded zeolite H-ZSM-5 by heating under a nitrogen flow.

4.4.2 Regeneration of metal ion-exchanged zeolites

After the adsorption of pure thiophene on Cu^+ -Y and drying at 100 °C in a flow of nitrogen, the regeneration of the thiophene-loaded adsorbent was studied by thermal gravimetric analysis in a flow of air. Figure 4.32 shows the weight loss and the heat flow profile of the used adsorbent (TG-DTA). The two different exothermic peaks at ca. 160 °C and ca. 280 °C can in principle be attributed to the burning of chemically bonded thiophene. Alternatively, the different peaks may also be attributed to two different mode of interaction of thiophene with metal species present inside the framework of zeolites. It is also evident from the IR spectrum of thiophene adsorbed on Cu^+ -Y that two different types of interaction are possible and they are most probably due to the interaction of thiophene with Cu^+ -ion by π -complexation and the interaction of thiophene with structural hydroxyl groups, respectively.

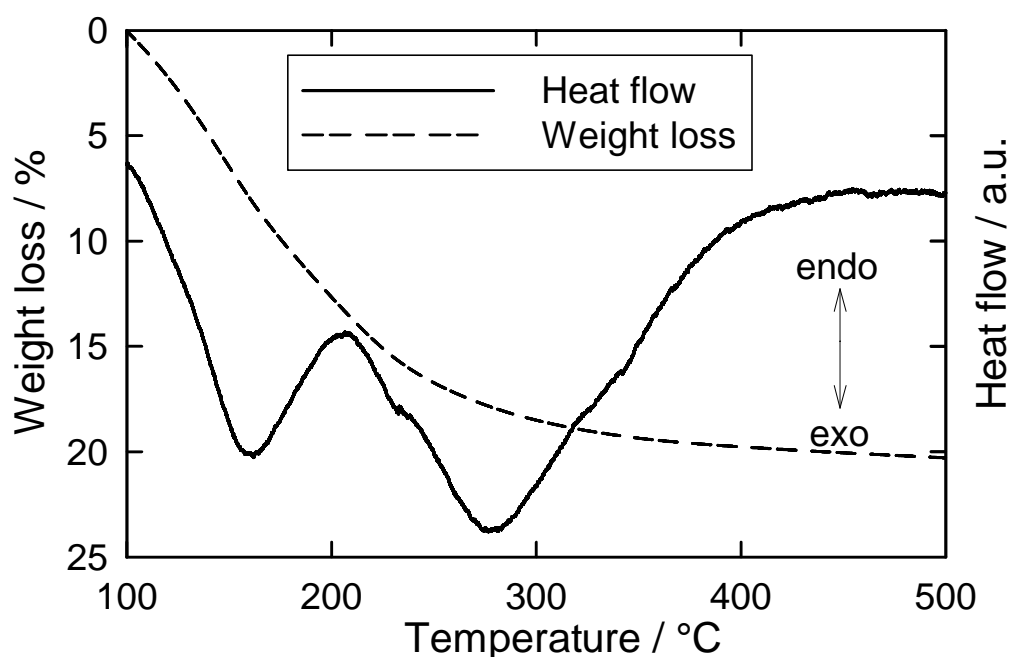


Figure 4.32: TG-DTA analysis of thiophene-loaded Cu^+ -Y zeolite.

The colour of the thiophene-loaded Cu^+ -Y zeolite was controlled before and after regeneration. It was found that the colour of the adsorbent change from deep violet to light blue. The blue colour is most probably due to the presence of Cu^{2+} -ions as charge compensating ions. It is therefore anticipated that the oxygen from air used to burn off adsorbed thiophene has oxidised Cu^+ -Y to Cu^{2+} -Y zeolite. To reduce the ionic state again

from Cu^{2+} to Cu^+ , the material was heated under nitrogen flow. As a consequence, the colour of the material changes from blue to white indicating a reduction of the Cu^{2+} ions. Figure 4.33 shows the comparison of the breakthrough curve with fresh adsorbent and with the regenerated adsorbent using model solution 1. The breakthrough for the adsorption of thiophene on regenerated zeolite Cu^+ -Y appears earlier and the adsorption reaches the equilibrium slowly when compared to the breakthrough curve for the adsorption of thiophene on fresh Cu^+ -Y zeolite. The adsorption capacity for thiophene on Cu^+ -Y is almost completely regained. With all the above results, it can be concluded that Cu^+ -Y can be regenerated thermally by first treating in the flow of air at ca. 400 °C (to burn off thiophene) and then by autotereduction at 450 °C (Cu^{2+} to Cu^+) in the flow of nitrogen.

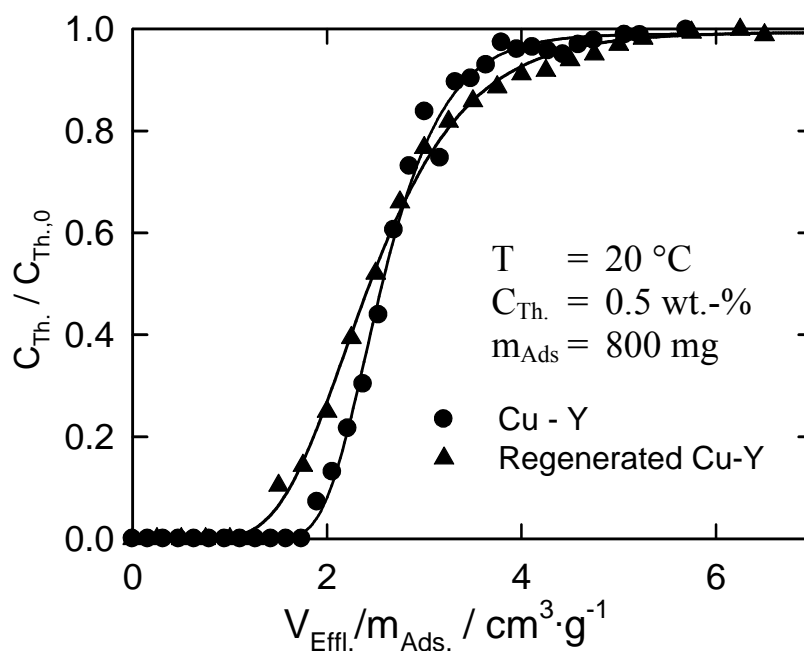


Figure 4.33 Breakthrough curves for the adsorption of thiophene from model solution 1 on fresh zeolite Cu^+ -Y and regenerated zeolite Cu^+ -Y.

Figure 4.34 shows the thermal gravimetric and differential thermal analysis (TG-DTA) curves of the used adsorbent Ce^{3+} -Y after adsorption of pure thiophene. Similar to the TG-DTA of thiophene-loaded Cu^+ -Y zeolite, here too, two exothermic peaks are observed. But these peaks are observed at temperatures (260 and 430 °C) higher than that observed on Cu^+ -Y (shown in Figure 4.32). The peak at 430 °C can be attributed to the burning of thiophene interacted to metal ion via sulphur atom (M-S interaction). Similar TG-DTA profiles are

observed for La^{3+} -Y and Y^{3+} -Y adsorbents (Figure 4.35 and 4.36). These adsorbents (Ce^{3+} -Y, La^{3+} -Y and Y^{3+} -Y) can be highly selective for the adsorption of sulphur-containing compounds because, the sulphur-containing compounds may dominate over other hydrocarbons in adsorbing on metal ion species via M-S interaction. These adsorbents might require higher temperatures for regeneration than Cu^+ -Y zeolite, which is evident from the TG-DTA profiles (Figures 4.34, 4.35 and 4.36).

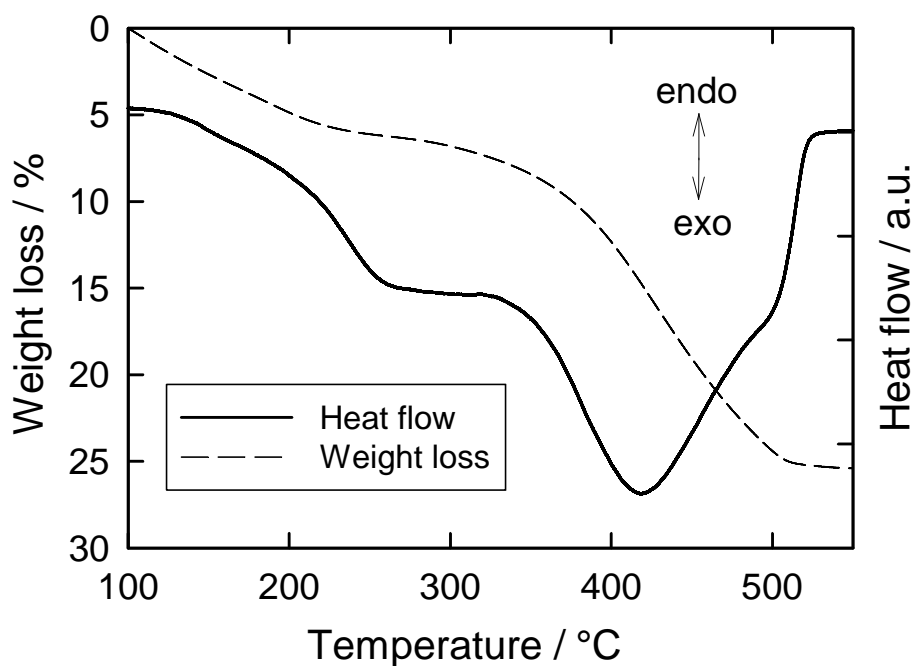


Figure 4.34: TG-DTA analysis of thiophene-loaded Ce^{3+} -Y zeolite in air.

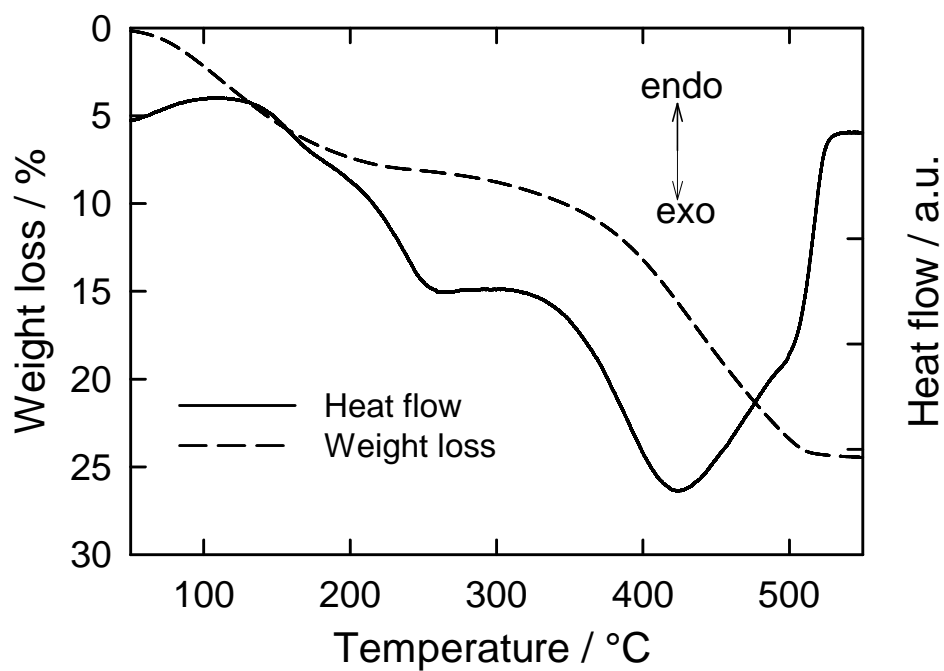


Figure 4.35: TG-DTA analysis of thiophene-loaded La³⁺-Y zeolite in air.

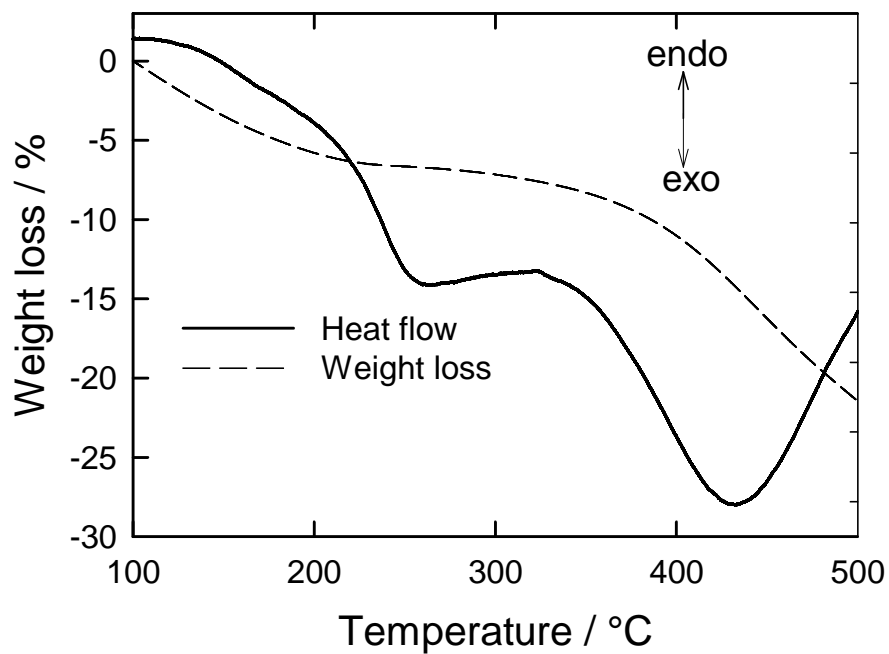


Figure 4.36: TG-DTA analysis of thiophene-loaded Y³⁺-Y zeolite in air.

5 Selective adsorption of 4,6-DMDBT from toluene

Using the currently available catalytic hydrodesulphurization (HDS) technology, the sulphur content in fuels can be reduced to as low as 10 ppm. However, removing the traces of sulphur containing compounds, particularly dialkyl dibenzothiophenes, requires increasingly severe reaction conditions and consumes large amounts of hydrogen. The position of the alkyl groups in these dialkyl dibenzothiophenes plays an important role in controlling the reactivities of these molecules [70-73]. For example, the ability to remove sulphur from dimethyl dibenzothiophenes (DMDBTs) via HDS technology over a Co-Mo/Al₂O₃ catalyst is reported to have the order [70]



The primary reason for the poor activity of the 4,6-DMDBT has been attributed to the steric hindrance of the methyl groups, which hinders the approach of the sulphur atom to the active sites of the catalyst. As a result, the HDS of 4,6-DMDBT does not tend to follow the direct desulphurization route typical of other reactive sulphur compounds over Co-Mo/Al₂O₃ catalyst [15]. Therefore it would be interesting to find an alternative method to remove these traces of dialkyl dibenzothiophene molecules.

Therefore, Cu⁺-Y and Ce³⁺-Y zeolites were screened in the present study to explore their adsorptive ability for selectively removing 4,6-DMDBT from toluene. The kinetics of adsorption from a starting solution with 0.5 wt.-% of 4,6-DMDBT in toluene are shown in Figure 4.37. Approximately 7.0 and 7.4 mg of 4,6-DMDBT per gram of adsorbent were adsorbed on Ce³⁺-Y and Cu⁺-Y, respectively within 10 hours of stirring in a batch system. With these results, it can be concluded that the sulphur-containing molecules left over after hydrodesulphurization viz. dialkyl dibenzothiophene, can be removed by subsequent application of selective adsorption on Ce³⁺-Y or Cu⁺-Y zeolite after catalytic hydrodesulphurization.

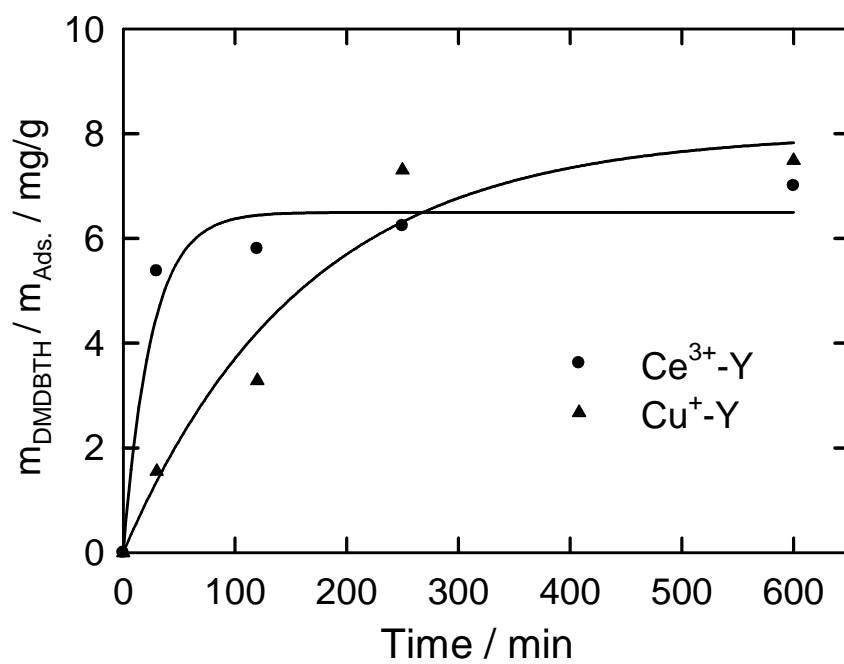


Figure 4.37: Adsorption of 4,6-DMDBT at 20 °C from a solution of 0.5 wt.-% 4,6 DMDBT in toluene on $\text{Ce}^{3+}\text{-Y}$ and $\text{Cu}^{+}\text{-Y}$, respectively.

6 Conclusions

Acidic zeolites like H-Y, H-ZSM-5, H-MCM-22 and H-MOR zeolites were found to be the selective adsorbents for the removal of thiophene from toluene or *n*-heptane as solvent. The competitive adsorption of toluene is found to influence the adsorption capacity for thiophene and is more predominant when high-alumina zeolites are used as adsorbents. This behaviour is also reflected by the results of the adsorption of thiophene on H-ZSM-5 zeolites with varied $n_{\text{Si}}/n_{\text{Al}}$ ratios (viz. 13, 19 and 36) from toluene and *n*-heptane as solvents, respectively.

UV-Vis spectroscopic results show that the oligomerization of thiophene leads to the formation of dimers and trimers on these zeolites. The oligomerization in acid zeolites is regarded to be dependent on the geometry of the pore system of the zeolites. The sulphur-containing compounds with more than one ring viz. benzothiophene, which are also present in substantial amounts in certain hydrocarbon fractions, are not adsorbed on H-ZSM-5 zeolites. This is obvious, as the diameter of the pore aperture of zeolite H-ZSM-5 is smaller than the molecular size of benzothiophene.

Metal ion-exchanged FAU-type zeolites are found to be promising adsorbents for the removal of sulphur-containing compounds from model solutions. The introduction of Cu^+ -, Ni^{2+} -, Ce^{3+} -, La^{3+} - and Y^{3+} - ions into zeolite Na^+ -Y by aqueous ion-exchange substantially improves the adsorption capacity for thiophene from toluene or *n*-heptane as solvent. More than the absolute content of Cu^+ -ions, the presence of Cu^+ -ions at the sites exposed to supercages is believed to influence the adsorption of thiophene on Cu^+ -Y zeolite. It was shown experimentally for the case of Cu^+ -Y and Ce^{3+} -Y that the supercages present in the FAU zeolite allow for an access of bulkier sulphur-containing compounds (viz. benzothiophene, dibenzothiophene and dimethyl dibenzothiophene). The presence of these bulkier compounds compete with thiophene and are preferentially adsorbed on Cu^+ -Y zeolite.

IR spectroscopic results revealed that the adsorption of thiophene on Na^+ -Y, Cu^+ -Y and Ni^{2+} -Y is primarily a result of the interaction of thiophene via π -complexation between C=C double bond (of thiophene) and metal ions (in the zeolite framework). A different mode of interaction of thiophene with Ce^{3+} -, La^{3+} - and Y^{3+} -metal ions was observed in the IR spectra of thiophene adsorbed on Ce^{3+} -Y, La^{3+} -Y and Y^{3+} -Y zeolites, respectively. On these

adsorbents, thiophene is believed to interact via a lone electron pair of the sulphur atom with metal ions present in the adsorbent (M-S interaction).

The experimental results show that there is a large difference in the thiophene adsorption capacities of π -complexation adsorbents (like $\text{Cu}^+\text{-Y}$, $\text{Ni}^{2+}\text{-Y}$) between the model solution with toluene as solvent and the model solution with *n*-heptane as solvent. The lower capacity of these zeolites for the adsorption of thiophene from toluene than from *n*-heptane as solvent is the clear indication of competition of toluene in interacting with adsorbent in a way similar to thiophene. The difference in thiophene adsorption capacities is very low in the case of adsorbents $\text{Ce}^{3+}\text{-Y}$, $\text{La}^{3+}\text{-Y}$ and $\text{Y}^{3+}\text{-Y}$, which are believed to interact with thiophene predominantly by direct $\text{M}^{3+}\text{-S}$ bond (thiophene interacting with metal ion via a lone pair of electrons).

TG-DTA analysis was used to study the regeneration behaviour of the adsorbents. Acid zeolites can be regenerated by simply heating at 400 °C in a flow of nitrogen whereas thiophene is chemically adsorbed on the metal ion. By contrast, it is not possible to regenerate by heating under idle inert gas flow. The only way to regenerate these adsorbents is to burn off the adsorbate, which eventually brings about an undesired emission of SO_x . The exothermic peaks appeared at different temperatures in the heat flow profiles of $\text{Cu}^+\text{-Y}$, $\text{Ce}^{3+}\text{-Y}$, $\text{La}^{3+}\text{-Y}$ and $\text{Y}^{3+}\text{-Y}$ are also indicating that two different types of interaction are present as revealed by IR spectroscopy, too.

One major difficulty in reducing the sulphur content in fuels to value below 10 ppm is the inability in removing alkyl dibenzothiophenes, viz. 4,6 dimethyl dibenzothiophene, by the existing catalytic hydrodesulphurization technique. $\text{Cu}^+\text{-Y}$ and $\text{Ce}^{3+}\text{-Y}$ were found in the present study to adsorb this compound from toluene to a certain extent. To meet the stringent regulations on sulphur content, selective adsorption by zeolites could be a valuable post-purification method after the catalytic hydrodesulphurization unit.

7 Abbreviations and indices

a.u	arbitrary units
BET	Brunauer-Emmet-Teller
C_{Th}	Concentration of thiophene
$C_{Th,0}$	Initial concentration of thiophene
DMDBT	Dimethyl dibenzothiophene
DTA	Differential thermal analysis
EDAX	Energy dispersive X-ray analysis
ΔH_{ads}	Enthalpy of adsorption
FAU	Faujasite
FID	Flame ionisation detector
HDS	Hydrodesulphurization
H_{vap}	Heat of vaporization
IR	Infrared
IZA	International Zeolite Association
LPIE	Liquid-phase ion-exchange
m_{Th}	Mass of thiophene
m_{Ads}	Mass of adsorbent
MCM-22	Mobil composition of matter No. 22
MOR	Mordenite
MS	Mass spectrometer
SBU	Secondary building unit
SEM	Scanning electron microscope
SSIE	Solid state ion-exchange
TGA	Thermogravimetric analysis
TG-DTA	Thermogravimetric and differential thermal analysis

UV-Vis	Ultraviolet-visible
V _{Eff.}	Volume of effluent
VPIE	Vapour-phase ion-exchange
λ	Wavelength
XRD	X-ray diffraction
ZSM-5	Zeolite Socony Mobil No. 5
ZSM-11	Zeolite Socony Mobil No. 11

8 References

- [1]. I.V. Babich and J.A. Mozlijn, *Fuel* **82**, 607-631(2003).
- [2]. S. Labana, G. Pandey and R.K. Jain, *Lett. in Appl. Microbiol.* **40**, 159-163 (2005).
- [3]. Z. Varga and J. Hancsók, *Petroleum and Coal* **45**, 3-4, 135-141 (2003).
- [4]. G.A. Purdy, „*Petroleum Refining and Treating*“, McGraw-Hill, p. 216 (1958).
- [5]. A.P. Singh, P.C. Singh, K.K. Pandey and V.N. Singh, *Can. J. Chem. Eng.* **66**, 501-504 (1988).
- [6]. A.P. Singh, P.C. Singh and V.N. Singh, *Ind. Eng. Chem. Res.* **27**, 2101-2104 (1988).
- [7]. D. Nicholson, *Anal. Chem.* **32**, 1365-1366 (1960).
- [8]. D. Nicholson, *Anal. Chem.* **34**, 370-374 (1962).
- [9]. A.S. Sultanov, U.B. Khakimov, G. Talipov and J.J. Shchekochinin, *React. Kinet. Catal. Lett.* **2(3)**, 243-250 (1975).
- [10]. B.A.D. Angelis and G. Appierto, *J. Colloid Interface Sci.* **53(1)**, 14-19 (1975).
- [11]. A.D. Ulendeeva, V.I. Lygin and N.K. Lyapina, *Kinet. Katal.* **20(4)**, 978-983 (1979).
- [12]. A.S.H. Salem, *Ind. Eng. Chem. Res.* **33**, 336-340 (1994).
- [13]. A.S.H. Salem and H.S. Hamed, *Chem. Eng. Technol.* **20**, 342-347 (1997).
- [14]. J. Weitkamp, M. Schwark and S. Ernst, *J. Chem. Soc., Chem. Commun.*, 1133-1134 (1991).
- [15]. C.L. Garcia and J.A. Lercher, *J. Phys. Chem.* **96**, 2669-2675 (1992).

- [16]. A. Chica, K. Strohmaier and E. Iglesia, *Langmuir* **20**, 10982-10991 (2004).
- [17]. D. Richardeau, G. Joly, C. Canaff, P. Magnoux, M. Guisnet, M. Thomas and A. Nicolaos, *Applied Catalysis A: General* **263**, 49-61 (2004).
- [18]. A. Chica, K.G. Strohmaier and E. Iglesia, *Applied Catalysis B: Environmental* **60**, 223-232 (2005).
- [19]. Patent EP0275855 (A1), 27. July 1988, N.V. SOPOR S.A. (W.Mingels, E.M. Enody and E.F.M. Vasant).
- [20]. T.I. Korányi, A. Jentys and H. Vinek, *Studies in Surface Science and Catalysis* **94**, 582-589 (1995).
- [21]. A. Takahashi, F.H. Yang and R.T. Yang, *Ind. Eng. Chem. Res.* **41**, 2487-2496 (2002).
- [22]. R.T. Yang, „*Adsorbents: Fundamentals and Applications*“, Wiley-Interscience, p.192, 219-222 (2003).
- [23]. S. Velu, X. Ma and C. Song, *Ind. Eng. Chem. Res.* **42**, 5293-5304 (2003).
- [24]. A.J. Hernández-Maldonado and R.T. Yang, *J. Am. Chem. Soc.* **126**, 992-993 (2004).
- [25]. A.J. Hernández-Maldonado and R.T. Yang, *Ind. Eng. Chem. Res.* **43**, 6142-6149 (2004).
- [26]. A.J. Hernández-Maldonado and R.T. Yang, *Ind. Eng. Chem. Res.* **43**, 1081-1089 (2004).
- [27]. M. Xue, R. Chitrakar, K. Sakane, T. Hirotsu, K. Ooi, Y. Yoshimura, Q. Feng and N. Sumida, *J. Colloid Interface Sci.* **285**, 487-492 (2005).
- [28]. S. Velu, C. Song, M.H. Engelhard and Y.H. Chin, *Ind. Eng. Chem. Res.* **44**, 5740-5749 (2005).
- [29]. K. Chatterjee, R. Wolny and L.M. Stock, *Energy and Fuels* **4**, 402-406 (1990).

- [30]. A.J. Hernández-Maldonado, F.H. Yang, G. Qi and R.T. Yang, *Applied Catalysis B: Environmental* **56**, 111–126 (2005).
- [31]. R.A. Sanchez-Delgado, *J. Mol. Catal.* **86**, 287-307 (1994).
- [32]. R.J. Angelici, *Bull. Soc. Chim. Belg.* **104**, 268 (1995).
- [33]. D.L. Hughes, R.L. Richards, C. Shortman, *J. Chem. Soc., Chem. Commun.*, 1731 (1986)
- [34]. C. Potrin, J.M. Bregalt, J.M. Manoli, *J. Chem. Soc., Chem. Commun.*, 664-665 (1980).
- [35]. X. Ma, L. Sun and C. Song, *Catalysis Today* **77**, 107–116 (2002).
- [36]. Ch. Baerlocher, W.M. Meier and D.H. Olson, „*Atlas of Zeolite Framework Types*“, p. 6 (2001).
- [37]. H.G. Karge and J. Weitkamp, „*Molecular sieves: Science and Technology*“, Springer, p. 165 (1999).
- [38]. A. Mersmann, „*Ullmanns Encyclopedia of Industrial Chemistry*“, VCH, Weinheim, B3, p. 9 (1998).
- [39]. R. M. Dessau, *American Chemical Society Symp. Ser.*, 135, 123 (1980).
- [40]. S.M. Csicsery, *Pure & Appl. Chem.* **58**, 841-856, 1986.
- [41]. J.V. Smith, *Adv. Chem. Ser.* **101**, 171 (1971).
- [42]. US Patent 4954325, 9. March 1990, Mobil Oil Corporation (M.K. Rubin and P. Chu).
- [43]. S. Yongchen, Y. Piaoping, J. Mingjun, Z. Wenxiang, and W. Tonghao, *Catal. Commun.* **9(5)**, 907-912 (2008).

- [44]. H.G. Karge and J. Weitkamp, „*Molecular sieves: Science and Technology*“, p. 76 (1999).
- [45]. S. Brunauer, L. S. Deming, W.S. Deming and E. Teller, *J. Am. Chem. Soc.* **62**, 1723-1732 (1940).
- [46]. S. Brunauer, P.H. Emmett and E. Teller, *J. Am. Chem. Soc.* **60**, 309-319 (1938).
- [47]. E.M. Flanigen, H. Khatami, and H. A. Szymanski, *Adv. Chem. Ser.* **10**, 201 (1971).
- [48]. M. Rico, J.M. Orza and J. Morcillo, *Spectrochimica Acta* **21**, 689-719 (1965).
- [49]. P. Mills, S. Korlann, M. E. Bussell, M.A. Reynolds, M.V. Ovchinnikov, R.J. Angelici, C. Stinner, T. Weber and R. Prins, *J. Phys. Chem. A.* **105**, 4418-4429 (2001).
- [50]. M. Schwark, Ph. D. thesis, Institut für Technische Chemie I, Universität Stuttgart, p. 23 (1991).
- [51]. S. Ernst, Ph. D. Thesis, Universität Karlsruhe, p. 23 (1987).
- [52]. M. Schwark, Ph. D. thesis, Institut für Technische Chemie I, Universität Stuttgart, p. 24 (1991).
- [53]. S. Unverricht, M. Hunger, S. Ernst, H. G. Karge, J. Weitkamp, in: J. Weitkamp, H.G. Karge, H. Pfeifer, W. Hölderich (ed.), „*Zeolites and Related Microporous Materials: State of the Art, Studies in Surface Science and Catalysis*“, Vol. 84, Teil A, Elsevier, Amsterdam, P. 37-44. (1994).
- [54]. F. Geolbaldo, G.T. Palmomino, S. Bordiga, A. Zecchina, C.O. Areal, *Phys. Chem., Chem. Phys.* **1**, 561-569 (1999).
- [55]. R.F. Curis, D.M. Jones and W.A. Thomas, *J. Chem. Soc. C: Organic* **2**, 234-238 (1971).

- [56]. A.H. Jackson „*chemistry of heterogenous compounds*“, ed. E.C. Taylor and A. Weissenberg, Interscience, John Wiley & Sons, New York **48**, part I, P.305 (1987).
- [57]. E. Ruiz-Hitzky, *Adv. Mater.* **5**, 334-340 (1993).
- [58]. E. Ruiz-Hitzky, P. Aranda, B. Casal and J.C. Galván, *Adv. Mater.* **7**, 180-184 (1995).
- [59]. T. Bein and P. Enzel, *Angew. Chem.* **28**, 1692-1694 (1989).
- [60]. J.R. Blanking, G.L. Millar, A. Bowmaker and R.P. Cooney, *J.Raman Spectros.* **24**, 523-526 (1993).
- [61]. P. Enzel and T. Bein, *J. Chem. Soc., Chem. Commun.* **18**, 1326-1327 (1989).
- [62]. S. Bordiga, G. Ricchiardi, G. Spoto, D. Scarano, L. Carnelli, A. Zecchina and C.O. Areán, *J. Chem. Soc., Faraday Trans.* **89**, 1843-1855 (1993).
- [63]. G. Spoto, S. Bordiga, G. Ricchiardi, D. Scarano, A. Zecchina and E. Borello, *J. Chem. Soc., Faraday Trans.* **90**, 2827-2835 (1994).
- [64]. F. Geobaldo, G. Spoto, S. Bordiga, C. Lamberti and A. Zecchina, *J. Chem. Soc., Faraday Trans.* **93**, 1243-1249 (1997).
- [65]. R. Chiappetta, S. Bodoardo, F. Geobaldo, F. Fajula and E. Garrone, *Res. Chem. Int.* **25(1)**, 111-129 (1999).
- [66]. G. Spoto, F. Geobaldo, S. Bordiga, C. Lamberti, D. Scarano and A. Zecchina, *Topics in Catalysis* **8**, 279-292 (1999).
- [67]. J. Datka, M. Bocjen, P. Rymarowicz, *J. Catal.* **114**, 368-376 (1988).
- [68]. P.A. Jacobs, W.D. Wilde, R.A. Schoonheydt, J.B. Uytterhoeven and H. Beyer *J. Chem. Soc., Faraday Trans. 1*, **72**, 1221-1230 (1976).
- [69]. J. Howard, J.M. Nicol, *J. Chem. Soc., Faraday Trans. 1*, **85**, 1233-1244 (1989).

- [70]. S. K. Bej, S. K. Maity and U. T. Turaga , *Energy and Fuels* **18**, 1227-1237 (2004).
- [71]. K. Segawa, K. Takahashi, S. Satoh, *Cataylsis. Today* **63**, 123-131 (2000).
- [72]. V. Meille, E. Schulz, M. Lemaire, M. Vrinat, *Appl. Catal. A: General* **187**, 179 (1999).
- [73]. H. Schulz, W. Böhringer, P. Waller and F. Ousmanov, *Catalysis Today* **49**, 87 (1999).

Curriculum Vitae

Name	Sridhar Adapa
Address	101, Central Towers Apt. Balaji Nagar, Wyra Road Khammam-507002, A.P. India
Date of Birth	22.08.1978
Place of Birth	Warangal (India)
Education	
07/2004 – 08/2008	Ph. D. at Technical University of Kaiserslautern
02/2002 – 01/2004	Master of Science in Chemical Engineering at University of Applied Sciences, Muenster
07/2003 – 01/2004	Master Thesis at EADS, Friedrichshafen
07/1997 – 05/2001	Bachelor of Technology in Chemical Engineering at Osmania University, Hyderabad, India
05/1995 – 05/1997	Intermediate Education, Khammam, India
06/1985 – 04/1995	Secondary School Education, Khammam, India
Work Experience	
07/2004 – 08/2008	Research Co-worker at Technical University of Kaiserslautern